INSTITUTE OF APPLIED PHYSICS

Manuscript
C.Z.U. 530.145+535.14

Ceban Victor

QUANTUM BEHAVIORS OF OPTICAL AND OPTOMECHANICAL SYSTEMS POSSESSING ARTIFICIAL ATOMS

131.01 - Mathematical Physics

Thesis in physics

Ph.D. supervisor: MACOVEI Mihai, Dr. Sci., Assoc. Prof.

Author: CEBAN Victor

CHIŞINĂU, 2020

INSTITUTUL DE FIZICĂ APLICATĂ

Cu titlu de manuscris
C.Z.U. 530.145+535.14

CEBAN Victor

DINAMICA CUANTICĂ A SISTEMELOR OPTICE ŞI OPTOMECANICE CU ATOMI ARTIFICIALI

Specialitatea: 131.01 - Fizică matematică

Teză de doctor în ştiinţe fizice

Conducător Ştiinţific: MACOVEI Mihai, dr. hab. în şt. fiz.-mat., conf. cerc.

Autorul: CEBAN Victor

CHIŞINĂU, 2020

OUTLINE

ACKNOWLEDGEMENTS

I would like to cordially thank my supervisor Mihai Macovei for his inspiring guidance through all my work presented here. I’m very thankful to him for enlightening me into the world of quantum physics and for his unconditional assistance to my formation.

I’m very grateful to all my colleagues, Profirie Bardețchi, Corneliu Gherman, Viorel Ciornea, Sergiu Cârlig, Elena Cecoi, Alexandra Mîrzac and Ion Cojocaru, for their fruitful discussions and friendly support they have provided me since my first day at the Institute of Applied Physics.

I’m heartfully thankful to my beloved parents and specially to my grandparents, who have nourished my curiosity about the universe I’m living in, since I remember myself.

SUMMARY

to the thesis ”Quantum behaviors of optical and optomechanical systems possessing artificial atoms”, presented by Victor Ceban for conferring the scientific degree of Ph.D. in Physics, Speciality 131.01 ”Mathematical Physics”, Chişinau, 2020.

The thesis has been written in English language and consists of the introduction, 5 chapters, general conclusions and recommendations, and the list of 200 references. The thesis contains 127 pages of basic text, 25 figures and 145 formulas. The results presented in the thesis are published in 20 scientific publications.

Key words: sub-Poissonian phonon laser, quantum interferences, phonon superradiance, fast phonon dynamics, phonon assisted population inversion, artificial atoms, quantum-dots, quantum-wells, quantum optomechanics, cavity quantum electrodynamics.

The goal: The determination and analysis of different quantum properties of the dynamics of an optical or mechanical resonator interacting with semiconductor artificial atoms.

Research objectives: The identification of various emitter-resonator coupling schemes related to different characteristic features of artificial atoms; The demonstration of the quantum statistics of an optical or mechanical resonator when interacting with an artificial atom; The identification of possible quantum interferences in systems possessing multi-level artificial atoms; The observation of the behaviour of the quanta distribution of a nanomechanical resonator under different interaction conditions; The demonstration of the influence of collective phenomena to the behaviour of an optomechanical system.

Scientific novelty and originality of the results: the phonon superradiant behaviour has been demonstrated in solid matter quantum nanomechanical resonators; the phenomenon of destructive quantum interference has been manipulated in order to effectively decouple an artificial atom from an optical cavity; a perturbation treatment of moderately strong quantum-dot-acoustic-resonator dynamics has allowed the observation of sub-Poissonian distributed phonon fields, i.e., quantum phonon lasing.

The main scientific problem solved consists in analysing the phenomena related to the quantum statistics of different types of quantum oscillators interacting with artificial atoms, in order to predict the conditions required to prepare the quantum oscillator in a specific quantum state.

Theoretical significance and applicative value: in this thesis it was demonstrated the quantum dynamics of open quantum systems with an elevated degree of complexity, which include diverse interactions among various components such as artificial atoms, laser light, optical cavities, nanomechanical resonators and the surrounding environment.

The model of a pumped two-level quantum-dot coupled to a quantum mechanical resonator operating in a moderately strong coupling regime has been solved. A coherent phonon generation scheme with sub-Poissonian quantum distribution of the vibrational quanta of the acoustic nanomechanical resonator has been proposed in order to improve phonon based sensing techniques.

A setup made of an equidistant ladder-type three-level quantum-well with perpendicular dipoles placed in an optical cavity has been investigated in the good cavity limit. A scheme for a quantum switch based on quantum interference effect was proposed. The cavity electromagnetic field is turned on and off by varying the parameters of the input pumping lasers.

The collective behaviour of a sample of initially excited two-level quantum-dots placed on a quantum mechanical resonator has been reported among the firsts investigations in the current literature. Therefore, a mechanism generating phonons with fast dynamics has been established. Ultra-short intense phonon pulses are generated via this mechanism, similarly to the superradiance effect.

The implementation of the scientific results: the research presented in this thesis has been successfully implemented in the framework of the bilateral moldo-german project 13.820.05.07/GF and national institutional project 15.817.02.09F, and may be further used for educational purposes.

ADNOTARE

la teza ”Dinamica cuantică a sistemelor optice și optomecanice cu atomi artificiali”, elaborată de Victor Ceban pentru conferirea gradului științific de doctor în științe fizice la specialitatea 131.01 ”Fizică matematică”, Chișinău, 2020.

Teza este scrisă în limba engleză și constă din introducere, 5 capitole, concluzii generale și recomandări, și lista a 200 titluri bibliografice. Teza conține 127 pagini de text de bază, 25 figuri și 145 formule. Rezultatele prezentate în teză sunt publicate în 20 lucrări științifice.

Cuvinte cheie: laser fononic de tip sub-Poissonian, interferențe cuantice, superradianță fononică, dinamică rapidă a fononilor, inversia populației asistată de fononi, atomi artificiali, puncte cuantice, gropi cuantice, optomecanică cuantică, electrodinamica cuantică de cavitate.

Scopul tezei: Determinarea și analiza diferitor proprietăți cuantice ale dinamicii unui rezonator optic sau mecanic care interacționează cu un atom artificial pe bază de semiconductor.

Obiectivele tezei: Identificarea diferitor scheme de cuplare emițător-rezonator legate de diferite proprietăți caracteristice atomilor artificiali; Demonstrarea statisticii cuantice a unui rezonator optic sau mecanic, când acesta interacționează cu atomii artificiali; Identificarea eventualelor interferențe cuantice în sisteme care conțin atomi artificiali cu mai multe nivele; Observarea comportamentului distribuției cuantelor unui rezonator nanomecanic pentru diferite condiții de interacțiune; Demonstrarea influenței fenomenelor colective asupra comportamentului sistemelor optomecanice.

Noutatea științifică și originalitatea rezultatelor: Comportamentul superradiant al fononilor a fost demonstrat pentru rezonatoare nanomecanice cuantice pe bază de materie solidă; Fenomenul de interferență destructivă a fost manipulat pentru a decupla efectiv un atom artificial de o cavitate optică; Tratarea dinamicii la nivel perturbativ a permis observarea fononilor distribuiți sub-Poissonian, adică observarea efectului laser fononic cuantic, pentru regimuri de cuplare moderat intens a punctului cuantic cu rezonatorul acustic.

Problema științifică soluționată constă în analiza fenomenelor legate de statistica cuantică ale diferitor tipuri de oscilatoare cuantice care interacționează cu atomi artificiali, cu scopul de a prezice condițiile necesare pentru a pregăti oscilatorul cuantic într-o stare cuantică specifică.

Semnificația teoretică și valoarea aplicativă: în această teză, este demonstrată dinamica cuantică a sistemelor cuantice deschise cu un grad înalt de complexitate, care includ diverse interacțiuni între diferite componente, cum ar fi: atomi artificiali, lumină laser, cavități optice, rezonatoare nanomecanice și mediul ambiant.

Modelul unui punct cuantic pompat, cu două nivele, care interacționează cu un rezonator nanomecanic a fost rezolvat pentru un regim de cuplare moderat intens. A fost popusă o schemă de generare a fononilor coerenți, în care a fost obținută o distribuție sub-Poissoniană ale cuantelor vibraționale a rezonatorului nanomecanic acustic.

Un dispozitiv constituit dintr-o groapă cuantică cu trei nivele echidistante amplasată într-o cavitate optică a fost investigat în limita cavității cu factor de calitate înalt. A fost propusă o schemă a unui întrerupător cuantic bazată pe efectul de interferență cuantică. Câmpul electromagnetic a cavității apare și dispare variind parametrii laserelor de pompare.

Comportamentul colectiv a unui eșantion de puncte cuantice cu două nivele, inițial excitate, amplasate pe un rezonator nanomecanic, a fost studiat printre primii în literatura de specialitate. Astfel, a fost stabilit un mecanism de generare a fononilor cu dinamică rapidă. Prin intermediul acestui mecanism sunt generate pulsuri ultra-scurte și intense de fononi, similar efectului de superradianță.

Implementarea rezultatelor științifice: studiile prezentate în această teză au fost cu succes implementate în cadrul proiectului bilateral moldo-german 13.820.05.07/GF și proiectului național instituțional 15.817.02.09F, și pot fi utilizate cu scop didactic pentru studenții ciclului universitar și post-universitar.

АННОТАЦИЯ

к диссертации «Квантовая динамика оптических и оптомеханических систем искусственных атомов», представленной Виктором Чебан на соискание ученой степени доктора физических наук по специальности 131.01 «Математическая физика», Кишинэу, 2020

Диссертация написана на английском языке и состоит из введения, пяти глав, общих заключений и рекомендаций, и списка цитируемой литературы из 200 источников. Диссертация содержит 127 страниц базового текста, 25 графиков и 145 формул. Результаты диссертационной работы опубликованы в 20 научных публикациях.

Ключевые слова: фононный лазер субпуассоновского типа, квантовая интерференция, фононное сверхизлучение, инверсия населенности обусловленной фононами, искусственные атомы, квантовая оптика и квантовая оптомеханика.

Цель диссертации: Определение и изучение различных квантовых свойств оптического либо механического резонатора, взаимодействующего с искусственными атомами, возникающими в полупроводниковой среде.

Задачи диссертации: Выявление различных схем соединения излучатель-резонатор в зависимости от характеристических свойств искусственных атомов. Доказательство квантовой статистики оптического либо механического резонатора при его взаимодействии с искусственными атомами. Выявление возможных явлений квантовой интерференции в системах, содержащих многоуровневые искусственные атомы. Изучение поведения распределения квантов возбуждения наномеханических резонаторов в различных условиях их взаимодействия с искусственными атомами. Доказательство влияния коллективных явлений на поведение оптомеханической системы.

Научная новизна и оригинальность результатов: Выяснены особенности поведения фононов в сверхизлучательном состоянии в случае твердотельных квантовых наномеханических резонаторов; установлена возможность манипулирования явлением деструктивной квантовой интерференции с целью эффективного отключения взаимодействия искусственного атома и оптического резонатора; доказана возможность получения субпуассоновских фононов, т.е. возможность осуществления квантового фононного лазера.

Основная научная задача, решаемая диссертацией, заключается в исследовании явлений, обусловленных видами статистики различных квантовых осцилляторов, взаимодействующих с искусственными атомами, в целях определения условий, необходимых для создания квантового осциллятора в определенном квантовом состоянии.

Теоретическая значимость и прикладная ценность: в настоящей диссертационной работе изучена квантовая динамика сложных открытых квантовых систем, включающих различные виды взаимодействия между разными компонентами системы, такими как искусственные атомы, лазерное излучение, оптические и наномеханические резонаторы, и окружающая среда. Исследована динамика двухуровневой модели квантовой точки в поле лазера, умеренно сильно взаимодействующей с наномеханическим резонатором. Предложен способ генерации когерентных фононов, которым получено субпуассоновское распределение вибрационных квантов акустического наномеханического резонатора, способствующий улучшению сенсорных технологий, основанных на фононах. Теоретически предложена схема устройства, состоящего из эквидистантной многозвенной трехуровневой квантовой ямы с перпендикулярными диполями, расположенной в оптическом резонаторе высокой добротности. На базе последней предлагается создать квантовый триггер на основе явления квантовой интерференции. Показано, что изменяя параметры лазеров накачки возникает возможность манипулирования интенсивностью электромагнитного поля в резонаторе. Впервые изучен коллектив возбужденных двухуровневых квантовых точек, расположенных на квантовом наномеханическом резонаторе и показана возможность излучения интенсивных ультракоротких импульсов фононов по аналогии со сверхизлучательным эффектом.

Внедрение научных результатов: представленные в настоящей диссертации результаты были успешно применены в рамках двухстороннего молдавско-немецкого проекта 13.820.05.07/GF и национального институционного проекта 15.817.02.09F.

SHORTCUTS

QD - Quantum dot

QW - Quantum well

EMF - Electromagnetic field

RWA - Rotating wave approximation

$\{a, a^\dagger\}$ - photonic operators

$\{b, b^\dagger\}$ - phononic operators

$\{S^i, S_i\}$ - atomic bare-state operators

$\{R^i, R_i\}$ - atomic dressed-state operators

γ - spontaneous emission rate

κ - damping rate of a reservoir

$\bar{n}$ - mean phonon number of a thermal reservoir

$\langle n \rangle$ - mean phonon (or photon) number of a resonator

$g^{(2)}(0)$ - second-order phonon-phonon (or photon-photon) correlation function

$\mathcal{L}$ - the Liouville superoperator

ρ - density operator

H - Hamiltonian

Ω - Rabi frequency

INTRODUCTION

Actual research status:

Light is the best carrier of quantum information. Photons are good at transporting a specific quantum state over long distances due to reduced noise and strong correlations, which are the key features for technological applications such as quantum communications and quantum cryptography. The feasibility of such technologies have been recently justified by remarkable reports where a quantum state of a single-photon have been successfully teleported from Earth to an orbit satellite over a distance of about 1400 km [1], while cryptographic quantum keys have been successfully distributed in optical fibre over distances of about 400 km with a rate of 6.5 kbps [2].

New horizons open up with the possibility of distribution of quantum states to multiple sources via information nodes, leading to light based quantum networks [3]. Quantum information processing would allow the use of photons for computational operations [4]. A quantum simulation with less than a hundred of photons would bypass the calculation capacity of modern classical computers. The concept of simulating quantum systems with different photon based quantum system would significantly improve current modelling capacity of complex structures in such fields as chemistry and biology. A successful realisation of a waveguide circuit able to operate with four input photons have been recently reported [5].

The implementation of quantum information technologies, as well as various light based sensing and imaging applications, requires a good degree of control and manipulation of photon emission, propagation and detection phenomena. Artificial atoms possess some important features which make them perspective candidates for such technological implementations. Various types and architectures of artificial atoms allow one to engineer optical emitters with some particular characteristics suitable for a specific setup requirements. Especially in the framework of low-loss integrated quantum photonics circuits and on-chip realisation of optical setups, the technical aspects of a setup may impose important limitations and constraints. In this context, superconducting circuits and semiconductor artificial atoms, such as quantum-dots, have shown good efficiency as on-demand single-photon sources [6], which is a key ingredient for quantum information technologies.

Artificial atoms also possess several important differences from real atoms, as they interact with electrical signals and with the mechanical motion. Their optoelectrical and optomechanical couplings suggest various applications in optical sensing and metrology techniques, as well as, applications for hybrid quantum technologies as an interface for the integration of photonic devices into modern electronics. Moreover, their optomechanical coupling opens a new door to quantum confinement of the mechanical motion of matter at mesoscopic scales.

The optomechanical interactions become an important actor for nanoscale optical devices such as nanofibres, superconducting detectors, photonic crystal cavities and various photonic integrated circuits. At this size scales, the mechanical vibrations of the device intrinsically influence the quantum optical effects via the light radiation force. Reciprocally, the manipulation of the quantum mechanical motion can be achieved via optical control. For example, recent reports on optical cooling of a macroscopical mechanical resonator down to its quantum ground state [7] represents an important experimental breakthrough in the quantum manipulation of the mechanical motion via light sources.

Various optomechanical devices have been developed in order to manipulate the quantum optical and quantum mechanical phenomena [8]. Quantum mechanical resonators with high quality factors have been engineered via different architectural approaches, e.g., suspended micro-mirrors and membranes, microtoroids, microspheres, microdisks, nanobeams, nanorods and multi-layered acoustical cavities. A particular interest represents semiconductor based resonators which allow on-chip fabrication and integration to more complex photonic devices. As such, a photonic crystal nanobeam represents a photonic crystal nanocavity shaped as a beam, while a semiconductor microdisk mecahnical resonator represents a whispering-gallery-mode optical cavity. Both of these nanoscale devices allow the confinement of co-localised optical and mechanical modes with high optical and mechanical quality factors. Another important feature consists in the possibility to embed semiconductor artificial atoms such as quantum-dots into these devices.

The implementation of artificial atoms into optomechanical devices introduces a completely new coupling regime between the optical and mechanical parts, as the effective optomechanical coupling strength is increased a few orders of magnitude [9]. Among various coupling schemes, quantum-dots embedded on different mechanical resonators possess a particularity to not require any additional electric or magnetic fields to couple to the mechanical motion. The intrinsic optomechanical coupling of the quantum-dot embedded on a crystal originates from the deformations of the quantum-dot which appear due to the mechanical vibrations of the crystal lattice. Enhanced optomechanical couplings could induce strong photon-phonon correlations observed when optically cooling a nanomechanical resonator with an embedded quantum-dot on it [10].

Strong optomechanical coupling regimes had introduced a series of investigations on optical phenomena which can be influenced by the coupling of the emitters to the mechanical motion such as the surrounding thermal vibrations interacting with a quantum-dot. Phenomena as asymmetry in the side-peaks of the Mollow triplet [11] and phonon assisted population inversion [12] appear due to the interaction of the quantum-dot with the environmental thermal phonons. If comparing to real atoms, the entanglement of a pair of quantum-dots is enhanced due to their coupling to a common environmental phonon reservoir [13].

In a different manner, the optomechanical coupling can be explored to optically control the quantum state of the mechanical motion. Quantum optics dispose of a broad gamut of precise tools able to manipulate the optomechanical setup. Unprecedentedly, this have allowed the preparation of various exotic quantum states of motion of matter at macroscopic scales. In this regard, important achievements have been reported in the recent years due to a continuous advance in the state-of-the-art techniques of engineering of optomechanical devices [9]. A single-phonon state has been observed in an optically cooled nanomechanical resonator [7]. Quantum squeezed states of mechanical motion had been successfully observed within a micrometre-scale mechanical resonator [14]. The acoustic analogue of the optical laser has been experimentally observed in various optomechanical setups based on electromechanical resonators [15], compound microcavities [16] or pumped ions [17]. Meanwhile, theoretical investigations suggest a large variety of phonon laser schemes, whereas setups based on quantum-dots embedded on quantum mechanical resonators have been described in [18, 19, 20].

In the context of quantum statistics, the coherently distributed quanta refers as a reference limit among classical and quantum states of a quantum resonator. Hence, a particular attention has been paid to identify optomechanical setups able to prepare the mechanical resonator in a pure quantum state. In this regard, remarkable optomechanical schemes had been identified for the generation of phonon fields with specific quantum statistics such as antibunching [20], negative Wigner function of the phonon states [21] and sub-Poissonian phonon distributions [22].

A major technological challenge to the implementation of artificial atoms into optical and optomechanical experiments arises when collective phenomena are considered. Collective effects often require the use of ensembles of identical emitters. Although this condition is easily validated by setups based on real atoms, in the case of artificial atoms there is a severe limitation in engineering quasi-identical artificial atoms. The current limitations of quantum-dot growth techniques are defined by the required high degree of resemblance in size and geometry of the quantum-dots. Moreover, the physics of collective phenomena also impose additional restrictions to the spatial distribution of the considered emitters, which becomes particularly challenging in the case of experimental setups based on quantum-dots.

A brilliant experimental realisation of a two-photon interference scheme has been reported in [23]. The considered setup is based on two separate quasi-identical quantum-dots with a high degree of resemblance. Remarkably, a different experiment based on Dicke collective states of closely-spaced quantum-dots have successfully reported the observation of superradiance effect [24], which have required the implementation of quasi-identically engineered artificial atoms.

The purpose of the thesis:

The determination and analysis of different quantum properties of the dynamics of an optical or mechanical resonator interacting with semiconductor artificial atoms.

Objectives of the thesis:

- Identification of various emitter-resonator coupling schemes related to different characteristic features of artificial atoms.
- Estimation of the quantum statistics of the dynamics of the quantum harmonic resonator when interacting with the artificial atom.
- Identification of possible quantum interferences when a multi-level artificial atom is considered.
- Observation of the behaviour of the distribution of quanta of the resonator under different interaction conditions.
- Investigation of the influence of collective phenomena to the behaviour of a considered resonator.

Research hypothesis:

Artificial atoms possess distinctive features when compared to real atoms. Quantum systems with unique properties can be identified when exploring the characteristics of the coupling of the artificial atoms with phonon and photon fields.

Analytical methods:

- The density matrix formalism has been adopted in order to apply the general reservoir theory to characterize the damping phenomena required for the description of open quantum systems. The effect of the surrounding environment to each component of the quantum system have been considered.
- The rotating wave approximations, the secular approximation, the dressed-state transformation, the perturbation theory and different changes of representations have been applied to the system dynamics in order to accurately reduce its complexity without loosing much of the generality of the problem.
- The method of projection of the master equation into the system state basis has been applied in order to define a solvable system of coupled equations for the modified density matrix elements. The quantum statistics of the investigated boson fields have been estimated from the variables of the solved system of equations.
- The method of determination of the equations of motion directly from the master equation has been applied in order to define a solvable system of coupled equation for the parameters of interest. The method allows one to solve the equation of motion of the investigated parameters describing the system dynamics.
- The method of factorization of high order correlations has been applied in order to reduce the complexity of system of equations involving collective operators. This method is applied when building the equations of motion directly from the master equation does not allow one to close and solve the system equation. The factorization of some high order correlation addresses this issue.

Thesis's structure:

In the **first Chapter** it is discussed various approaches of implementation of artificial atoms into modern nanoscale quantum optics. Important experimental realisations in cavity-electrodynamics and optomechanical devices containing different types of artificial atoms are described. Various challenges, advantages and limitations related to specific types of artificial atoms and their integration into optical cavities and quantum mechanical resonators are discussed. The general discussion aims to give an overview on how optical and optomechanical nanoscale devices develop nowadays in order to define the framework of this thesis.

In the **second Chapter**, the general theoretical framework of the thesis is presented. A synthesis of various theoretical approaches have been demonstrated and adapted to the following investigations. The quantum optical and optomechanical interactions are presented and discussed. The physical interpretation and the various theoretical assumptions are given for the Hamiltonian terms corresponding to the analytic models presented in the following chapters. A separate discussion is presented for the reservoir theory approach used to define various damping effects. The decoherent phenomena appear from imperfections of a quantum systems and its interaction with surrounding environment. The possibility to introduce this kind of phenomena to the analytic descriptions of the following quantum systems, is crucial for a realistic treatment of eventual quantum effects.

In the **third Chapter** it is discussed a particular case of interaction of a pumped two-level artificial atom with a quantum mechanical resonator. The theoretical framework defining the model is presented and analysed from the perspective of strong coupling regimes which may be reached when a quantum-dot coupled with a semiconductor mechanical resonator is considered. The related coupling strengths require a novel treatment of the quantum dynamics in order to accurately describe the quantum statistics of the mechanical resonator. The corresponding analytic approach is using a perturbation treatment which is compared to the treatment applied to systems with weaker coupling regimes where the perturbation treatment is not justified. The improved accuracy which is obtained from the novel analytic approach is investigated in various scenarios such as phonon generation setup, quantum cooling and bad cavity limits. The changes and important features related to the observed quantum phenomena are presented.

In the **fourth Chapter** it is discussed the case when a particular type of artificial atom interacts with an optical resonator. An artificial atom made of a quantum-well which may be engineered as a three-level ladder-type emitter with equidistantly shifted energetic levels is considered. The particularity of this type of emitter consists in its interaction with the optical resonator, where both of its transitions are coupled to the cavity. As the optical resonator indistinguishably interacts with both atomic transitions in the good cavity limit, the interaction amplitudes may interfere with each other. The artificial atom is prepared in a superposition of states via two lasers each pumping a different transition. Consequently, the interaction amplitudes are also influenced by how the atom is prepared and the configuration of the pumping lasers may be used to tune the interference phenomena up to a completely destructive interference case. The laser pumping introduces another effect into the system, which consists in the energy splitting of the emitter's spectra where side-bands appear. Different possibilities of control and manipulation of the quantum interference phenomena are investigated by tuning the cavity in resonance with each of spectra peaks. Each case requires a particular adaptation of the analytic treatment applied to solve the system dynamics, which is presented and discussed.

In the **fifth Chapter** it is discussed the influence of the collective behaviour of multiple two-level artificial atoms interacting with a quantum mechanical resonator. The chapter considers a closely-spaced sample of quantum-dots which allows for superradiant dynamics to occur. The investigation is focused on two different approaches, one considering samples made from a few quantum-dots where a complete analytical solution is found for the system dynamics and a different approach considering large quantum-dot samples where several approximations may be applied in order to solve the system dynamics. The two approaches are complementary, where one approach allows for a analytic interpretation of the observed collective phenomena, while the other allows the investigation of the effect at larger scales. The atomic superradiance effects lead to several essential changes of the collective dynamics. Comparing to the case of separate individual emitters, the collective superradiance is characterized by faster decay dynamics with more intense fluorescence spectra peaks. The coupling to the mechanical motion is different than the coupling to electromagnetic field. Therefore, the changes in the collective dynamics of the quantum systems affects the mechanical vibrations differently than the optical counterpart. The investigation of the quantum statistics of the vibrational motion of the quantum mechanical resonator is presented and discussed.

1 NANOSCALE QUANTUM OPTICS

This thesis treats the fundamental problem of the interaction of an emitter with a quantum harmonic oscillator through the prism of quantum optics. One has chosen to use artificial atoms as emitters and explore the related features when comparing to real atoms. Various quantum phenomena have been theoretically observed when combining these features with either an optical or a mechanical resonator. This chapter gives an overview on modern nanoscale quantum optics and the phenomena related to the implementation of artificial atoms, in order to build a general picture which lead to the formulation of the problems treated in this thesis.

The chapter is organized as follows. In the introductory paragraph 1.1, one shortly describes how quantum optics have evaluated since the beginning to the modern days. In paragraph 1.2, one discusses various types of artificial atoms and their implementation into integrated cavity-quantum electrodynamic setups, with a particular attention given to quantum interference phenomena. In paragraph 1.3 one presents the treatment of modern micro- and nano-scale quantum optical devices from the point of view of optomechanics. In paragraph 1.4 one discusses how the interaction of the artificial atoms with the quantum mechanical vibrations influences the optical processes and vice versa. In this context, some particular quantum effects, which appear within the dynamics of the mechanical vibrations, are presented. The collective interaction of artificial atoms and the related phenomena is discussed in paragraph 1.5. A summary is given in paragraph 1.6.

1.1 Modern quantum optics from the beginning

The quantum optics studies various phenomena related to the granular aspect of light. The story of this realm of quantum physics starts at the beginning of the previous century with the blackbody radiation model introduced by Max Plank [25, 26], where the light emission was treated in discrete units of energy. Einstein went further with this topic and have stated the light wave-particle duality via the energy fluctuations of the blackbody radiation [27, 28], a few years later after his Nobel Price worth paper on the photoelectric effect [29] was published.

After a half-century research of quantum optics, another Nobel Price worth experimental realisation had been achieved by Gordon, Zeicer and Townes [30] based on the theoretical approach proposed by Basov and Prokhorov [31] on the microwave amplification by stimulated emission of radiation, i.e., the maser. A few years later the first experiment on light amplification by stimulated emission, i.e., laser, had been performed by Maiman [32], whereas the major theoretical background explaining the physics of coherent light processes including the statistical approach have been developed by Glauber [33], Mandel [34] et al..

The understanding of the phenomena related to the nature of light and the nature of its interaction with the matter are broadly required by most of the fundamental and many interdisciplinary research fields, as well as, by various industrial applications. Modern quantum optics are used to understand the surrounding universe from the macro-scale to molecular and sub-atomic scales, while its industrial application broad palette vary from heavy industry and communications to hi-tech appliances and gadgets. This broad gamut of research and applications requires a permanent innovation in the fundamental understanding of quantum optical processes.

One powerful domain of quantum optics focused on addressing the problems of its fundamentals is the cavity quantum electrodynamics. It was established by Purcell's investigations on the spontaneous emission behaviour, which led to the effect of enhancement of the emission rate of an atom when it is placed in a cavity [35]. The enhancement of the spontaneous emission rate was proportional to the quality factor of the cavity, when the cavity was tuned in resonance with the atomic transition. In empty space, the spontaneous emission appears due to atom interaction with the surrounding electromagnetic vacuum. The cavity electromagnetic field is different than the vacuum as it accepts only several frequencies. In contrast, the electromagnetic vacuum is made of a continuous spectra of frequencies. Therefore, the Purcell effect originates from the change in the density of modes of the electromagnetic field. The ratio of the spontaneous emission rates within the cavity and in free space is proportional to the ratio of the densities of modes, which is proportional to the cavity quality factor. Moreover, if the cavity is detuned from the atomic transition frequencies, an opposite effect occurs as out of resonance the cavity would not accept a photon of different frequency. This will lead to a decrease in the spontaneous emission rate. Pioneering experimental investigations on this effect were presented in [36] and later in [37]. In the following paragraph, one will discuss the importance of the Purcell effect in the context of cavity quantum electrodynamics with quantum-dots.

The realm of cavity quantum electrodynamics have evolved since theoretically and experimentally in identifying and describing the atom-field interaction. The experimental realisation of one-atom maser [38], i.e., micromaser, have added another dimension to this realm of research by introducing the strong atom-cavity coupling regimes. The theoretical description of strong-coupling cavity dynamics was given by Jaynes and Cummings [39], where the quantum interaction of a two-level atom with a single-mode cavity field was given. This model is used in following studies presented in this thesis and its detailed description is given in the next chapter. The strong-coupling dynamics has allowed the prediction and the experimental observation of many fundamental quantum optical phenomena, e.g., collapse and revival of Rabi oscillations [40] where the oscillation of the population of a two-level atom between its ground and excited states disappears and re-appears because of the granular aspect of the cavity electromagnetic field, sub-Poissonian photon statistics [41] which represent a pure quantum feature of the light that cannot be obtained from classical sources, single-atom effects [42], trapping states [43] where the atom is prepared in a specific superposition of states and cases when light prepared in a pure Fock photon state [44].

One issue of modern cavity quantum electrodynamics is the discrepancy between the theoretical and experimental progress, as the experimental possibilities in the state-of-the-art of the modern techniques and methods are limited if comparing to the permanently increasing requirements of the theoretical framework. Therefore, novel approaches in this realm of research are permanently investigated. An important actor in this investigation represents the use of artificial atoms, which brings several opportunities over the real-atom-cavity models. The possibility to engineer a single emitter permanently confined within the cavity allows one to reach larger cavity-emitter interaction times if comparing to atom trapping techniques. Moreover, it is possible to create artificial atoms adopted for a specific experimental requirement, such as the energetic levels of artificial atoms which are related at a certain degree to their design.

With more and more integration of quantum physics in modern technologies, new progress vectors appear such as quantum computation and quantum information treatment and transfer. The classical computers deal with the notion of bits, which can be associated in quantum physics with two-level state systems, also called qubits. Here, the photons are good candidates to substitute electrons in computational operations [4]. Many of cavity quantum electrodynamics features are brought in this new dimension, as photons in cavities are good candidates to create computational quantum simulators [45] or nodes of a quantum network [3].

The quantum communications are more focused on quantum cryptography processes [46] in order to ensure a secure treatment of information. The quantum information transfer studies focus on confining quantum entangled states over large distances. Recently, the world record of maintaining two quantum entangled photons was set over a distance of about 1400 km [1]. This remarkable result allowed to teleport the state of a qubit made of an independent single-photon from a ground observatory to a low-Earth-orbit satellite. The most remarkable in this kind of processes, is that the state of the qubit is instantaneously transferred at the moment when the entanglement is broken, i.e., the ”spooky action at a distance” as commented by Einstein.

In this context of novel quantum technologies, the field of integrated quantum photonics have been successfully developing during the last decades [47, 48]. This realm of quantum optics and condensed matter engineering techniques is driven by the requirement to build on-chip devices able to produce on demand various optical effects. With the possibility to build optical cavities of a few hundred nanometres in size, the semiconductor based artificial atoms present a major interest for a on-chip integration of a cavity quantum electrodynamic model within the strong coupling cavity-emitter regime [49].

Considering the tendencies of modern development of quantum optics, perspective candidates for further scientific investigations are the artificial atoms. Various related scientific research directions had been established during the last decades. Artificial atoms possess a discrete electronic structure similarly to real atoms. This allows various quantum optic effects which had been previously obtained with real atoms, to be produced by setups based on artificial atom. There are several important differences among real and artificial atoms from the point of view of quantum optics. Namely, one would highlight the following major features of artificial atoms, comparing to real atoms:

$\rightarrow$ on-chip integration of various quantum setups

$\rightarrow$ interaction with mechanical vibrations, i.e., the phonons

$\rightarrow$ the possibility to engineer different designs and architectures in order to tune the characteristics of the artificial atom, e.g., the transition frequency and the coupling strengths

$\rightarrow$ a few orders of magnitude higher coupling regimes with the optical cavity

$\rightarrow$ significantly higher operating temperatures

$\rightarrow$ additional control by applying a voltage

$\rightarrow$ the single-atom like experiments where large type of emitter-cavity interaction times may be achieved, i.e., no need to trap the atom.

While many other differences among real and artificial atoms may be considered either an advantage or a downside depending on the context, it is to note that artificial atoms have a major disadvantage in comparison with real atoms, which is the impossibility to engineer completely identical artificial atoms. Particularly, it affects the quantum collective effects which will be discussed later in this chapter, however the reproducibility of an investigated setup should be considered separately for each case.

In following paragraphs one will discuss various implementations of these features. In the next paragraph 1.2, one will discuss how artificial atoms are implemented in systems with optical resonators. One will discuss the current state-of-the-art in experimental realisation of various phenomena related to cavity quantum electrodynamics with this type of emitters.

In this context, a more focused description is made on the quantum interference phenomena. Various cavity quantum interference phenomena is obtained depending on the characteristics of the considered emitter, while artificial atoms may be engineered in order to fit some requirements such as degenerate transition frequencies in some particular case. In chapter 4 of this thesis one will show how these two particularities may be combined in order to obtain a quantum interference phenomena with a three-level artificial atom with degenerate transition frequencies when it is placed in an optical resonator.

In paragraph 1.3 one will discuss the impact of mechanical vibrations on cavity quantum electrodynamics. The treatment of modern micro-sized optical cavities converge to the realm of optomechanics situated at the frontier of quantum optics and condensed matter physics. Various approaches related to studies of the interaction of cavity fields and mechanical vibrations will be presented.

In paragraph 1.4 one will discuss how the coupling of artificial atoms with the mechanical vibrations adds another dimension to the optomechanical treatment. One will present the technological framework required for the implementation of artificial atoms in order to generate coherent or even sub-Poissonian phonon statistics. In chapter 3 of this thesis one will show how this effect is obtained when an artificial atom is placed in an acoustical cavity or on a nanomechanical resonator.

In paragraph 1.5 one will discuss how collective effects may be obtained with artificial atoms. Particularly, one will focus on Dicke type interactions which occur among closely spaced atoms. The possibility to obtain such type of interactions with artificial atoms will be presented. In chapter 5 of this thesis one will show how superradiant collective interaction of an ensemble of artificial atoms influences the dynamics of a quantum mechanical resonator.

1.2 Artificial atoms in optical systems

In this paragraph one will present the different artificial atom architectures which are among the most applied in modern quantum optics, such as:

$\rightarrow$ quantum-dots

$\rightarrow$ quantum-wells

$\rightarrow$ quantum-wires

$\rightarrow$ superconducting circuits

$\rightarrow$ nitrogen-vacancy centres in diamonds.

Further studies of this thesis will be focused on semiconductor based artificial atoms as quantum-dots and quantum-wells. Therefore, more detailed discussions on the artificial atom implementation in quantum optics will be related to this type of emitters.

The common aspects of real and artificial atoms, is that their electronic discrete energetic levels appear as a consequence of the electron confinement in space. The real atom electrons are confined via their natural attraction force to the positively charged protons localised in the centre of the atom.

In semiconductor based artificial atoms, the confinement is achieved when a semiconductor material with a smaller band gap is embedded on a material with a larger gap. As the electron is confined within the material with the smaller gap, the shape of the embedded crystal will define the properties of the artificial atom. Quantum-dots represent point-like crystals where the electron is confined in all three dimensions, a quantum-wire allows for a two-dimensional confinement within an one-dimensional crystal, the quantum-well represents a single dimensional electron confinement within a two-dimensional embedded layer. Only quantum-dots represent a discrete spectrum of energies, while the quantum-wires and quantum-wells energy levels refers to the formation of mini-bands within their spectra.

The difference in materials in nitrogen-vacancy centres in diamonds is created by an impurity made of a nitrogen atom which substitutes a vacancy of a missing carbon atom in the diamond lattice [50]. Similarly to quantum-dots, they allow a three-dimensional confinement and have a discrete energy spectrum. However, this type of artificial atoms have different properties due to their size of a single atom, comparing to the size of quantum-dots which are made at different scales varying from a few hundred atoms to tens of thousands. This difference is expressed in their optical and optomechanical properties.

The superconducting circuits have various architectures [51], but they all are based on an RLC superconducting circuit which implements Josephson junctions [52]. This allows one to include a non-linear element into the quantum harmonic behaviour of the circuits. As within the superconducting regime the circuit resistance vanishes, the dynamics is reduced to a LC circuit case. Due to the quantum harmonic behaviour of LC circuits, their infinite energetic levels are degenerated. The inclusion of a non-linearity, i.e., a Josephson junction, allows one to break the degeneracy of energetic levels. As the energy levels are not equally distributed anymore, one is able to select some particular levels, such as the first two levels in order to form a qubit.

The implementation of a specific type of artificial atom into an optical system may be determined by some experimental limitations [53]. Superconducting circuits are mostly operable in microwave frequencies, whereas quantum-dots transitions are more suited to optical frequencies. The temperature conditions for coherent manipulations vary significantly for each particular type of emitter. Real atoms are operated at temperatures varying from nanokelvins to microkelvins. Ions require better conditions within the scale of millikelvins. Superconducting circuits are operated within similar conditions of millikelvins. Quantum optical experiments with quantum-dots are manipulated at significantly higher temperatures of a few kelvins. A remarkable feature of the nitrogen-vacancy centres in diamonds is that they are operable at room temperatures.

Another differentiation among various types of artificial atoms is their characteristic sizes [53]. Superconducting circuits dimensions are of order of micrometres, while quantum-dots dimensions are significantly smaller of order of a few nanometres. Another important feature is the interatomic distance, which is important for two-emitter or collective phenomena. Quantum-dots may be spaced at distances of tens of nanometres, while superconducting circuits are spaced at micrometre distances.

It is to note that experimental challenges in using a particular type of artificial atoms are related to many more characteristics e.g., the phonon assisted quantum optical effects when the artificial atom couples to mechanical vibrations, the possibility of additional control via magnetic or electric fields or via an applied voltage, dephasing processes and many more. Although all these challenges, remarkable on-chip realisation of various cavity quantum electrodynamics experiments have been implemented with quantum-dots [49] and superconducting circuits [6]. For example, an on-chip realisation of a superconducting circuit interacting with a microwave waveguide optical cavity is presented in Fig.1.1.

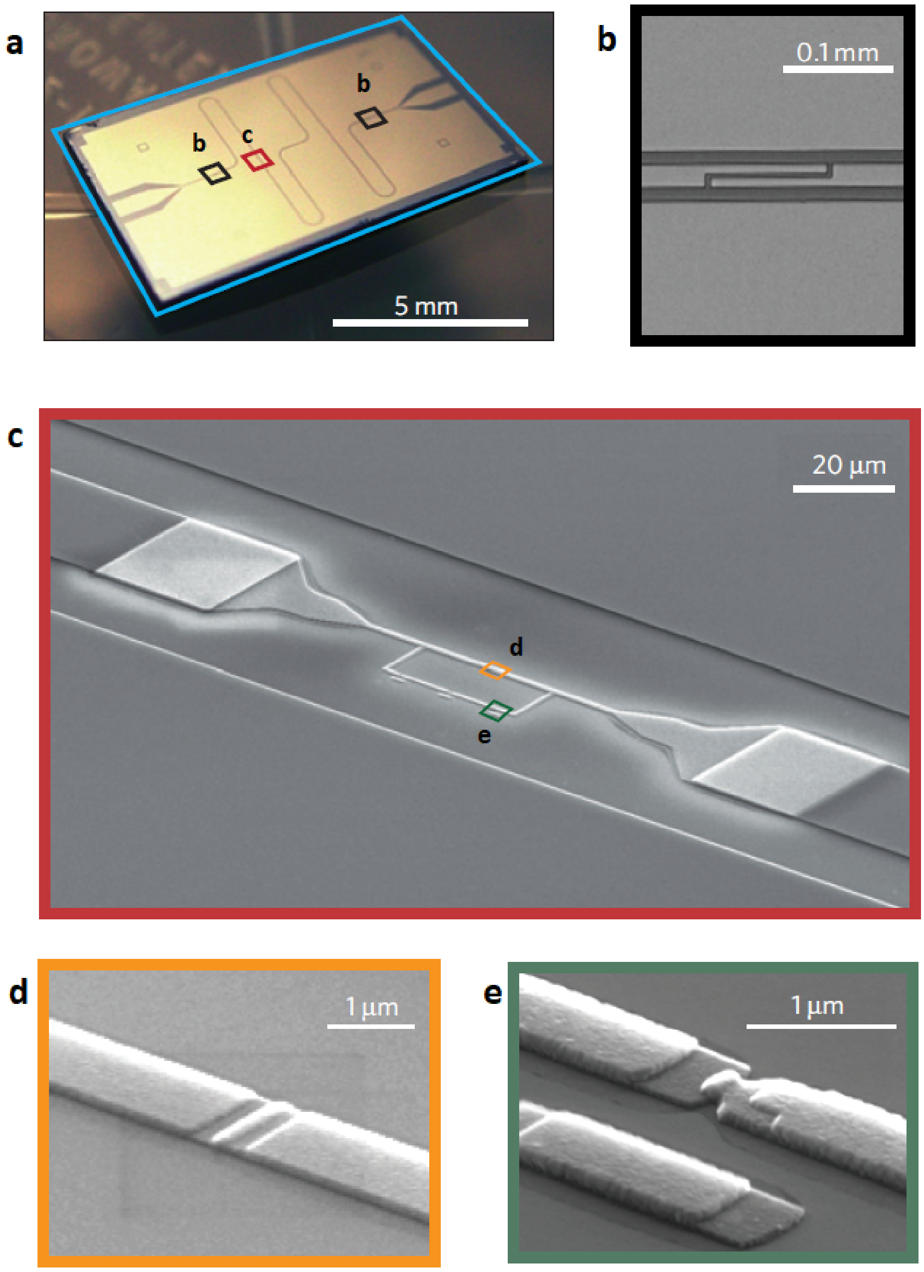

Fig. 1.1: **a.** An on-chip realisation of a superconducting circuit interacting with a microwave optical resonator; **b.** interdigital coupling capacitors defining the edges of the optical waveguide resonator; **c.** the superconducting flux qubit; **d,e.** various Josephson junctions. The figure is taken from [54].

In what follows, one will focus on semiconductor based artificial atoms such as quantum-dots. Their fabrication techniques have rapidly advanced during the last two decades and nowadays many fundamental quantum optic effects have been experimentally observed. Among the most wide-spread types of quantum-dots one will highlight here the colloidal quantum-dots and the epitaxially grown quantum-dots.

The colloidal quantum-dot nanocrystals are formed in chemical solutions. The manipulation of their growth kinetics allows a good control degree of their shape and size. Scales of a few nanometres may be achieved in size for quantum-dots composed of a few hundreds of atoms, while their shape may be controlled to obtain architectures such as dot-in-rods or tetrapods. This kind of emitters have shown good potential for single-photon sources. Strong photon anti-bunching effect have been observed in the fluorescence of single colloidal CdSe/ZnS quantum-dot [55]. Moreover, similar effect have been found for a cavity quantum electrodynamics setup operated at room temperature, made of a single colloidal CdSe/ZnS quantum-dot placed in a vertical microcavity [56]. The possibility of operating the setup at room temperature suggests a good candidate of single-photon source for technological purposes.

An even more widespread type of quantum-dots for quantum optic experiments are the self-assembled quantum-dots. Their synthesis is based on molecular beam epitaxy growth, where small crystals are formed due to the relaxation of the strain which appears from the difference in the lattice constants of the two materials. For example, many optic experiments are implementing InAs/GaAs self-assembled quantum-dots obtained via the Stranski-Krastanov self-organized growth [57]. The strained InAs lattice form small nanocrystals shaped as flat lenses deposed on the GaAs substrate. They are made a few nanometres in heigh and a few tenths of nanometres in diameter. The InAs material has a smaller bandgap among the valence and conduction bands, if compared to the GaAs substrate, which allows one to spatially confine the exciton formed within the quantum-dot. The formation of the exciton may be obtained under optical or electrical pumping, both pumping methods being experimentally available for this type of quantum-dots. When operated at cryostat temperatures of a few kelvins, these type of artificial atoms have narrow emission lines. This makes them suitable candidates for experiments based on cavity quantum electrodynamics effects.

When implementing this type of artificial atoms into cavity quantum electrodynamics setups, several major experimental challenges arise. An important challenge appears from the quantum-dot architecture as it is deposed on a substrate. Thus, the light emitted from the quantum-dot may be trapped in the substrate surrounding it. This challenge becomes more prominent when weak cavity fields are considered. Different techniques based either on using quantum optics effects or by engineering the spatial cavity modes are applied to address the issue [58].

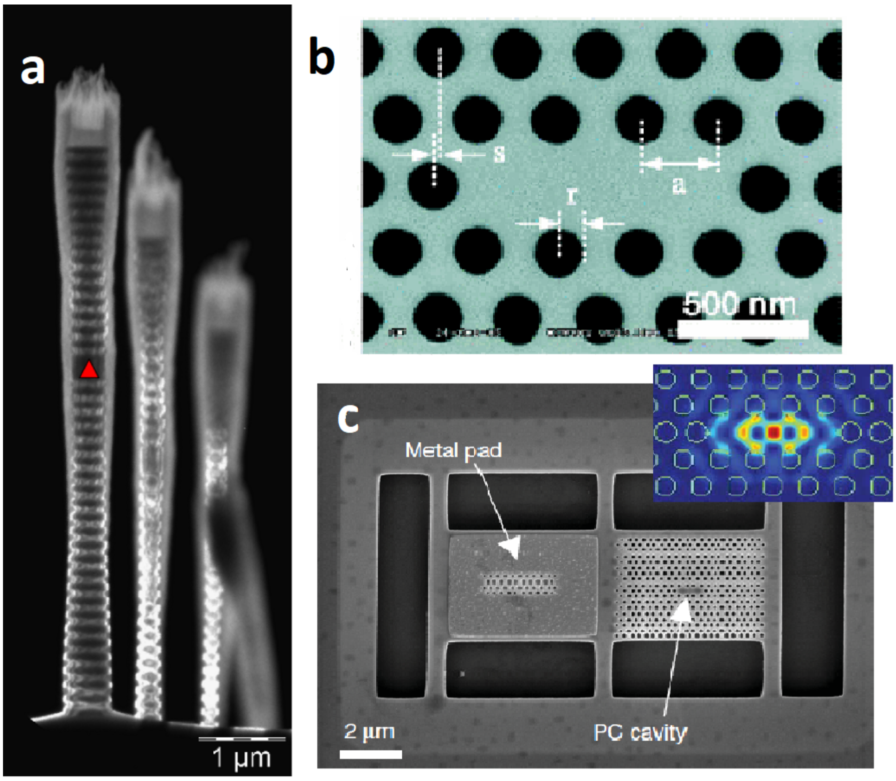

Fig. 1.2: **a.** A pillar microcavity with a quantum-dot inside. The position of the quantum-dot is represented as a red triangle. The figure is taken from [6].; **b., c.** Photonic crystal cavities with embedded quantum-dots. The figures are taken from [60, 61], respectively.

For technological applicability of quantum optic effects, micro- or nano-scale optical cavities are considered. A particular interest is focused on pillar microcavities [59] and photonic crystal cavities [60, 61] as this type of optical cavities can be engineered with an embedded quantum-dot inside, as presented in Fig.1.2. Considering the ensemble of engineering limitations, additional experimental challenges related to the Purcell effect appear. As previously mentioned, different frequency tuning of the atom-cavity defines how the emitter will emit. One may achieve suppression or enhancement of photon spontaneous emission in the cavity depending on the fine tuning of the engineered quantum-dot-microcavity setup.

Various techniques are applied in order to tune either the cavity or the quantum-dot frequencies. The nanocavity frequency may be tuned by varying its refractive index via a photodarkening effect. It is achieved when deposing a thin chalcogenide glass layer on the top of the cavity [62]. Another method of fine tuning is achieved by deposing nitrogen or xenon gas condensate onto the cavity at kelvin temperature [63]. Both methods have reported a shift of a few nanometres in the wavelength of the photonic crystal nanocavity. The quantum-dot can be tuned by shifting its transition frequency when applying a magnetic or an electric field. Correspondingly, the Zeeman shift [64] and the Stark shift [65] effects have been successfully observed in self-assembled quantum-dots.

More experimental challenges appear when an optical pump is introduced. For example, the observation of the Mollow triplet is possible when a two-level emitter is resonantly pumped with an intense laser. Under the pumping effect, the fluorescence spectra of the emitter is described by a central peak centred at the emitter transition frequency and two side-bands equally shifted in both directions from the central peak. The distance between the side-bands and the central peak is related to the intensity of the applied laser. Note that the corresponding theoretical framework will be presented in the next chapter.

The experimental observation of this effect had had to address a major problem of eliminating the scattered laser light from the quantum-dot emission light, as the laser is in resonance with the quantum-dot transition. It had been achieved via the polarization and spectral selection [66] or by engineering an integrated cavity-quantum-dot setup with orthogonal excitation and emission directions [67].

All the previously presented remarkable achievements in quantum optics setups based on quantum-dots and the corresponding experimental breakthroughs have allowed for further observation of more complex fundamental quantum effects. The photon blockade effect have been successfully observed for a quantum-dot put inside a photonic crystal nanocavity [68]. The photon blockade phenomenon appears when a first photon is emitter in a cavity. The single-photon-cavity system has a different resonance frequency than the empty cavity. Therefore, the probability of emitting a second photon at the cavity frequency is significantly decreased due to this difference, resulting in the so called blockade of emitting the second photon. The possibility to create the experimental setup on a chip, makes it a good candidate for a single-photon transistor.

The first experimental realisation of quantum teleportation using single quantum-dots have been reported in [69]. Two independently generated indistinguishable photons had been prepared in a polarization entangled state by sending the photons on two different arms of an interferometer. With an observed fidelity of 80%, quantum-dots are making good opportunities for technological applications in the realm of quantum teleporting and communications. Another method of preparation of entangled photons have been reported in [70], where time-bin entangled photons have been observed out of a biexciton cascade from a resonantly excited quantum-dot.

Progress for technological applications of quantum optics with artificial atoms have been achieved in various major developing challenges. On-chip realisation of a quantum-dot-based setup able to emit, guide and detect a few-photon electromagnetic field have been reported in [71]. A cryptographic key had been successfully distributed over a distance of 35 km of optic fibre using single-photons from quantum-dot-microcavity system [72]. An optic two-qubit logic gate based on indistinguishable photons emitted from a self-assembled quantum-dot in an optical pillar microcavity have been achieved in [73]. As the setup is realized from semiconductor based components, it suggests a future development for scalable optical quantum computing devices.

A particular phenomenon investigated in this thesis is the quantum interference. Quantum interference effects involving various atomic transition amplitudes have been intensively investigated recently [74, 75, 76]. It originates from indistinguishability of the corresponding transition pathways. As a consequence, quenching of spontaneous emission occurs due to quantum interference effects between decaying pathways which are dependent on mutual orientation of corresponding transition dipoles [77, 78, 79]. Laser- or phase-control of spontaneous emission processes were demonstrated there. Also, quantum interference effects lead to very narrow spectral lines in the spontaneous emission spectrum of pumped molecular, semiconductor or highly charged ion systems [80, 81]. Furthermore, such spontaneously generated coherences in a large ensemble of nuclei operating in x-ray regime and resonantly coupled to a common cavity environment were experimentally demonstrated in [82].

Previously it was shown that multi-level atoms interacting with the vacuum of a preselected cavity mode, in the bad-cavity limit, exhibit cavity induced quantum interference which is similar to the spontaneously generated coherences due to parallel transition dipoles [83, 84]. Quantum interference effects in an ensemble of ^{229}Th nuclei interacting with coherent light were demonstrated too, in [85]. Destructive or constructive interference effects were observed even in a strongly pumped few-level quantum- dot sample [86, 87]. Protection of bipartite entanglement [88] or continuous variable entanglement [89] via quantum interferences were shown to occur as well. Finally, electromagnetic induced transparency is an another phenomenon of quantum destructive interference which makes a resonant opaque medium highly transparent and dispersive within a narrow spectral band [90].

A powerful tool in the control and manipulation of interference effects originates from an additional degree of freedom of the system given by its phase dependence. For example, quantum interference effects influence the collective fluorescence of a driven sample of emitters, which becomes sensitive to phase dependence. Thus, the phase difference of the two lasers pumping a collection of three-level emitters may decrease and cancel its fluorescence when quantum interferences appear from a coherently driven source [91]. The superfluorescent behaviour of a sample of four-level emitters is modified by the vacuum induced quantum interferences and may be enhanced by varying the phase difference of the pumping lasers [92]. Moreover, for a well-chosen phase the sample may be trapped in its excited state and thus decoupled from the surrounding environment.

The phase dependent complete or partial cancellation of the spontaneous emission is reached when a single four-level emitter is considered [93]. The spontaneous emission properties may also be controlled via the phase difference of the pumping laser and a squeezed surrounding reservoir for a three-level ladder-type emitter [94]. In a different scenario, phase dependent systems may be used to study the phase itself, e. g. , the carrier-envelope phase of a few-cycle laser pulse may be determined via the behaviour of the populations of a qubit system [95].

A more challenging goal has been the realization of quantum effects in systems made of artificial atoms such as quantum-wells, as these systems possess additional degrees of freedom, which leads to stronger decoherent phenomena [96]. The particular interest in this type of artificial atoms for the current realm is the possibility to tailor their energetic states via the layer thicknesses and materials used for the quantum-well [97]. Quantum interference phenomena as gain without inversion have been experimentally obtained for pumped three-level ladder-type coupled triple wells [98], while electromagnetically induced transparency has been observed in three-level quantum-well systems with Λ-type transitions [99] as well as ladder-type intersubband transitions [100, 101].

A direct detection of ac Stark splitting, i.e. , dressed-state splitting, has been experimentally achieved in [100] for Ξ-type quantum-wells. This type of quantum-well is particularly interesting as it may be engineered as an equidistant three-level emitter [96, 97], an emitter difficult to implement with real atoms. A quantum switch based on a quantum interference scheme composed of a Ξ-type quantum-well with equidistant energetic levels had been suggested in [102, 103].

1.3 From optical to optomechanical systems

Shortly after the firsts remarkable achievements in cavity quantum electrodynamics investigations described in the previous sections, the realm of optomechanics emerged. First predicted by Maxwell, the electromagnetic radiation force had been experimentally observed for more than a century ago [104]. It appears when the matter is irradiated by a beam of light and one of the first investigations in optomechanics have been questioning what would happen if one of the cavity mirrors would be engineered in order to be able to move under the action of this force. A large variety of modern optomechanical devices have been developed since, many of which are presented in Fig.1.3. In what follows, one will discuss different experimental and engineering approaches in optomechanics, in order to highlight how it combines with the previously discussed realm of cavity quantum electrodynamics.

Although the model of an optical cavity with a vibrating mirror have been intensely investigated for half of century, it still presents a major interest for modern research. Various setups have been implemented at different scales, from micrometre size mirrors suspended on various types of micromechanical resonators to massive mirrors of tens of kilograms in mass.

At macro-scale, a tremendous research have been done to stabilise the mechanical motion of the large mirrors of the LIGO (Laser Interferometer Gravitational Wave Observatory) interferometer. With each mirror weighing about ten kilograms, one was able to cool down the mirrors up to an effective temperature of $1.4\mu K$, which corresponds to a phonon occupation number value of ~ 200 [105].

Similarly to the realm of cavity quantum electrodynamics, the optomechanical setups have evolved in order to reduce their sizes, with micro-mirrors currently reaching the scale of tens of micrometres in size. There are various techniques to either couple a micrometre mirror to a micromechanical resonator such as an AFM cantilever [106] or to fabricate a mechanical resonator which would substitute the classical mirror, e.g., a mirror made from a doubly-clamped monocrystalline resonator made from an epitaxial AlGaAs Bragg-type reflector [107] or a mirror made from micro-optomechanical trampoline resonator composed of a SiO_2/Ta_2O_5 dielectric reflective thin layer deposed on a silicon nitride resonator [108]. The last two types of devices are presented in Fig.1.3.b and Fig.1.3.d, respectively.

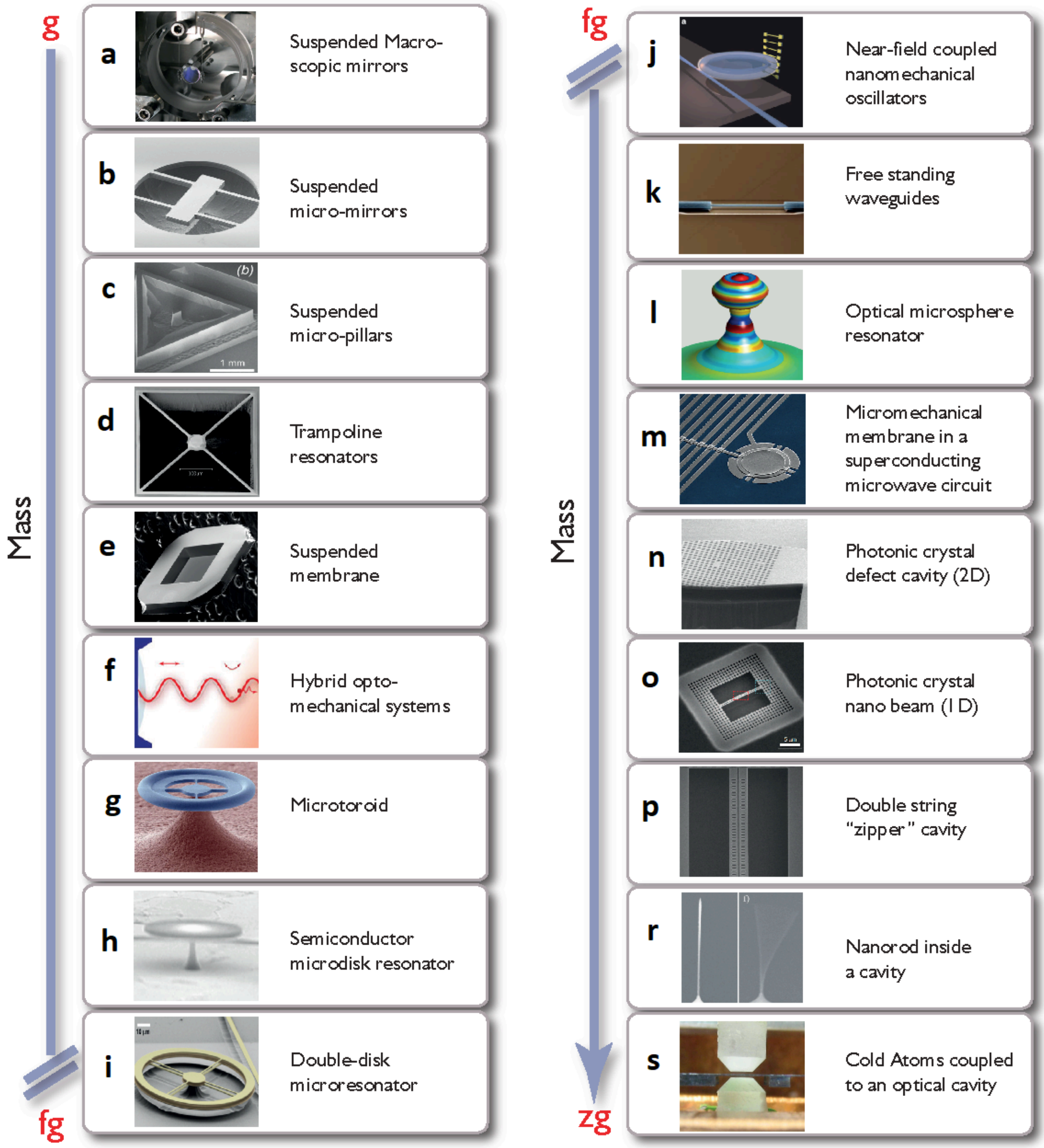

Fig. 1.3: Various types of optomechanical devices. The figure is taken from [8].

Instead of considering an optical cavity where a mirror vibrates, a different approach in optomechanics consists in considering a rigid cavity with a mechanical resonator inside. In this type of systems, the optical and the mechanical components are distinct objects. The major advantage is the possibility to focus more on the mechanical part of the system without being limited by the design of the optical cavity. Namely, one is able to consider smaller and lighter mechanical resonators with diverse optomechanical properties, as well as resonators that allow artificial atoms to be embedded.

One may differentiate the various mechanical resonators in two categories: nanomechanical resonators and membranes. The nanomechanical resonators represent an one-dimensional object, i.e., the length is significantly higher than the dimensions of its cross-section. It can be singly or double-clamped, i.e., it may have one or both ends fixed to a substrate. Various resonance frequencies and quality factors can be obtained by varying the length, the shape of the cross-section or the material of the nanomechanical resonator.

An optomechanical setup made of a singly clamped carbon-based nanorod inserted in a fibre-based optical cavity have been reported in [109]. The nanorods are grown on a AFM cantilever via electron-beam deposition and measure a few micrometres in length and about a hundred nanometres in diameter as shown in Fig.1.3.r. At room temperature, they oscillate at a resonance frequency in the range of a few MHz with a low quality factor of order of hundreds. Similar quality factors at room temperatures, but significantly different dimension ratios can be achieved with nanomechanical resonators made from suspended carbon nanotubes [110]. The resonator consists of a bundle of a few carbon nanotubes, a few tens of micrometres in length and less than ten nanometres in diameter, which resonantly vibrates at a frequency of about 500 kHz. A significant increase of the mechanical quality factor up to orders of $10^5 - 10^6$, is observed at room temperature for high stress silicone nitride nanomechanical resonators [111]. The resonator is similar in size to nanorods, but has a doubly-clamped geometry and a resonance frequency of 580KHz. Moreover, nanomechanical resonators with tunable resonance frequency up to few GHz of magnitude and high quality factors of order $\sim 10^4$ are obtained from stressed doubly-clamped carbon nanotubes operated at cryogenic temperatures [112].

The second type of mechanical resonators that can be inserted in an optical cavity are thin membranes which represent a two-dimensional object with a micrometre sized cross-section and under a hundred nanometres width. An example of a suspended membrane is shown in Fig.1.3.e. The main difference between membranes and nanomechanical resonators are defined by their mass, size and geometry which defines different mechanical resonance frequency ranges and optomechanical couplings. However, a more important difference is related to the flat shape of the membrane that scatters the light in a defined direction which may be controlled in order to reach stable cavity modes. The considerably larger overall sizes of the membranes, when comparing to one-dimensional resonators, influences the cavity modes as the membrane changes the effective refractive index of the cavity. Besides the changes of the cavity mode induced by the static membrane, the mechanical vibration of the membrane may perturb and mix the cavity modes.

Successful experimental realisations of optomechanical setups consisting of membranes placed in optical cavities have been recently reported. A mechanical resonance frequency of 261kHz and a high mechanical quality factor of order of $\sim 10^6$ have been observed at cryogenic temperatures for a high-stress stoichiometric Si_3N_4 membrane interacting with an optical cavity of frequency of 1064 nm [113]. A fibre-based optical cavity interacting with an inserted silicon nitride membrane had been investigated in [114], where a fundamental mechanical frequency of 1.74 MHz and a quality factor of order of $\sim 10^4$ had been reported.

Although the optomechanics had initially derived from the domain of cavity quantum electrodynamics, the two realms have inevitably meet again due to technological progress in engineering small optical setups at micrometre scales for on-chip applications. The experimental treatment of modern cavity quantum electrodynamics based on micro-scale optical cavities [59, 60] cannot be realistically applied without considering the intrinsic optomechanical effects which become prominent at this size scales. Moreover, the optomechanical coupling of this kind of systems can be manipulated in various ways in order to influence either the optical or the quantum mechanical effects.

A good example of combining a photonic crystal cavity with a mechanical resonator is the case of photonic crystal nanobeams. Such a device is presented in Fig.1.3.o. Similarly to the geometry of a nanomechanical resonators, a photonic crystal cavity had been shaped as a beam, i.e., with its length a few order of magnitude longer than its width and height. The architecture of the crystal cavity allows one to confine not only optical modes, but also mechanical modes. The resulting optomechanical device allows an additional control of the co-localized optical and mechanical modes, if comparing to simple photonic crystal cavities where bulk phonon modes are considered. Even better confinement of mechanical modes are obtained by engineering the photonic crystal nanobeam into a phononic shield [115]. In this experiment, one was able to confine an optical mode resonance at a wavelength of 1544.8 nm and a mecahnical mode resonance at a frequency of 5.1GHz. At a cryogenic temperature about ten Kelvins, the phonon mode quality factor of the device was of order of 10^6, which is two order of magnitude higher than the quality factors of unshielded photonic crystal nanobeams.

Another example of obtaining co-localized optical and mechanical modes are the whispering-gallery-mode microresonators. Various architectures of this type of optomechanical devices such as microtoroids [116], microdisk resonators [117] and optical microsphere resonators [118] are presented in Fig.1.3.g, Fig.1.3.h and Fig.1.3.l, respectively. The optical properties of whispering-gallery-mode cavities allow exceptional high photon lifetimes to be obtained, reaching quality factor values up to 10^9 order. The possibility to fabricate such resonators at micro-scale sizes make them good candidates for optomechanical purposes. Moreover, the radial symmetry leads to strong optomechanical coupling if comparing to previously described devices, as well as good mechanical quality factor values of order of hundreds or even higher depending on particular type of resonator geometry.

A particular interest for potential devices based on artificial atoms are the microdisk resonators made from semiconductor material, shown in Fig.1.3.h. Engineered a few micrometres in diameter and a few hundreds of nanometres in width, they show good perspective for on-chip fabrication purposes. An optomechanical GaAs disk resonator with high mechanical and optical quality factors had been recently reported in [117]. A mechanical quality factor of order of 10^3 at room temperature and 10^4 under vacuum and cryogenic conditions had been achieved for the fundamental breathing mode of frequency of 1.37 GHz.

Although the presented optomechanical devices have led to various technological and scientific breakthroughs [8, 119, 120] far beyond the description given in this section, they all have a severe physical limitation, which is the weak coupling of the electromagnetic field with the mechanical motion via the radiation force. Going beyond this limitation, would reveal even more optical and optomechanical effects. Adding artificial atoms into the previously discussed optomechanical devices would address this issue, while giving new degrees of freedom of control and manipulation to the optomechanical setups.

1.4 Artificial atoms in optomechanical systems

A new dimension of research in optomechanics is related to the insertion of various artificial atoms into optomechanical devices. A mature technological framework have been developed in engineering semiconductor artificial atoms and superconducting qubits into optomechanical setups and firsts experimental achievements had been already reported during the past decade. Various concepts on how artificial atoms can be implemented are presented in Fig.1.4 and will be discussed further.

A key particularity in phenomena related to optomechanical systems based on artificial atoms is the strong effective optomechanical coupling which can be achieved. This introduces a new perspective in the coherent control of quantum mechanical motion of matter, as well as a new degree of manipulation of quantum optical processes. While each type of artificial atom couples in its own way to a mechanical system, a different theoretical framework is required for each case. However, the overall dynamics of this interaction is similar, which allows one to compare the various systems from the point of view of the effective optomechanical coupling that can be achieved [9].

Superconducting circuits may couple with a mechanical resonator in different ways depending on their type. In Fig.1.4.a, a superconducting circuit qubit made of a Cooper pair confined on a small superconducting island interacts with a vibrating gate electrode. An strong effective coupling in range of $5 - 50$ MHz is achieved for such configuration [121]. In Fig.1.4.b, a flux superconducting qubit formed by the direction of the current circulating within a loop is interacting with the mechanical vibrations of the loop via the Lorentz force created by an applied magnetic field. An optomechanical coupling strength in the range of $0.1 - 1$ MHz have been observed in [122].

Qubits associated with electronic or nuclear spin states such as quantum-dots or defect centres may interact with the vibrations of a magnetized nanomechanical resonator tip as shown in Fig.1.4.c. An effective coupling constant value in the range of $10 - 100$ kHz have been reported for a spin qubit made of a nitrogen-vacancy centre in diamond [123].

In Fig.1.4.d a qubit made from a quantum-dot or a defect centre is embedded on a nanomechanical resonator and couples to the mechanical vibration through the deformations which appear from the flexural motion of the resonator. The intrinsic coupling of the quantum-dot with the nanomechanical resonator is different from the previous optomechanical coupling schemes which require an external applied field. In the case of a quantum-dot coupled to a double-clamped semiconductor beam resonator, an optomechanical coupling value of the order of $1 - 10$ MHz is expected [124]. One of the firsts experimental reports have observed a coupling strength of 450 kHz, for a singly-

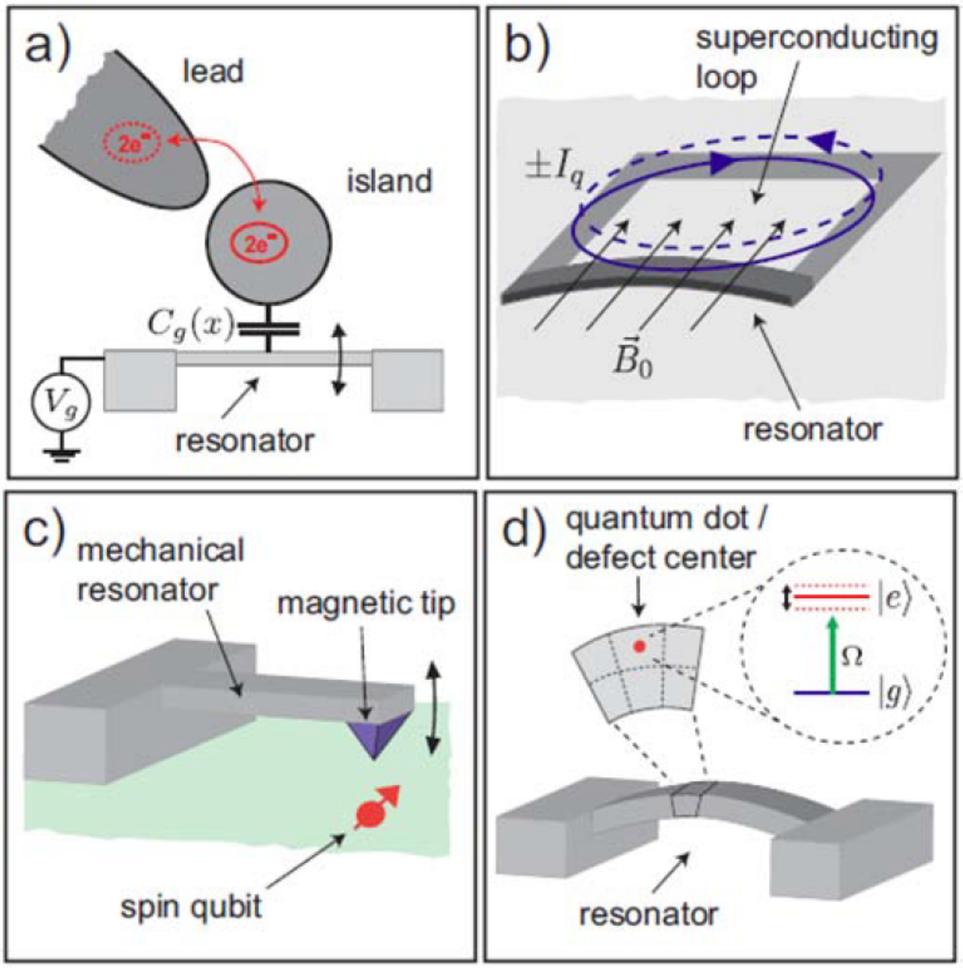

Fig. 1.4: Schematic representations of the interaction of different artificial atoms with quantum mechanical resonators. Namely: **a)** a superconducting circuit qubit made of a Cooper pair; **b)** a flux superconducting qubit; **c)** a spin qubit; **d)** a quantum-dot or a defect centre. The figure is taken from [9].

clamped cone-shaped nanowire oscillating at a mechanical frequency of 530 kHz with a quality factor of the order of 10^3 [125].

The strong interaction strengths which appear from the intrinsic coupling of quantum-dots with the phonon environment may significantly influence some quantum optical phenomena. For example, broader spectral lines and asymmetrical Mollow triplet side-peaks had been observed for a coherently pumped quantum-dot [11], while a decrease in the side-band splitting with increasing temperature of the quantum-dot had been observed in [126]. The population inversion of a pumped quantum-dot occurs due to its coupling to the surrounding mechanical vibrations [12]. A significant enhancement of the entanglement a pair of pumped quantum-dots coupled to a phonon reservoir have been suggested in [13].

Strong optomechanical coupling strength effects works in both directions. Not only the optical processes are influenced by the mechanical vibration, but the mechanical motion may be controlled and manipulated by optical influence. This opens important opportunities in various quantum cooling techniques as well as in the preparation of pure quantum states of mechanical motion via a coherent control of phonon generation. These aspects of optomechanical phenomena will be discussed further.

Various techniques have been used to cool down the matter close to its ground vibrational state. First related experimental achievements were obtained on single atoms using two-level sideband cooling [127] and resolved-sideband Raman cooling [128] techniques. The last technique was further expanded to cool a collection of atoms trapped in a two-dimensional optical lattice [129]. Since then, various techniques had been theoretically suggested and experimentally applied, in order to diversify and enhance the quantum cooling mechanism in different ways. Thus, cooling schemes using quantum optical effects as electromagnetically induced transparency for multiple multilevel trapped atoms [130] have shown a good applicability. The use of quantum interferences for laser cooling has been further extrapolated for the nonresolved-sideband regimes [131]. The process of two-photon cooling have allowed distinguishing different matter states of a nonlinearly coupled qubit-resonator system [132]. Furthermore, more exotic schemes were proposed to give additional control to quantum cooling processes as well as to cool the matter at larger scales. For example, cooling at laser-qubit resonance can be obtained in a photonic-crystal environment [133]. Faster cooling dynamics may be achieved via quantum interferences within a two-mode cavity with a movable mirror [134] or via the collective effects of a collection of coupled qubits interacting with a superconducting circuit [135].

A big step forward for the state-of-the-art in the quantum control of the matter at mesoscopic scales had been reported for cooling experiments which involves nanomechanical resonators [7, 136]. Remarkably, near-ground state cooling of the fundamental mechanical mode had been achieved. The addition of a quantum-dot to a setup based on a nanomechanical resonator would allow even stronger cooling effects to occur [137]. Moreover, for this kind of optomechanical setup, strong correlations of the electromagnetic and quantum mechanical vibrations had been predicted in [10].

Earlier experiments in laser generation of coherent phonons in different bulk materials [138, 139, 140] were succeeded by new optomechanical and electromechanical setups, achieving important experimental results in the acoustical analog of the optical laser by using piezoelectrically excited electromechanical resonators [15] and laser driven compound microcavities [16] or trapped ions [17]. In the meantime, theoretical models propose improvements in the background theory of the experiments like the PT-symmetry approach [141] and two cavity optomechanics [142], as well as new possible setups using vibrating membranes [142, 143], quantum-dots embedded in semiconductor optomechanical resonators [18, 19, 20] and Bose-Einstein condensate under the action of magnetic cantilever [144].

Pure quantum behaviour of the mechanical motion such as phonon antibunching [20], squeezing [145, 146] and negative Wigner function of phonon states [21] had been reported. Sub-Poissonian statistics of vibrational states is another pure quantum property. The domain of this statistics starts at the limit of a classical coherent state having a Poissonian distributed quanta and may end up with a pure Fock state at the other limit. Studies on the quanta statistics had already revealed many pure quantum features for different physical systems and remarkable results were achieved in a large spectrum of photonic quantum electrodynamics's applications [41, 147] as well as in Bose-Einstein condensate's physics [148, 149]. As for optomechanics, sub-Poissonian distributed phonon fields have been already predicted in setups based on vibrating mirrors [145, 22] and in single-electron transistors [150]. Within strong optomechanical coupling regimes, sub-Poissonian statistic may also occur for quantum-dots embedded on a nanomechanical resonator or multi-layered acoustical cavities [151].

1.5 Collective effects with artificial atoms

Two-atom quantum systems are one of the most trivial models for the study of collective effects and have an important role in the theoretical and experimental research of quantum optical effects such as quantum interferences, atomic entanglement and superradiance. Quantum interferences had been observed for two photodissocciated atoms of a Ca_2 molecule where a single photon is shared among the atoms [152]. A two-atom-cavity interferometer was first built in analogy with the Young's interferometer, where each trapped atom acts as slit and the interference occurs due to indistinguishable pathways of the atoms-field interaction [153]. Depending on the superposition of the pathways, this type of interferences shows cavity-induced saturation of the resonance fluorescence spectra or photon bunching effect [154]. One of the basic model of quantum atomic entanglement effects is the two-atom system either placed in a cavity [155] or interacting with the surrounding vacuum field [156].

The observation of the Rydberg blockade regime between two neutral atoms was reported in [157, 158], which is a crucial prerequisite towards the creation and control of atomic entanglement. The dipole-dipole interaction may also be manipulated when the environmental vacuum field is considered in the case of two three-level Λ-type atoms, where the surrounding reservoir induces the coupling of orthogonal transitions. Therefore, the spatial orientation of these atoms determines the steady-state dynamics of the system [159]. The coherent trapping effect is influenced as well by the dipole-dipole interaction of the two two-level atoms trapped in a cavity [160].

First discovered by Dicke [161], the phenomenon of superradiance can be understood as a collective giant dipole resulting from an ensemble of closely packed emitters. As a result, the spontaneous emission dynamics is modified, leading to a reduced radiative lifetime as well as an enhanced emission intensity proportional to the square of the number of excited emitters. Two-atom systems may be considered as the edge for collective effects. Superradiance and subradiance was first observed in the spontaneous emission variation for two trapped Ba138+ ions [162]. Non-decaying atomic collective states were predicted for two-atom systems prepared in a subradiant state [163].

Interestingly, the speed up of the spontaneous decay also occurs for single-photon excitations [164], *i.e.*, when only a single emitter of the atomic sample is excited. From early experiments with driven gases [165], superradiance has been investigated intensely in various theoretical and experimental approaches [166, 167, 168, 169, 170]. Since then, remarkable results have been achieved and superradiance was observed in molecular aggregates [171] and crystals [172], as well as in

Bose-Einstein condensates where Dicke phase transition occurs [173].

As previously mentioned, artificial atoms have a major a disadvantage in comparison with real atom as they cannot be engineered to be completely identical. This issue creates a severe technological challenge when it comes to collective processes. Remarkably, two-photon interferences have been observed in a setup based on two separate quantum-dots [23] which requires a high degree of resemblance among the two qubits. Another important goal was achieved in the realm of condensed matter physics, where superradiance was observed within a collection of quantum-dots [24].

In the realm of optomechanics, significant results have been achieved for collective effects in condensed matter physics [170]. Particularly, superradiance was observed in a collection of artificial atoms as quantum-dots [24]. Moreover, phonon superradiance effects were predicted for molecular nanomagnets [174] and nanomechanical resonators as vibrating membranes [175], while subradiance with phonons was reported for a system using coupled quantum-dots, in analogy with the subradiant photon effect for a two-ion system [176]. Single-photon superradiance has been reported recently for artificial atomic samples [177], whereas an analytical framework for the engineering of single-photon superradiance in extended media was developed in [178]. quantum-wells allow for even more exotic superradiant behaviour as their excited states, i.e., the excitons, are created in a two-dimensional layer [170], which is different from the quantum-dot case where excitons are well localized in space.

1.6 Conclusions to Chapter 1

Modern quantum optics progresses towards the fields of quantum communications and quantum computing. Among various technological concepts related to these fields, a strong requirement arises in engineering small optical devices at micro- and nano-scales. Photon emitters made of artificial atoms are good candidates for such proposes as they possess several advantages over real-atom-based sources. Various types of artificial atoms such as superconducting circuits and semiconductor based artificial atoms may be embedded within the optical device and some of them allow on-chip engineering. Beyond optical interactions, artificial atoms may be electrically controlled which suggest different applications in modern electronics. quantum-dots are particularly interesting as single-photon sources required for quantum communications, being able to emit photons on-demand.

With decreasing sizes of the optical setups, optomechanical interactions become more prominent. Specially, when considering semiconductor based artificial atoms such as quantum-dots, which intrinsically couple to the mechanical vibrations. Their optomechanical coupling strength is several orders of magnitude higher than the coupling resulting from the action of the radiation force. Within such strong coupling regimes, optical processes are co-existing with quantum mechanical ones. Which allows one to use quantum optical treatment to manipulate the quantum mechanical motion of solid matted at mesoscopic scale.

Various technological approaches related to the implementation of artificial atoms to nano-scale quantum optics have been presented in this chapter. One have separately treated the achievements and the challenges related to optical and optomechanical systems. Various implementation of such systems, as well as, the related phenomena, have been discussed.

2 THE OPTOMECHANICAL INTERACTION

The fundamentals of this thesis relies on the theory of an emitter interacting with a quantum harmonic oscillator. One uses artificial atoms as emitters and considers their specific properties if comparing to atoms. Namely, artificial atoms as quantum-dots may be deposed on different types of quantum mechanical resonators and interact with phonons in the good cavity limit. While other type of artificial atoms as quantum-wells allow to engineer their energetic levels to form an equidistant three-level emitter, which allows one to obtain strong quantum interferences when interacting with an optical resonator. Investigations following in the next chapters rely on the same fundamental theory, although each particular case requires a specific treatment. Therefore, this chapter regroups the fundamental physics of all the following investigations, in order to give the reader a clearer overview on the physical processes to be discussed.

The optical part of the quantum systems is discussed in the first paragraph of this chapter. Both, optical and opto-mechanical setups are directly related to the quantum interaction of the emitter with an electromagnetic field. Moreover, damping processes as the spontaneous emission decay, which is omnipresent in quantum system with atomic-like emitters, may be fully explained only through the prism of the qubit-field interaction. All the necessary details for the description of a system interacting with an electromagnetic field are deduced and discussed and will be applied into the following chapters. The description of the laser pumping effect of a two-level quantum-dot, given in the Chapter 3, will rely on the semi-classic interaction given here. Also, a fully quantum description of the interaction of the electromagnetic field with a quantum-well will be required in Chapter 4.

The mechanical part of opto-mechanical systems is treated in the second paragraph of this chapter. This type of treatment may affect both, the optical and the mechanical behaviour of such systems. The particularity of the treatment consists in considering phonons as bosonic fields and, therefore, all the tools of the quantum optics theory can be applied in order to describe them. Although phonons and photons are treated as bosons from the analytical point of view, their physical meaning is completely different and requires a separate approach. The quantum systems studied in Chapters 3 and 5, are focused on the investigation of the quantum statistics of the mechanical resonator's phonons.

All quantum systems presented in this thesis are open quantum systems, where each of its elements, e.g., the artificial atoms, the phonons and the photons, are exposed to the damping effect of the surrounding environment. The photon leaking into the electromagnetic vacuum, the thermal phonon surroundings or the spontaneous emission of the artificial atoms will be described and defined in the third paragraph of this chapter. For each type of damping mechanics, one will apply the general reservoir theory for the specific type of interaction.

2.1 The optical part

The two-level artificial atom is described by its excited state $|e\rangle$, the ground state $|g\rangle$ and the transition frequency among these two states ω_{qd}. The atomic operators describing the artificial atom's dynamics are defined as $S^{+} = |e\rangle\langle g|$, $S^{-} = |g\rangle\langle e|$ and $S_z = \frac{1}{2}\left(|e\rangle\langle e| - |g\rangle\langle g|\right)$. They obey the standard commutation relations for SU(2) algebra:

$$\begin{aligned}
&\left[S^{\pm}, S^{\mp}\right] = \pm 2 S_z, \\
&\left[S^{\mp}, S_z\right] = \pm S^{\mp}.
\end{aligned} \tag{2.1}$$

As the qubit state basis is represented via its two states $\{|e\rangle, |g\rangle\}$, the identity operator is defined as $|g\rangle\langle g| + |e\rangle\langle e| = 1$. The free qubit Hamiltonian is deduced by applying the identity operator on both sides of H_{QD}:

$$H_{QD} = \left(|g\rangle\langle g| + |e\rangle\langle e|\right) H_{QD} \left(|g\rangle\langle g| + |e\rangle\langle e|\right) = \hbar\omega_g |g\rangle\langle g| + \hbar\omega_g |e\rangle\langle e|, \tag{2.2}$$

where $\hbar\omega_g = \langle g|H_{QD}|g\rangle$ and $\hbar\omega_e = \langle e|H_{QD}|e\rangle$ are the two eigenenergies of H_{QD} and the off-diagonal terms of H_{QD} are null, i.e., $\langle e|H_{QD}|g\rangle = \langle g|H_{QD}|e\rangle = 0$, as this Hamiltonian does not contain any interactional terms. For the sake of simplicity, one may consider a different origin in the energy coordinate, so that:

$$H_{QD} = \hbar\frac{(\omega_e - \omega_g)}{2}|e\rangle\langle e| - \hbar\frac{(\omega_e - \omega_g)}{2}|g\rangle\langle g| = \hbar\omega_{qd} S_z, \tag{2.3}$$

where $\omega_{qd} = \omega_e - \omega_g$.

The quantum-dot-laser interaction is described within the dipole approximation where the field variations in the proximity of the qubit are considered irrelevant, i.e., when $\mathbf{k}\cdot\mathbf{r} \ll 1$, where $\mathbf{k}$ is the wavevector and $\mathbf{r}$ is the coordinate fixed on the atom position $\mathbf{r}_0$. Considering a gauge-independent field $\mathbf{E}(\mathbf{r}_0, t)$, linearly polarized along the $\mathbf{x}$ axis, one defines the quantum-dot-laser Hamiltonian in the dipole approximation as:

$$H_{QD-laser} = -e\mathbf{r}\cdot\mathbf{E}(\mathbf{r}_0,t) = -exE(\mathbf{r}_0,t) = -ex\mathcal{E}\cos(\omega_L t), \tag{2.4}$$

where e is electron charge, x is the atom's coordinate, $\mathcal{E}$ is the laser field amplitude and ω_L is the laser frequency. In the first equality of eq.(2.4) was given the general expression of the interaction of the qubit's electron with a gauge-independent electromagnetic field. In the second equality, one has projected the scalar product among the polarization axis. While, in the last equality one has inserted the classic expression of an electromagnetic field $E(\mathbf{r}_0,t) = \mathcal{E}\cos(\omega_L t)$ which is justified as long as intense laser fields are considered. This type of interaction is called the semi-classical quantum-dot-laser interaction as the laser field is treated classically. In order to introduce the atomic induced dipole momenta, one applies the identity operator $|g\rangle\langle g| + |e\rangle\langle e| = 1$ on both sides of the position operator x as follows:

$$\begin{aligned} H_{QD-laser} &= -e\left(|g\rangle\langle g| + |e\rangle\langle e|\right)x\left(|g\rangle\langle g| + |e\rangle\langle e|\right)\mathcal{E}\cos(\omega_L t) \\ &= -\left(\wp_{ge}|g\rangle\langle e| + \wp_{eg}|e\rangle\langle g|\right)\mathcal{E}\cos(\omega_L t), \end{aligned} \tag{2.5}$$

where, within the second equality of the equation, one has introduced the off-diagonal elements of the qubit's dipole matrix $\wp_{ge} = e\langle g|x|e\rangle$ and $\wp_{eg} = e\langle e|x|g\rangle$. The off-diagonal elements obey the relation $\wp_{ge} = \wp_{eg}^*$. As the quantum-dot possess only an induced dipole and not a permanent one, the diagonal elements of the dipole matrix are null, i.e., $\{\langle g|x|g\rangle, \langle e|x|e\rangle\} = 0$. This relations were used in the calculus of eq.(2.5), where one has eliminated the diagonal elements.

For the sake of simplicity and without loosing the generality of the actual problem, one will further consider the off-diagonal dipole matrix elements to be real, i.e., $\wp_{ge} = \wp_{eg} = \wp$:

$$\begin{aligned} H_{QD-laser} &= -\left(\wp_{ge}S^- + \wp_{eg}S^+\right)\left(e^{i\omega_L t} + e^{-i\omega_L t}\right)\mathcal{E}/2 \\ &= -\hbar\Omega\left(S^- + S^+\right)\left(e^{i\omega_L t} + e^{-i\omega_L t}\right), \end{aligned} \tag{2.6}$$

this assumption allows one to define the Rabi frequency $\Omega = \wp\mathcal{E}/2\hbar$, which is the frequency of the oscillation of the atomic population between its ground and excited states under the effect of the laser pumping. One has also used the trigonometric relation $\cos(\omega_L t) = \left(e^{i\omega_L t} + e^{-i\omega_L t}\right)/2$.

In order to simplify the previous expression of the laser-quantum-dot interaction Hamiltonian, one expresses it in the interaction picture according to the free Hamiltonian of the considered system $H_{QD} = \hbar\omega_{qd}S_z$. This is done by applying to the interaction Hamiltonian, the corresponding unitary transformation $U(t) = exp(-iH_{QD}t/\hbar)$:

$$
\begin{aligned}
H_{QD-laser} &= U^{\dagger}(t)\{-\hbar\Omega\left(S^{-}+S^{+}\right)\left(e^{i\omega_L t}+e^{-i\omega_L t}\right)\}U(t) \\
&= -\hbar\Omega\left(S^{-}e^{i(\omega_L-\omega_{qd})t}+e^{-i(\omega_L-\omega_{qd})t}S^{+}\right) \\
&\quad -\hbar\Omega\left(S^{-}e^{-i(\omega_L+\omega_{qd})t}+e^{i(\omega_L+\omega_{qd})t}S^{+}\right), \qquad (2.7)
\end{aligned}
$$

where in the last equality of the equation one has used the relations $U^{\dagger}(t)S^{-}U(t) = S^{-}e^{-i\omega_{qd}t}$ and $U^{\dagger}(t)S^{+}U(t) = S^{+}e^{i\omega_{qd}t}$. These relations have been deduced by applying the atomic commutation relations of eqs.(2.1) to the mathematical expansion:

$$
e^{A}Be^{-A} = B + [A,B] + \frac{1}{2!}[A,[A,B]] + \frac{1}{3!}[A,[A,[A,B]]] + ... \qquad (2.8)
$$

which leads to a Taylor expansion of the exponential functions $e^{\pm i\omega_{qd}t}$.

Within the interaction picture, a secular approximation is applied to the interaction Hamiltonian. In this approximation, the atomic terms rotating at frequencies $\pm(\omega_L+\omega_{qd})$ were neglected as they are rapidly oscillating and their contribution at time scales larger than $1/(\omega_L+\omega_{qd})$ is null. As the characteristic time scale of the dynamics of the laser-quantum-dot interaction is given by $1/\Omega$, the secular approximation is valid as long as this time scale is big enough to consider the contribution of the fast terms null, i.e., $1/(\omega_L+\omega_{qd}) \ll 1/\Omega$ or $\Omega \ll (\omega_L+\omega_{qd})$. Therefore, the interaction Hamiltonian, within the secular approximation is given as:

$$
\begin{aligned}
H_{QD-laser} &= -\hbar\Omega\left(S^{-}e^{i(\omega_L-\omega_{qd})t}+e^{-i(\omega_L-\omega_{qd})t}S^{+}\right) - \hbar\Omega\left(S^{-}e^{-i(\omega_L+\omega_{qd})t}+e^{i(\omega_L+\omega_{qd})t}S^{+}\right) \\
&\simeq -\hbar\Omega\left(S^{-}e^{i(\omega_L-\omega_{qd})t}+e^{-i(\omega_L-\omega_{qd})t}S^{+}\right). \qquad (2.9)
\end{aligned}
$$

One obtains the final form of the laser-quantum-dot interaction Hamiltonian by returning into the initial representation, i.e., the Schrödinger picture. It is done by applying an inverse unitary transformation $U^{\dagger}(t)$, in a similar way that the calculus of eq.(2.7). Therefore, one obtains:

$$
H_{QD-laser} = -\hbar\Omega\left(S^{-}e^{i\omega_L t}+e^{-i\omega_L t}S^{+}\right). \qquad (2.10)
$$

This term represents the semi-classical light-qubit interaction, as a classical treatment was applied to the electromagnetic field in eq.(2.4). This treatment is justified for intense coherent light. A general description of the light-qubit interaction requires, however, a fully quantum treatment of the interacting electromagnetic field.

One shall begin to characterize the quantum electromagnetic field by identifying its free Hamiltonian. The classical Hamiltonian is found from the solutions of the Maxwell's equations for a single-mode linearly polarized gauge-independent electromagnetic field in empty space [179, 180] and may be expressed as:

$$H_{harmonic\ oscillator} = \frac{1}{2}\left(m\omega^2 q^2 + \frac{p^2}{m}\right). \tag{2.11}$$

This expression is equivalent to the Hamiltonian of a harmonic oscillator, where m is a constant with the dimension of a mass which equals the unitary value $m = 1$ for the case of an electromagnetic field, q is the position and p is the momentum of the oscillator. The Hamiltonian of the quantum field is deduced via the correspondence rule by inserting the canonical position and momentum operators q and p, respectively, into eq.(2.11). Similarly to the quantum harmonic oscillator case, one performs the second quantization by defining the non-hermitian creation operator $a^\dagger$ and annihilation operator a as:

$$\begin{aligned} ae^{-i\omega t} &= (\omega q + ip)/\sqrt{2\hbar\omega}, \\ a^\dagger e^{i\omega t} &= (\omega q - ip)/\sqrt{2\hbar\omega}, \end{aligned} \tag{2.12}$$

which obey the commutation relation:

$$[a, a^\dagger] = 1. \tag{2.13}$$

With the new set of operators, the free field Hamiltonian within the second quantization is given as:

$$H_{photons} = \hbar\omega\left(a^\dagger a + \frac{1}{2}\right). \tag{2.14}$$

The photon field basis is defined via the eigenfunctions of the Hamiltonian of the free field $H_{photons}$. The lowest eigenenergy is given by the non-vanishing part of the Hamiltonian term $\hbar\omega/2$ and the corresponding eigenfunction $|0\rangle$ is called the vacuum state. This state describes the empty field, i.e., the field with no photons. The non-zero energy of the vacuum state is generally explained by the quantum fluctuations of the quantum harmonic oscillator at rest. In our particular case, those are the quantum fluctuations of the electromagnetic vacuum responsible for different fundamental quantum phenomena as the spontaneous emission effect or the Casimir effect [181].

The Hermitian quantity $n = a^\dagger a$ is called the number operator and defines the eigenenergies corresponding to $H_{photons}$ as:

$$E_n = \hbar\omega(n + 1/2), \tag{2.15}$$

where two near eigenenergies differ by the amount $\hbar\omega$ corresponding to a single elementary excitation of the oscillator, i.e., a photon in the current case. Therefore, the number operator counts the number of photons corresponding to a particular field state.

After the vacuum state, the next higher eigenenergy is increased by the amount $\hbar\omega$. The corresponding eigenfunction $|1\rangle$ is obtained by applying the creation operator to the vacuum state, i.e., $|1\rangle = a^\dagger|0\rangle$, and is called the first Fock state. The complete Fock basis $\{|n\rangle, n \in \mathcal{N}\}$ is built by successively applying the creation operator, so that n^{th} Fock state is defined after a normalization as :

$$|n\rangle = \frac{1}{\sqrt{n!}}(a^\dagger)^n|0\rangle. \tag{2.16}$$

The Fock basis represents an infinite basis of orthogonal vectors, i.e., $\langle m|n\rangle = \delta_{m,n}$, where δ is the Kronecker function.

Note that this quantum description of a single-mode electromagnetic field, may be generalized for the case of a multi-mode field by considering that each mode of the field is described by a different independent harmonic oscillator. Therefore, the dynamics of the multi-mode field will be described via the Hamiltonian:

$$H_{multi-mode} = \sum_j \hbar\omega_j \left(a_j^\dagger a_j + \frac{1}{2}\right), \tag{2.17}$$

where one has indexed the frequency, the creation and annihilation operators of each of the field modes and one has summed over all the field modes. As the field modes are described via independent oscillators, each mode is described via a set of independent creation and annihilation operators $a_j^\dagger$ and a_j, so that $[a_j, a_i^\dagger] = \delta_{j,i}$ and an independent Fock basis $\{|n_j\rangle, n_j \in \mathcal{N}\}$, so that $\langle n_j|n_i\rangle = \delta_{j,i}$.

The quantum treatment applied to the electromagnetic field in eqs.(2.11-2.17), may be applied to any other type of dynamics that can be expressed via the model of a quantum harmonic oscillator. The fields that obey this dynamics are called bosonic fields, the creation and annihilation are called the bosonic operators. For example, the phonon fields that will be discussed in the next paragraph, have a harmonic dynamics and obeys the same quantization rules as the electromagnetic fields, therefore they are expressed via a similar set of bosonic operators.

Once one has quantized the field's dynamics and defined the field operators. One may apply the bosonic operators of eqs.(2.12) to the general form of the quantum-dot-laser interaction term given in the first equality of eq.(2.4). More precisely, the expression of the single-mode gauge-independent linearly polarized field obtained from the solution of the classic Maxwell's equations, within the second quantization is obtained as follows:

$$\mathbf{E}(\mathbf{r},t) = \mathcal{E}\mathbf{q}(t)\sin(\mathbf{k}\cdot\mathbf{r}) = \mathcal{E}\sqrt{\frac{\hbar}{2\omega}}(a^{\dagger}e^{i\omega t}+ae^{-i\omega t})\sin(\mathbf{k}\cdot\mathbf{r}), \tag{2.18}$$

where in the first equality one has used the correspondence rule on the position operator $\mathbf{q}(\mathbf{t})$, while in the second equality one has expressed the position operator via the bosonic operators. Similarly to the semi-classical treatment, one applies the dipole approximation by considering the field invariant in the proximity of the qubit, i.e., $\mathbf{k}\cdot\mathbf{r} \ll 1$. Therefore, within the dipole approximation, the field expression becomes:

$$\mathbf{E}(\mathbf{r}_0,t) = \mathcal{E}_0(a^{\dagger}e^{i\omega t}+ae^{-i\omega t}), \tag{2.19}$$

where $\mathbf{r}_0$ is the position of the artificial atom and one defines $\mathcal{E}_0 = \mathcal{E}\sqrt{\frac{\hbar}{2\omega}}\sin(\mathbf{k}\cdot\mathbf{r}_0)$. Inserting the field expression in the general form of the interaction term of eq.(2.4), the artificial-atom-field quantum interaction for a field polarized along the **x** axis, is defined as:

$$H_{QD-field} = -e\mathbf{r}\cdot\mathbf{E}(\mathbf{r}_0,t) = -exE(\mathbf{r}_0,t) = -ex\mathcal{E}_0(a^{\dagger}e^{i\omega t}+ae^{-i\omega t}), \tag{2.20}$$

where x is the atom's position operator **r** projected along the field's polarisation axis **x**. Similarly to eqs.(2.5-2.6), one defines the induced transition dipole momenta $\wp$ by inserting the identity operator $|g\rangle\langle g|+|e\rangle\langle e|=1$ on both sides of x as follows:

$$\begin{aligned} H_{QD-field} &= -e\left(|g\rangle\langle g|+|e\rangle\langle e|\right)x\left(|g\rangle\langle g|+|e\rangle\langle e|\right)\mathcal{E}_0(a^{\dagger}e^{i\omega t}+ae^{-i\omega t}) \\ &= -\left(\wp_{ge}|g\rangle\langle e|+\wp_{eg}|e\rangle\langle g|\right)\mathcal{E}_0(a^{\dagger}e^{i\omega t}+ae^{-i\omega t}) \\ &= -\wp\left(S^{-}+S^{+}\right)\mathcal{E}_0\left(a^{\dagger}e^{i\omega t}+ae^{-i\omega t}\right). \end{aligned} \tag{2.21}$$

This Hamiltonian form may be simplified by applying a secular approximation, similarly to the semi-classical treatment aproach of eqs.(2.7-2.9). Within the interaction picture, the system Hamiltonian is expressed as:

$$H_{QD-field} = \hbar g\left(S^{-}e^{-i\omega_{qd}t}+S^{+}e^{i\omega_{qd}}\right)\left(a^{\dagger}e^{i\omega t}+ae^{-i\omega t}\right), \tag{2.22}$$

where one defines the coupling constant $g = -\wp\mathcal{E}/\hbar$. Within this representation, one is able to split the fast-rotating terms from the slow-rotating ones. Considering that the characteristic time scale of the quantum-dot-field interaction $1/g$ is larger than the period of the fast-oscillating terms $1/(\omega+\omega_{qd})$, i.e., $g \ll (\omega+\omega_{qd})$, one may apply the secular approximation and neglect the contribution of the fast terms. Within this approximation, the system Hamiltonian is expressed as:

$$H_{QD-field} \;=\; \hbar g\big(S^{-}a^{\dagger}e^{i(\omega-\omega_{qd})t} + e^{-i(\omega-\omega_{qd})t}aS^{+}\big). \tag{2.23}$$

Back in the Schrödinger representation, the Hamiltonian describing the two-level quantum-dot interacting with a single-mode quantum field is given as:

$$H \;=\; \hbar\omega_{qd}S_z + \hbar\omega a^{\dagger}a + \hbar g\big(S^{-}a^{\dagger} + aS^{+}\big). \tag{2.24}$$

This Hamiltonian is known as the Jaynes-Cummings model [39] describing a two-level emitter interacting with a single-mode quantum field. Note that within the quantum treatment of the atom-field interaction, the Rabi frequency does not explicitly appear within the interaction term, however it may be deduced by solving the dynamics of the Hamiltonian. One of the main differences between the semi-classic and quantum treatments, is that for the last case one obtains different Rabi frequencies for each of the states of the field. As the photons are distributed among different possible field states, the overlap of different Rabi oscillations leads to the pure quantum phenomena of collapse and revivals of the oscillations of the population of the pumped atom [180]. However, with increasing the photon number, the Rabi frequencies corresponding to high photon occupation numbers become very close to each other. Therefore, the overlap of these oscillations lead to longer population oscillation lifetimes. In this manner, for infinitely large photon numbers, the population collapse is completely cancelled and the two theories converge.

Finally, within the case of a multi-mode electromagnetic field, the interaction of the emitter with each of the field's mode is considered separately. Therefore, the free field and the interaction terms of eq.(2.24) are indexed according to each field mode and summed over all the modes. Therefore:

$$H \;=\; \hbar\omega_{qd}S_z + \sum_j \hbar\omega_j a_j^{\dagger}a_j + \sum_j \hbar g_j\big(S^{-}a_j^{\dagger} + a_jS^{+}\big), \tag{2.25}$$

where j is the index of the j^{th} field mode.

2.2 The mechanical part

The nature of the quantum vibrations of the mechanical resonator are described via the model of a one dimensional lattice made of a chain of N ions connected with their closest neighbours through a linear force field, as in they were connected via springs. The atoms are all identical and equally spaced, described via a mass m, momentum p_j and position q_j of the j^{th} ion. The interaction occurring among two neighbouring atoms is described via the force constant K, which for the case of a spring describes its rigidity. The system Hamiltonian is obtained by summing the kinetic energies of the ions and the spring potential energies as:

$$H_{ph} = \sum_{j=1}^{N} \left(\frac{p_j^2}{2m} + \frac{K}{2}(q_j - q_{j-1})^2 \right). \tag{2.26}$$

The quantum version of the Hamiltonian is obtained by applying the correspondence rule and introducing the canonical position and momentum operators that obey the commutation relation $[p_j, q_i] = -i\hbar\delta_{j,i}$, where $\delta_{j,i}$ is the Kronecker function. In order to treat the many-body Hamiltonian of eq.(2.26) in a collective manner, one applies a discrete Fourier transformation, i.e., an inverse decomposition in Fourier series, to the atomic canonic operators. Namely, the canonic operators, in the reciprocal space are defined as:

$$\begin{aligned} q_{\mathbf{k}} &= \frac{1}{\sqrt{N}} \sum_{j=1}^{N} q_j e^{-i\mathbf{k}\mathbf{R}_j^0}, \\ p_{\mathbf{k}} &= \frac{1}{\sqrt{N}} \sum_{j=1}^{N} p_j e^{-i\mathbf{k}\mathbf{R}_j^0}, \end{aligned} \tag{2.27}$$

where $\mathbf{R}_j^0$ are equilibrium position of the ions. Note, that as one considers a finite lattice of length L, the interatomic distance is given as L/N. As the lattice is made of identical atoms, the lattice constant a is the same as the interatomic distance, hence, $a = L/N$. Therefore, the k space of the Fourier transform is defined within the lattice first Brillouin zone as:

$$k \in \left\{ \frac{2\pi n}{Na} - \frac{\pi}{a}, n \in \mathcal{N} \right\}. \tag{2.28}$$

With the new set of operators, the expression of the Hamiltonian of eq.(2.26) becomes:

$$H_{ph} = \sum_{\mathbf{k}} \left(\frac{1}{2m} p_{\mathbf{k}} p_{\mathbf{-k}} + \frac{K}{2} q_{\mathbf{k}} q_{\mathbf{-k}} (2 - e^{ika} - e^{-ika}) \right). \tag{2.29}$$

From the definition of the discrete Fourier transformations of eq.(2.27), one may further express the Hermitian conjugate of the canonical operators as:

$$
\begin{aligned}
q_{\text{-}\mathbf{k}} &= q_{\mathbf{k}}^{\dagger}, \\
p_{\text{-}\mathbf{k}} &= p_{\mathbf{k}}^{\dagger}.
\end{aligned} \tag{2.30}
$$

The analogy with the case of the quantum harmonic oscillator is highlighted by defining the lattice eigenfrequencies as:

$$
\omega_k^2 = \frac{2K}{M}(1-\cos ka), \tag{2.31}
$$

which in the neighbouring of $k \to 0$, behaves as $\omega_{k\to 0} \simeq ka\sqrt{K/M}$. It represents the dispersion relation of acoustical phonons. Note that optical phonons are not supported by the current model and requires to consider a lattice made of different kinds of atoms. However, a more sophisticated model will not change or improve the description of the acoustical phonons dynamics. Hence, the current model is suitable for the following studies as the investigations of the following optomechanic setups are related to the acoustical phonons only due to the couplings strengths of the light-matter mechanics.

The dispersion relation allows the lattice Hamiltonian to be expressed as a sum of independent harmonic oscillators over all the lattice modes, similarly to the free Hamiltonian of the electromagnetic field discussed in eq.(2.25):

$$
H_{ph} = \sum_{\mathbf{k}} \frac{1}{2}\left(\frac{p_{\mathbf{k}}p_{\mathbf{k}}^{\dagger}}{m} + m\omega_k^2 q_{\mathbf{k}}q_{\mathbf{k}}^{\dagger}\right). \tag{2.32}
$$

The only difference with the electromagnetic treatment is the quadratic terms that appear as $p_{\mathbf{k}}p_{\mathbf{k}}^{\dagger}$ and $q_{\mathbf{k}}q_{\mathbf{k}}^{\dagger}$, instead of $p_{\mathbf{k}}^2$ and $q_{\mathbf{k}}^2$, respectively. Therefore, the second quantization requires the following set of bosonic operators:

$$
\begin{aligned}
b_{\mathbf{k}}e^{-i\omega_{\mathbf{k}}t} &= (m\omega_{\mathbf{k}}q_{\mathbf{k}} + ip_{\mathbf{k}})/\sqrt{2m\hbar\omega_{\mathbf{k}}}, \\
b_{-\mathbf{k}}^{\dagger}e^{i\omega_{\mathbf{k}}t} &= (m\omega_{\mathbf{k}}q_{\mathbf{k}} - ip_{\mathbf{k}})/\sqrt{2m\hbar\omega_{\mathbf{k}}},
\end{aligned} \tag{2.33}
$$

which obey the commutation relation $[b_{\mathbf{k}}, b_{\mathbf{k}'}^{\dagger}] = \delta_{k,k'}$. With the new set of bosonic operators and by considering the dispersion relation property $\omega_{\mathbf{k}} = \omega_{-\mathbf{k}}$, the free lattice Hamiltonian is expressed as:

$$
H_{ph} = \sum_{\mathbf{k}} \hbar\omega_{\mathbf{k}}\left(b_{\mathbf{k}}^{\dagger}b_{\mathbf{k}} + \frac{1}{2}\right). \tag{2.34}
$$

In the case of a mechanical resonator a single-mode field is selected. The rest of lattice modes are considered through the reservoir theory as damping phenomenon and are expressed as a thermally distributed reservoir. Different architectures have been implemented in order to obtain single-mode phonon field for a quantum mechanical resonator [8]. Some of these architectures allow an artificial atom to be embedded on the mechanical resonator, e.g., multi-layered acoustical cavities use distributed Bragg reflectors in order to achieve high values of the cavity quality factors [182], just as the case of nano-mechanical beams [183] where single-mode phonons are achieved due to the beam geometry.

The quantum vibrations of the mechanical resonator are described by the single-mode phonon field of frequency ω_{ph} and the bosonic operators b and $b^\dagger$. The resonator free Hamiltonian is defined as:

$$H_{ph} \;=\; \hbar\omega_{ph}\left(b^\dagger b + \frac{1}{2}\right). \tag{2.35}$$

For simplicity, one may further neglect the $\hbar\omega_{ph}/2$ term of H_{ph} as it does not contribute to the following investigations of the phonon dynamics.

The phonon vibrations are expressed as an oscillation of the ions within the lattice of the mechanical resonator. If these oscillations are small comparing to the inter-atomic distance, the phonon-electron interaction may be treated as a perturbation of the ion-electron interaction. In a general form, the Hamiltonian of the interaction of a electron with a lattice of ions is given as [184]:

$$H_{e-ions} \;=\; \int d\mathbf{r}\varrho(\mathbf{r})\sum_m V_{e-ion}(\mathbf{r}-\mathbf{R}_m), \tag{2.36}$$

where $\varrho(\mathbf{r})$ is the electron charge density operator, V_{e-ion} is the electron-ion interaction potential that is summed over all the m ions. The electron and ion position are described by $\mathbf{r}$ and $\mathbf{R_m}$, respectively. The ion mechanical oscillation $\mathbf{q}$ around the equilibrium position $\mathbf{R_0}$ may be expressed as $\mathbf{R_m} = \mathbf{R_0} + \mathbf{q}$. For small oscillations $\mathbf{q}$, a first order Taylor expansion of the interaction potential around the equilibrium position may be performed as:

$$V_{e-ion} \;=\; V_{e-ion}(\mathbf{r}-\mathbf{R}_0) - \;\mathbf{q}\cdot\nabla V_{e-ion}(\mathbf{r}-\mathbf{R}_0) + \mathcal{O}(\mathbf{q}^2), \tag{2.37}$$

where the first term represents the interaction of the electron with the ions in equilibrium and the second is the phonon-electron interaction potential.

In order to introduce the boson operators instead of position ones, it is more convenient to expand the electron-phonon potential in Fourier series over the phonon wave-vectors $\mathbf{k}$, similarly to the discrete Fourier transformations of eq.(2.27). This transformation allows one to use the property of the spacial derivatives in the Fourier space on the ∇ operator of the electron-phonon potential term, as follows:

$$V_{e-ph} \quad = \quad -\mathbf{q}\cdot\nabla V_{e-ion}(\mathbf{r}-\mathbf{R}_0) = -\frac{i}{N}\sum_{\mathbf{k}}\mathbf{q}\cdot\mathbf{k}\,V(\mathbf{k})e^{i\mathbf{k}\cdot(\mathbf{r}-\mathbf{R}_0)}. \tag{2.38}$$

This expression describes the interaction of an electron with a single ion.

In order to define the quantum-dot-phonon interaction, one sums the electron-phonon interaction potential over all the quantum-dot's ions. This allows one to insert the canonic operators of eq.(2.27) expressed in the reciprocal space and generalized for the three dimensional case, as follows:

$$V_{e-ph} \quad = \quad -\frac{i}{N}\sum_{m}\sum_{\mathbf{k}}\mathbf{q}_m\cdot\mathbf{k}\,V(\mathbf{k})e^{i\mathbf{k}\cdot(\mathbf{r}-\mathbf{R}_{0,m})} = -\frac{i}{\sqrt{N}}\sum_{\mathbf{k}}\mathbf{q}_k\cdot\mathbf{k}\,V(\mathbf{k})e^{i\mathbf{k}\cdot\mathbf{r}}. \tag{2.39}$$

Here, the phonon operators of eq.(2.33) are inserted into the expression of V_{e-ph} by decomposing the lattice oscillation of the phonon mode **k** over the directions of **q**. Therefore, the second quantization of the electron-phonon interaction potential term, is given as:

$$V_{e-ph} \quad = \quad \sum_{\mathbf{k}}\frac{1}{\sqrt{2m\omega_{\mathbf{k}}N}}(b_{\mathbf{k}}^{\dagger}+b_{\mathbf{k}})k\,V(\mathbf{k})e^{i\mathbf{k}\cdot\mathbf{r}}. \tag{2.40}$$

The Hamiltonian of the interaction of the phonons with the quantum-dot's electron is obtained by introducing the expression of the electron-phonon interaction potential defined in eq.(2.40) into the general Hamiltonian form of the electron-ions interaction of eq.(2.36):

$$H_{e-ph} \quad = \quad \sum_{\mathbf{k}}\int d\mathbf{r}\varrho(\mathbf{r})\frac{1}{\sqrt{2m\omega_{\mathbf{k}}N}}(b_{\mathbf{k}}^{\dagger}+b_{\mathbf{k}})k\,V(\mathbf{k})e^{i\mathbf{k}\cdot\mathbf{r}}. \tag{2.41}$$

Here, a Fourier transformation can be applied to the charge density operator after a rearrangement of the terms of eq.(2.41), namely, $\varrho(\mathbf{k}) = \int d\mathbf{r}\varrho(\mathbf{r})e^{i\mathbf{k}\cdot\mathbf{r}}$. Therefore, the quantum-dot-phonon interaction Hamiltonian may be expressed as:

$$H_{e-ph} \quad = \quad \sum_{\mathbf{k}} M_{\mathbf{k}}\varrho(\mathbf{k})(b_{\mathbf{k}}^{\dagger}+b_{\mathbf{k}}), \tag{2.42}$$

where the term $M_{\mathbf{k}} = k\,V(\mathbf{k})/\sqrt{2m\omega_{\mathbf{k}}N}$, represents a constant that be carried out of the integral of eq.(2.41) and treated separately from $\varrho(\mathbf{k})$.

Generally, the quantum-dot-phonon interaction matrix elements are given as $M_{\mathbf{k}}^{i,j} = M_{\mathbf{k}}\varrho_{i,j}(\mathbf{k})$. These matrix elements are defined via the elements of the charge density operator given in matrix form, which is expressed as:

$$\varrho_{i,j}(\mathbf{k}) \quad = \quad \int d\mathbf{r}\psi_i^*\psi_j e^{i\mathbf{k}\cdot\mathbf{r}}|i\rangle\langle j|, \tag{2.43}$$

where ψ_i is the wave function of the electron in state i [184]. When a quantum-dot is considered, the dominant effect in the interaction of the electron with the phonons is the deformation potential, which for lowest deformation order is phenomenologically described via an experimentally defined constant. The deformation potential constants are given as D_c or D_v for the electron being in the conduction or valence band, respectively. Therefore the term $M_{\mathbf{k}} = k\,V(\mathbf{k})/\sqrt{2m\omega_{\mathbf{k}}N}$ represents a constant, as $V(\mathbf{k}) = \{D_c, D_v\}$.

Under the laser pumping, the quantum-dot is excited when an electron from the valence band is thrown to the conduction band and thus an exciton is formed. It is the quantum-dot's spacial confined exciton, that interacts with deformations induced via the phonon oscillations. The quantum-dot excited state is represented not only by the electron from the conduction band, but also by the positively charged "hole" left in the valence band, and the entire electron-hole system shall be considered in order to fully describe the quantum-dot-phonon interaction. As within the quantum-dot the exciton is strongly confined, the electron-hole wave function may be approximated by the product of the single electron and hole wave functions [184]. Therefore the complete quantum-dot-phonon interaction is obtained by applying a similar treatment of eqs.(2.36 - 2.42) separately to the hole dynamics, additionally to the electron-phonon coupling. The final interaction Hamiltonian is given as:

$$H_{QD-ph} = \sum_{\mathbf{k}} (M_{\mathbf{k}}^{(e)}\varrho_{e,e}^{(e)}(\mathbf{k}) + M_{\mathbf{k}}^{(h)}\varrho_{e,e}^{(h)}(\mathbf{k}))(b_{\mathbf{k}}^{\dagger} + b_{\mathbf{k}}), \tag{2.44}$$

where, one has applied the index (e) to the terms describing the electron in the conduction band and (h) for the ones describing the hole in the valence band. The diagonal quantum-dot-phonon interaction matrix elements of H_{QD-ph} are considering only the excited state which represents the exciton. Also, one has neglected the off-diagonal elements, by restricting to low energetic phonons that do not allow for interband transitions.

The final form of the quantum-dot-phonon interaction, is obtained by inserting the expression of $\varrho_{e,e}^{(h)}(\mathbf{k})$ and $\varrho_{e,e}^{(e)}(\mathbf{k})$ given by eq.(2.43), which leads to:

$$H_{QD-ph} = \hbar|e\rangle\langle e| \sum_{\mathbf{k}} g_{\mathbf{k}}(b_{\mathbf{k}}^{\dagger} + b_{\mathbf{k}}), \tag{2.45}$$

with $g_{\mathbf{k}} = k(\sqrt{2m\omega_{\mathbf{k}}N}\hbar)^{-1}\big(D_c \int d\mathbf{r}_e|\psi_{(e)}|^2 e^{i\mathbf{k}\cdot\mathbf{r}_e} - D_v \int d\mathbf{r}_h|\psi_{(h)}|^2 e^{i\mathbf{k}\cdot\mathbf{r}_h}\big)$.

The case of the mechanical resonator is described by a single-mode phonon field. One may note $S^+S^- = |e\rangle\langle e|$. Therefore, by selecting only one mode in eq.(2.45), one obtains:

$$H_{QD-ph} = \hbar g S^+S^-(b^{\dagger} + b). \tag{2.46}$$

2.3 The damping phenomena

The system dynamics is described by the master equation of the density matrix operator. The density operator is defined as $\rho = |\Psi\rangle\langle\Psi|$ and contains the same information as the system wave function $|\Psi\rangle$. The master equation of ρ in its general form is derived from the Schrödinger equation for the system wave function and describes the same dynamics. The general form of the master equation is called the Liouville-von Neumann equation and is given as:

$$\dot{\rho} \;=\; -\frac{i}{\hbar}[H,\rho]. \tag{2.47}$$

Although it is equivalent to the Scrödinger equation, the master equation allows to analytically describe the system damping processes in a simpler way through the formalism of the reservoir theory. The main concept of the reservoir theory relies on the assumptions that the surrounding reservoir is a subsystem that weakly interacts with the considered model and has no memory. The first assumption is applied via the Born approximation, where the changes within the reservoir originating from the weak interaction with the system, can be neglected and the reservoir rests at equilibrium all the time. The last assumption is expressed via a Markovian approximation and, in a general case, is validated if a infinite large system is considered for the reservoir, comparing to the studied system. In this case, once the quantum information goes from the system into the reservoir, it is irreversibly lost from the system.

Let us consider a system S interacting with a reservoir R, then the system reduced density matrix ρ_S is obtained by tracing the system-reservoir density matrix ρ_{SR} over the reservoir states, i.e., $\rho_S = Tr_R[\rho_{SR}]$. Within the interaction picture, the general master equation of the system-reservoir dynamics states is given via the von Neumann equation:

$$\dot{\rho}_{SR}(t) = -\frac{i}{\hbar}[V(t),\rho_{SR}(t)], \tag{2.48}$$

where the interaction potential $V(t)$ is expressed via the system Hamiltonian within the interaction picture.

The general solution of $\rho_{SR}(t)$ is given as function of the initial time of the interaction t_0 and may be expressed as:

$$\rho_{SR}(t) = \rho_{SR}(t_0) - \frac{i}{\hbar}\int_{t_0}^{t}[V(t'),\rho_{SR}(t')]dt'. \tag{2.49}$$

Inserting this solution of $\rho_{SR}(t)$ in the von Neumann equation (2.48) leads to:

$$\dot{\rho}_{SR}(t) = -\frac{i}{\hbar}[V(t), \rho_{SR}(t_0)] - \frac{1}{\hbar^2}\int_{t_0}^{t} \left[V(t), [V(t'), \rho_{SR}(t')]\right] dt', \tag{2.50}$$

where one applies the Born approximation which consists of the assumption of a weak system-reservoir interaction, i.e. $V(t) \ll 1$. Within the Born approximation, the solution of eq.(2.50) is treated as a first order development expressed as $\rho_{SR}(t) = \rho_S(t) \otimes \rho_R(t_0) + \rho_{int}(t)$. The first term represents the case when no system-reservoir interaction occurs, where one considers the reservoir always at equilibrium, i.e., as a time-independent term $\rho_R(t) \equiv \rho_R(t_0)$. The second term ρ_{int} is the interaction term of the linear development that satisfies the condition $Tr[\rho_{int}] = 0$ as it contains only off-diagonal elements. This assumption allows one to deduce the equation of the system reduced density matrix by tracing the system-reservoir density operator of eq.(2.50) over the reservoir states as follows:

$$\begin{aligned} \dot{\rho}_S(t) &= -\frac{i}{\hbar} Tr_R\left[[V(t), \rho_S(t_0) \otimes \rho_R(t_0)]\right] \\ &\quad -\frac{1}{\hbar^2} Tr_R\left[\int_{t_0}^{t} \left[V(t), [V(t'), \rho_S(t) \otimes \rho_R(t_0)]\right] dt'\right], \end{aligned} \tag{2.51}$$

where one has considered that the statistics of the systems do not have memory, i.e., the Markovian approximation, and therefore do not depend of the past, i.e., of the initial time t_0. This allows one to transform $\rho_S(t') \to \rho_S(t)$ within the integral of eq.(2.51). Therefore, the damping terms of the master equation are deduced by inserting the system-reservoir interaction Hamiltonian term expressed within the interaction picture into eqs.(2.47)-(2.51). The different interaction Hamiltonian terms depend on the nature of each damping phenomenon and will be discussed separately in what follows.

The effect of the surrounding temperature is described via a reservoir made of a multi-mode boson field with thermally distributed vibrational quanta. It may describe the thermal damping process either of the vibrations of the mechanical resonator or the oscillations of the electromagnetic field, as both cases are described via bosonic operators. In the case of the mechanical motion, the environmental damping reservoir is described via the surrounding temperature T, and the mechanical resonator may either receive or loose phonons from its interaction with the thermal bath. In the case of a electromagnetic field, the reservoir is represented by an empty thermal bath, i.e., a thermal reservoir of temperature $T = 0$ possessing no photons. In this case, the damping effect occurs when the photons irreversibly escape the cavity, which results only in a loosing effect for the optical resonator.

The field-reservoir interaction Hamiltonian is defined via a weak quantum interaction of a single mode field with the multi-mode reservoir field. In its general form, the interaction of two boson fields of same kind, e.g., photons or phonons, is given as:

$$H_{field-reservoir} = \sum_k \hbar g_k (a_k + a_k^\dagger)(a + a^\dagger), \tag{2.52}$$

where $a, a^\dagger$ are the single-mode field operators, $a_k, a_k^\dagger$ are the operators describing the k^{th} mode of the reservoir field. The total interaction term is obtained via the summation over the infinite independent reservoir's k modes. The interaction Hamiltonian may be simplified by eliminating the fast-rotating terms within the interaction picture, similarly to the method applied in eq.(2.9). The field and reservoir free Hamiltonians are expressed via the simplified form of eq.(2.35). In order to highlight the temporal dependency of the interaction terms, one goes in the interaction picture by applying the unitary transformation $U(t) = exp(-i(\omega a^\dagger a + \sum_k \omega_k a_k^\dagger a_k)t)$ and thus:

$$\begin{aligned} H_{field-reservoir} &= U^\dagger(t)\{\sum_k \hbar g_k (a_k + a_k^\dagger)(a + a^\dagger)\}U(t) \\ &= \sum_k \hbar g_k \left(a_k^\dagger a e^{-i(\omega-\omega_k)t} + a^\dagger a_k e^{i(\omega-\omega_k)t} + a a_k e^{-i(\omega+\omega_k)t} + a^\dagger a_k^\dagger e^{i(\omega+\omega_k)t} \right) \\ &\simeq \sum_k \hbar g_k \left(a_k^\dagger a e^{-i(\omega-\omega_k)t} + a^\dagger a_k e^{i(\omega-\omega_k)t} \right). \end{aligned} \tag{2.53}$$

The approximation performed in the last line of eq.(2.53) on the bosonic terms is called the rotating wave approximation (RWA) and is valid as long $g_k \ll (\omega + \omega_k)$, i.e., the characteristic time scale of the field-reservoir dynamics is larger than the oscillations of the fast-rotating terms. Inserting the Hamiltonian of eq.(2.53) in the general form of the master equation of the reduced density matrix of eq.(2.51) of the field-reservoir system, leads to:

$$\begin{aligned} \dot{\rho}_{field}(t) &= -i \sum_k g_k \left(\langle a_k^\dagger \rangle [a, \rho_{field}(t_0)] e^{-i(\omega-\omega_k)t} + \langle a_k \rangle [\rho_{field}(t_0), a^\dagger] e^{i(\omega-\omega_k)t} \right) \\ &- \int_{t_0}^t dt' \sum_{k,k'} g_k g_{k'} \Big\{ \Big(a a \rho_{field}(t') - 2a\rho_{field}(t') a + \rho_{field}(t') a a \Big) \\ &\quad \times e^{-i(\omega-\omega_k)t - i(\omega-\omega_{k'})t'} \langle a_k^\dagger a_{k'}^\dagger \rangle \\ &\quad - \Big(a^\dagger a^\dagger \rho_{field}(t') - 2a^\dagger \rho_{field}(t') a^\dagger + \rho_{field}(t') a^\dagger a^\dagger \Big) e^{i(\omega-\omega_k)t + i(\omega-\omega_{k'})t'} \langle a_k a_k \rangle \\ &\quad - \mathcal{L}(a^\dagger)(t') e^{-i(\omega-\omega_k)t + i(\omega-\omega_{k'})t'} \langle a_k^\dagger a_{k'} \rangle \\ &\quad - \mathcal{L}(a)(t') e^{i(\omega-\omega_k)t - i(\omega-\omega_{k'})t'} \langle a_k a_{k'}^\dagger \rangle \Big\}, \end{aligned} \tag{2.54}$$

where the Liouville superoperator is defined as $\mathcal{L}(\mathcal{O})(t) = 2\mathcal{O}\rho(t)\mathcal{O}^\dagger - \mathcal{O}^\dagger\mathcal{O}\rho(t) - \rho(t)\mathcal{O}^\dagger\mathcal{O}$ for a given operator $\mathcal{O}$. Here. the brackets $\langle ... \rangle$ describe the average value of the reservoir operator

$\mathcal{O}_k$ defined as the trace over the reservoir's states, i.e., $\langle \mathcal{O}_k \rangle = Tr_R[\mathcal{O}_k \rho_R]$. Depending on the reservoir properties, the eq.(2.54) may be simplified for each specific case. In the case of a thermal reservoir, the reservoir reduced density operator ρ_R is defined as (see p. 251, [179]):

$$\rho_R = \prod_k \left(1 - e^{-\hbar\omega_k/k_B T}\right) e^{-\hbar\omega_k a_k^\dagger a_k/k_B T}, \tag{2.55}$$

where k_B is the Boltzmann constant and T is the reservoir temperature. For this density operator, the average values of the reservoir operators are estimated as:

$$\begin{aligned}
\langle a_k a_{k'}^\dagger \rangle &= (\bar{n}_k + 1)\delta_{k,k'}, \\
\langle a_k^\dagger a_{k'} \rangle &= \bar{n}_k \delta_{k,k'}, \\
\langle a_k^\dagger \rangle &= 0, \\
\langle a_k \rangle &= 0, \\
\langle a_k^\dagger a_{k'}^\dagger \rangle &= 0, \\
\langle a_k a_{k'} \rangle &= 0,
\end{aligned} \tag{2.56}$$

where one has used the property $a_k^\dagger a_k |n_k\rangle = n_k |n_k\rangle$ where $|n_k\rangle$ is a state of the k^{th} mode of the reservoir field described within the Fock state basis. One has defined the mean number of quanta of the k^{th} mode of the reservoir field from the eq.(2.55) as:

$$\bar{n}_k = \frac{1}{e^{\hbar\omega_k/k_B T} - 1}. \tag{2.57}$$

What one highlights here is that $\bar{n}_k$ is found as the average value of n_k over all the mode's states.

Inserting the average values of the reservoir operators of eq.(2.56) into the eq.(2.54) leads to the following master equation:

$$\dot{\rho}_{field}(t) = \int_{t_0}^{t} dt' \sum_k g_k^2 \left(\bar{n}_k \mathcal{L}(a^\dagger)(t') e^{-i(\omega-\omega_k)(t-t')} - (1+\bar{n}_k)\mathcal{L}(a)(t') e^{i(\omega-\omega_k)(t-t')} \right). \tag{2.58}$$

In order to simplify the expression of eq.(2.58) one replace the sum over the modes of the field by an integral as the modes of the reservoir have infinitely closely-spaced frequencies. Therefore one may apply the transformation to a spherical coordinate volume element in k space as: $\sum_k \rightarrow \frac{\mathcal{C}}{4\pi} \int_0^{2\pi} d\phi \int_0^{\pi} d\theta \sin\theta \int_0^{\infty} dk k^2$, where $\mathcal{C}$ is a constant. This leads to:

$$\dot{\rho}_{field}(t) = \mathcal{C}\int_{t_0}^{t} dt' \int_0^\infty dk k^2 g_k^2 \Big(\bar{n}_k \mathcal{L}(a^\dagger)(t') e^{-i(\omega-\omega_k)(t-t')} - (1+\bar{n}_k)\mathcal{L}(a)(t') e^{i(\omega-\omega_k)(t-t')} \Big). \tag{2.59}$$

Finally, one assumes that the single-mode field of frequency ω interacts mostly with the modes of the reservoir with the frequency close to ω, e.g., the intensity spectrum of the cavity at the exit of its mirrors would be a peak centred around its frequency ω. Thus, one may replace $k = \omega/c$ within the k dependent integral quantity $k^2 g_k^2 = \omega^2 g_{k=\omega/c}^2/c^2$ and carry it out of the integral (see p. 207, [179]). Here, c is the speed of sound of the mechanical resonator. Carrying the quantity $k^2 g_k^2$ out of the integral, allows one to change the integration limit from $k = 0$ to $k \to -\infty$ and one obtains two similar delta functions in eq.(2.60), as $\int_{-\infty}^{\infty} d\omega_k e^{i(\omega-\omega_k)(t-t')} = 2\pi\delta(t-t')$ that allow to reduce the eq.(2.60) to:

$$\dot{\rho}_{field}(t) = \kappa\Big(\bar{n}\int_{t_0}^{t} dt' \mathcal{L}(a^\dagger)(t')\delta(t-t') + (1+\bar{n})\int_{t_0}^{t} dt' \mathcal{L}(a)(t')\delta(t-t')\Big), \tag{2.60}$$

where $\bar{n} = \bar{n}_{k=\omega/c}$ and $\kappa = 2\pi\omega^2 g_{k=\omega/c}^2 \mathcal{C}/c^3$ are the constants that appears after inserting the dispersion relation $k = \omega/c$ into the previous integral. By applying the property of the delta functions, one obtains:

$$\dot{\rho}_{field}(t) = \kappa\big(\bar{n}\mathcal{L}(a^\dagger)(t) + (1+\bar{n})\mathcal{L}(a)(t)\big). \tag{2.61}$$

Here the first term represents the pumping effect which describes the boson quanta that come into the single-mode field from the reservoir, while the second term represents the damping effect which describes the resonator's losses of quanta transferred into the reservoir. The damping constant κ may also be expressed in a simple form via the resonator quality factor Q as $\kappa = \omega/Q$. Note that for an empty thermal bath, i.e., when $\bar{n} = 0$, the pumping term vanishes, while the damping term doesn't as the oscillator quanta can leak into the empty reservoir. This is the case of an optical resonator interacting with the electromagnetic vacuum.

$$\dot{\rho}_{electromagnetic\ vacuum}(t) = \kappa\mathcal{L}(a)(t). \tag{2.62}$$

The spontaneous emission phenomenon originates from the interaction of the artificial atom with the surrounding electromagnetic vacuum. Although, the electromagnetic vacuum is an empty reservoir, i.e., $\bar{n} = 0$, its empty electromagnetic field possesses quantum fluctuations with a non-zero energy. More precisely, the energy of the vacuum fluctuations may be obtained from the field free Hamiltonian. Within the second quantization, the free Hamiltonian of the electromagnetic quantum field is defined via the bosonic creation and annihilation operators and is expressed similarly to the equation (2.35) but with a different frequency ω and a different set of bosonic operators a and $a^\dagger$. When the eigenenergy of the vacuum state is considered, it is given by the non-vanishing term of the Hamiltonian $\hbar\omega/2$. Therefore, the atom interaction with the surrounding vacuum leads to its decay to a less energetic state due to the fluctuation of the empty vacuum field.

In order to define the spontaneous emission damping term, one inserts the Hamiltonian quantum-dot-field quantum interaction term of eq.(2.23) generalized for a multi-mode field and expressed into the interaction picture, into the equation of the system reduced density operator of eq.(2.51). This leads to the following expression:

$$\begin{aligned}
\dot{\rho}_{SE}(t) \;=\;& -i\sum_k g_k\left(\langle a_k^\dagger\rangle[S^-,\rho_{SE}(t_0)]e^{-i(\omega_{qd}-\omega_k)t}+\langle a_k\rangle[\rho_{SE}(t_0),S^+]e^{i(\omega_{qd}-\omega_k)t}\right)\\
&-\int_{t_0}^{t}dt'\sum_{k,k'}g_kg_{k'}\Bigg\{\left(S^-S^-\rho_{SE}(t')-2S^-\rho_{SE}(t')S^-+\rho_{SE}(t')S^-S^-\right)\\
&\times e^{-i(\omega_{qd}-\omega_k)t-i(\omega_{qd}-\omega_{k'})t'}\langle a_k^\dagger a_k^\dagger\rangle\\
&-\left(S^+S^+\rho_{SE}(t')-2S^+\rho_{SE}(t')S^++\rho_{SE}(t')S^+S^+\right)e^{i(\omega_{qd}-\omega_k)t+i(\omega_{qd}-\omega_{k'})t'}\langle a_ka_k\rangle\\
&-\mathcal{L}(S^+)(t')e^{-i(\omega-\omega_k)t+i(\omega-\omega_{k'})t'}\langle a_k^\dagger a_{k'}\rangle\\
&-\mathcal{L}(S^-)(t')e^{i(\omega-\omega_k)t-i(\omega-\omega_{k'})t'}\langle a_ka_{k'}^\dagger\rangle\Bigg\},
\end{aligned} \tag{2.63}$$

where ρ_{SE} is the quantum-dot reduced density matrix operator of the quantum-dot-reservoir density matrix operator.

Note that the obtained equation is similar to the field-reservoir damping term, if replacing the field bosonic operators a and $a^\dagger$ of eq.(2.54) by the atomic operators S^- and S^+ respectively. Moreover, the assumptions and simplifications applied in eqs.(2.54 - 2.61) are valid for the quantum-dot-reservoir interaction case as well. Therefore, the spontaneous emission damping term has a similar form with the field damping term estimated in eq.(2.61). The only difference, is that for the spontaneous emission terms, one considers an empty thermally distributed vacuum reservoir. It corresponds to a thermal reservoir with a null temperature $T = 0$. Therefore, one sets $\bar{n} = 0$ and the pumping terms thus vanishes for the expression of the spontaneous decay damping term, similarly to the case of eq.(2.62), which leads to:

$$\dot{\rho}_{SE} \;=\; \gamma\mathcal{L}(S^-). \tag{2.64}$$

The spontaneous emission rate γ is estimated via the Weisskopf-Wigner theory of two-level-atom-reservoir interaction [185] and is given as $\gamma = \frac{1}{4\pi\epsilon_0}\frac{4\omega^3\wp^2}{3\hbar c^3}$, where ϵ_0 is the vacuum permitting constant and c is the speed of light constant.

The dephasing damping term is responsible for loss of coherence due to imperfections and impurities within the quantum-dot [186]. In its general form these processes may be expressed via the Hamiltonian form given in [187]:

$$H_{dephasing} = \hbar\mu(t)S_z, \tag{2.65}$$

where $\mu(t)$ is a delta-correlated Gaussian stochastic variable with zero mean value, which may be described as a noise term added to the quantum-dot transition frequency ω_{qd}. The term is given by the simplified version of the free quantum-dot Hamiltonian term of eq.(2.3) where one has applied the following transformation: $\omega_{qd} \to \omega_{qd} + \mu(t)$. The master equation of the dephasing term is deduced from the von Neumann equation as:

$$\dot{\rho}_{dephasing} = -\frac{i}{\hbar}[H, \rho_{dephasing}] = -i\mu(t)[S_z, \rho_{dephasing}]. \tag{2.66}$$

The master equation form after the stochastic average of the density operator is given via the dephasing rate γ_c as (see p. 173, [187]):

$$\dot{\bar{\rho}}_{dephasing} = \gamma_c\mathcal{L}(S_z), \tag{2.67}$$

where $\gamma_c = \lim_{t\to\infty}\Re\{\frac{1}{2}\int_0^t ds\int_0^t ds'\langle\mu(s)\mu(s')\rangle\}$ for Markovian processes and the bar over the density operator designates the stochastic average. For the sake of simplicity one will further use the simplified notation $\dot{\bar{\rho}}_{dephasing} \equiv \dot{\rho}_{dephasing}$ in the coming chapters.

2.4 Conclusions to Chapter 2

In this chapter one had described all the necessary components required to establish the system dynamics equations of the following optical and optomechanical setups. Thus, all of the further considered interaction terms of the system Hamiltonian, e.g., the atomic laser pumping effect, the qubit-electromagnetic-field and the quantum-dot-phonon interactions, have been deduced and described. Moreover, all the background theory necessary for the description of the quantum statistics have been discussed.

The decoherence effect which appears from the interaction of the quantum optomechanical and optical open systems with their environments have been treated though the general reservoir theory. This treatment have allowed one to implement the damping phenomena into the master equation separately from the coherent phenomena. In this way, one has reduced the complexity of the equations describing the system dynamics due to the adopted master equation formalism.

In what follows, the elements defined within this chapter will be used to build the analytical model of each particular investigated case. Each model consists of a system Hamiltonian describing all the coherent processes which appear within the quantum system. The system dynamics is described via the master equation of the quantum system, which is built from the damping terms and the Liouville-von-Neumann equation containing the Hamiltonian terms. However, in its ”rough” form, the master equation cannot be directly solved for more complex systems. It requires to adapt a set of various transformations and approximations in order to be solved without loosing too much of the generality of the problem. Therefore, each of the investigated quantum systems will require an additional particular treatment in order to be able to describe its dynamics and behaviour with enough precision.

3 AN ARTIFICIAL ATOM PLACED ON A MECHANICAL RESONATOR

In this chapter, one studies a system composed of an artificial atom placed on a quantum mechanical resonator. The system dynamics is investigated for moderate strong couplings of the artificial atom with the mechanical vibrations. For this coupling regimes, the analytic approach requires a treatment beyond the secular approximation of the system Hamiltonian in the interaction picture. One identifies that within strong coupling regimes, the generated mechanical vibrations show pure quantum features as sub-Poissonian distribution of the vibrational quanta. Moreover, within the cooling configuration, the quantum cooling effect is enhanced for this regime.

Let us consider a model consisting of a driven two-level quantum-dot embedded in a mechanical resonator made of a multi-layered acoustical nano-cavity, where the quantum-dot is pumped by an intense laser field and interacts with cavity single-mode phonon field as shown in Fig.3.1. This setup allows the cavity phonons to be created or annihilated depending on the chosen laser-quantum-dot detuning. The physics of this processes is explained as follows. The excitation of the quantum-dot corresponds to the formation of an exciton (electron-hole) localized within the quantum-dot. The interaction of the exciton charge with the deformation of the lattice is described via the deformation potential. Therefore, for a detuned laser, Raman-type transitions occur.

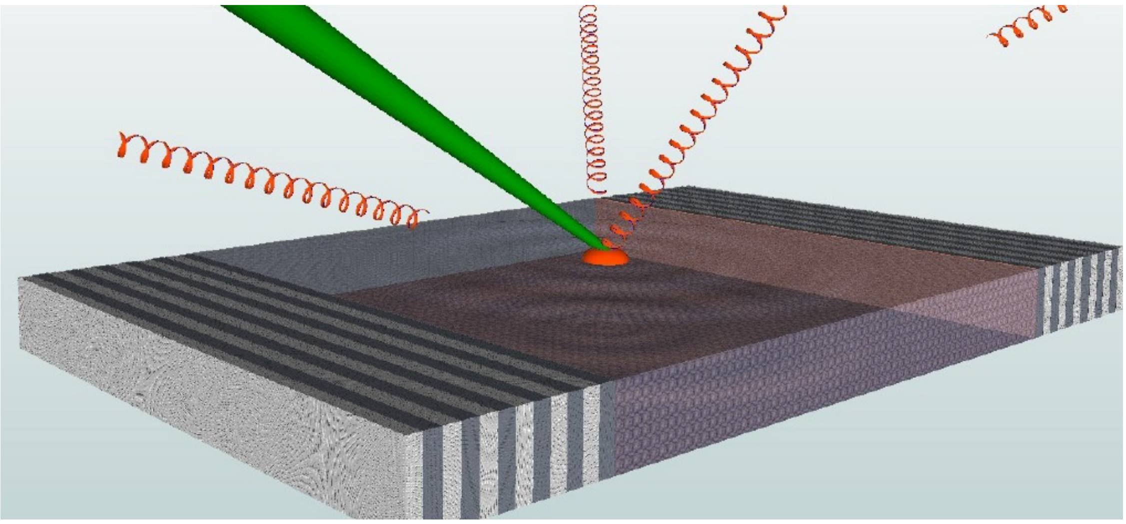

Fig. 3.1: The schematic of the investigated model: A two-level quantum-dot is embedded in a multilayered acoustical nanocavity. The quantum-dot is pumped near resonance with a coherent laser source and may spontaneously emit a photon.

For a blue-detuned laser, i.e., when the laser is set above the resonance frequency, the laser excitation leads to the creation of an exciton and phonons in the cavity through anti-Stokes-type transitions. This scheme does not lead to the generation of phonons as the created phonons are annihilated when the transition occurs in the opposite sense. This is valid as long as one does not consider the interaction of the quantum-dot with the surrounding electromagnetic vacuum, i.e., the quantum-dot spontaneous decay phenomenon. The last one, gives another possibility to the quantum-dot to decay, but this time without annihilating the mechanical vibrations. If considering both decay mechanisms, the system generates phonons but their field is infinitely increased as long as the mechanical resonator is considered perfect, i.e., no damping phenomena are introduced. Therefore, a third effect is introduced in order to describe a realistic system, which is the cavity damping by a thermal environmental reservoir. Thus, the leaking effect of the cavity will not allow the vibrational quanta to cumulate infinitely.

Red-detuned laser pumping leads to Stokes-type transitions, where a laser excitation of the quantum-dot occurs together with phonon annihilation. Similarly to the case of phonon generation, the cooling effect is achieved when the quantum-dot spontaneous emission and the thermal phonon reservoir are considered. When the quantum-dot spontaneously decay, the previously annihilated phonons are not created as it would be for the case of the decay under the laser pumping. Therefore, the cooling effect is achieved because of the spontaneous emission effect. But, if not considering the surrounding thermal environment, any cooling scheme would lead to an absolute cooling of the mode, which is not a realistic case. The thermal reservoir is required because of its pumping effect into the phonon mode, which balance the cooling effect and leads to a more realistic case.

In figure 3.2 a general overview of the system dynamics is given by the mechanical resonator mean phonon number as a function of the laser-quantum-dot detuning. At laser-quantum-dot resonance, there is no phonon emission or annihilation and the mechanical resonator is in equilibrium with the surrounding thermal bath. The blue-detuned laser pumping, i.e., negative detunings, leads to phonon generation, thus their mean number is increased over the value of the equilibrium with the thermal bath. The red-detuned case leads to cooling effect where the mean phonon number decreases down to the resonator near-ground-state.

In what follows, a more detailed description of the model is given in the next section, where the system Hamiltonian and its master equation are explained as well as its solving technique. The following three sections focus on the discussion of observed phenomena. Namely, the generation of sub-Poissonian distributed phonon fields is presented in section three, the quantum cooling effect and the phonon assisted population inversion in section four. The summary is given in section five.

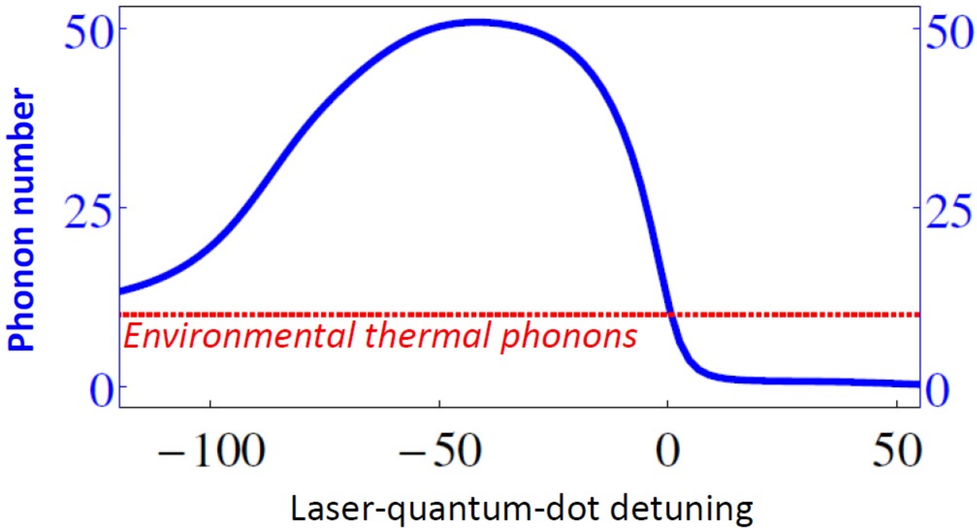

Fig. 3.2: The quantum dynamics of the mean phonon number of the mechanical resonator as function of the laser-quantum-dot detuning. The phonon generation and cooling regimes are defined by the sign of the detuning.

3.1 The model

The investigated dynamics is determined from the system Hamiltonian and its master equation which also includes the surrounding damping phenomena. The model consists of a pumped two-level quantum-dot with a transition frequency ω_{qd} described via Hamiltonian free term H_{QD} of eq.(2.3). The laser pumping effect is described via the semi-classic interaction term $H_{QD-laser}$ given in eq.(2.10) where the laser of frequency ω_L is treated in a classical way. The quantum-dot is embedded on a mechanical resonator of frequency ω_{ph}, which is described via the free term H_{ph} of eq.(2.35). The interaction of the quantum-dot with the quantum mechanical resonator is described via the term H_{QD-ph} given in eq.(2.46). Hence, the system Hamiltonian H is built as:

$$
\begin{aligned}
H &= H_{QD} + H_{ph} + H_{QD-laser} + H_{QD-ph} \\
&= \hbar\omega_{qd} S_z + \hbar\omega_{ph} b^\dagger b + \hbar\Omega(S^+ e^{-i\omega_L t} + e^{i\omega_L t} S^-) + \hbar g S^+ S^- (b^\dagger + b),
\end{aligned} \tag{3.1}
$$

where Ω is the Rabi frequency of the laser-quantum-dot interaction and g is the coupling strength of the interaction of the quantum-dot with the phonons of the mechanical resonator.

The master equation of the system density matrix operator ρ, is formed from the Liouville-von Neumann equation of eq.(2.47) of the Hamiltonian of eq.(3.1) together with the damping terms describing the resonator phonon field damping and pumping effects expressed via the term $\dot{\rho}_{field}$ of eq.(2.61) resulting from its interaction with a thermal environment, and the quantum-dot's spontaneous emission decay expressed via the term $\dot{\rho}_{SE}$ of eq.(2.64) and dephasing effect expressed via the term $\dot{\rho}_{dephasing}$ of eq.(2.67):

$$\begin{aligned}\dot{\rho} &= -\frac{i}{\hbar}[H,\rho] + \dot{\rho}_{field} + \dot{\rho}_{SE} + \dot{\rho}_{dephasing} \\ &= -\frac{i}{\hbar}[H,\rho] + \kappa(1+\bar{n})\mathcal{L}(b) + \kappa\bar{n}\mathcal{L}(b^{\dagger}) + \gamma\mathcal{L}(S^{-}) + \gamma_c\mathcal{L}(S_z),\end{aligned} \tag{3.2}$$

where κ is the phonon damping rate of a thermal reservoir described via its mean phonon number $\bar{n}$, γ is the spontaneous emission rate and γ_c is the dephasing rate.

In what follows, the system dynamics is found by projecting the master equation within the quantum-dot-phonon state basis. This leads to a system of coupled equations that may be numerically solved as the model's physical properties allows the system to be truncated. However, the master equation (3.2) with Hamiltonian of eq.(3.1) cannot be properly solved in its initial form, as it will require the implementation of drastic approximations leading to inaccurate results and even to a loss of quantum features. Hence, a series of transformations is applied in order to bring the master equation to a solvable form allowing the use of several approximations without loosing the generality of the investigation. More precisely, the system dynamics is solved via applying the dressed-state transformation to the quantum-dot state basis and then, in the interaction picture, one shall focus on simplifying the Hamiltonian and different master equation terms.

The semi-classical dressed-state transformation refers to the diagonalization of the Hamiltonian of the laser-quantum-dot sub-system defined via the free quantum-dot Hamiltonian term of eq.(2.3) and the quantum-dot-laser interaction term of eq.(2.10), where the laser is treated classically. The eigenstates of this subsystem are called the dressed-states and describe a new Hilbertian basis for the atomic states. The dressed-states are defined via a linear transformation of the initial, so called bare-states, defined as:

$$\begin{aligned}|+\rangle &= \sin\theta|g\rangle + \cos\theta|e\rangle, \\ |-\rangle &= \cos\theta|g\rangle - \sin\theta|e\rangle.\end{aligned} \tag{3.3}$$

where $\theta = \arctan(2\Omega/\Delta)/2$ and $\Delta = \omega_{qd} - \omega_L$. The new atomic operators are defined as:

$$
\begin{aligned}
R^{+} &= |+\rangle\langle-|,\\
R^{-} &= |-\rangle\langle+|,\\
R_{++} &= |+\rangle\langle+|,\\
R_{--} &= |-\rangle\langle-|,\\
R_{z} &= R_{++} - R_{--}. \qquad (3.4)
\end{aligned}
$$

Their expressions in the old basis, i.e., the bare-states, are deduced from the eqs.(3.3), which defines the new atomic commutation relation as:

$$
\begin{aligned}
[R^{\pm}, R^{\mp}] &= \pm R_z,\\
[R^{\mp}, R_z] &= \pm 2R^{\mp}. \qquad (3.5)
\end{aligned}
$$

Within the dressed-state basis, i.e., after diagonalization, the laser-quantum-dot sub-system Hamiltonian becomes:

$$
H_{sub-system} = \hbar\omega_{qd}S_z + \hbar\Omega(S^{+}e^{-i\omega_L t} + e^{i\omega_L t}S^{-}) = \hbar\bar{\Omega}R_z, \qquad (3.6)
$$

where $\bar{\Omega} = \sqrt{\Omega^2 + (\Delta/2)^2}$ is the generalized Rabi frequency for the detuned laser-quantum-dot interaction. Within the new basis, the Hamiltonian of the eq.(3.6) is significantly simplified up to a diagonal term and the full system Hamiltonian of eq.(3.1) is transformed as:

$$
\begin{aligned}
H &= \hbar\bar{\Omega}R_z + \hbar\omega_{ph}b^{\dagger}b\\
&+ \hbar g(b^{\dagger} + b)\{\sin^2\theta\, R_{--} + \cos^2\theta\, R_{++} - \frac{\sin(2\theta)}{2}(R^{+} + R^{-})\}. \qquad (3.7)
\end{aligned}
$$

In this form, all off-diagonal elements are related to the quantum-dot-phonon interaction term. Therefore, if changing the representation to the interaction picture of the Hamiltonian in its current form, this would allow one to distinguish the different off-diagonal terms according to their frequency of oscillation and to determine the criteria required for a rotating wave approximation (RWA) of the quantum-dot-phonon interaction. Note, that from a technical approach, the dressed-state transformation is a powerful analytical tool that allows one to apply some approximations to a particular set of off-diagonal elements after excluding the ones describing the laser-quantum-dot interaction. This method is used in various models and contexts, wherein the bare-state basis does not allow one to simplify the system dynamics and conserve the generality of the problem at the same time.

For the current model, the change of representation to the interaction picture of the dressed-state Hamiltonian is done via a unitary transformation $U(t) = e^{i(\bar{\Omega}R_z + \omega_{ph} b^\dagger b)t}$ according to the first two diagonal terms of eq.(3.7). Considering the phonon frequency ω_{ph} and the generalized Rabi frequency $\bar{\Omega}$ of same order, one splits the slow-rotating terms of the Hamiltonian oscillating at frequencies $\pm(\omega_{ph} - 2\bar{\Omega})$ from the fast-rotating ones corresponding to the frequencies $\pm\omega_{ph}$ and $\pm(\omega_{ph} + 2\bar{\Omega})$. Therefore, within the interaction picture, the system Hamiltonian is given as:

$$\begin{aligned}
H &= H_{slow} + H_{fast}, \\
H_{slow} &= -\hbar g \frac{\sin(2\theta)}{2}\{b^\dagger R^- e^{i(\omega_{ph}-2\bar{\Omega})t} + \text{H.c.}\}, \\
H_{fast} &= \hbar g(\sin^2\theta R_{--} + \cos^2\theta R_{++})\{b^\dagger e^{i\omega_{ph}t} + \text{H.c.}\} \\
&- \hbar g \frac{\sin(2\theta)}{2}\{b^\dagger R^+ e^{i(\omega_{ph}+2\bar{\Omega})t} + \text{H.c.}\}. \qquad (3.8)
\end{aligned}$$

Considering the criteria of splitting of the fast-terms, one may neglect H_{fast} via a secular approximation [179, 76] as long as $g \ll \omega_{ph}, \bar{\Omega}$, similarly to the approximation of eq.(2.9). This condition applied on the quantum-dot-phonon coupling strength defines the weak coupling regime. When the coupling constant g is increased closer to the magnitudes of ω_{ph} and $\bar{\Omega}$, the contribution of the fast-terms to the system dynamics continues to be small, however it cannot be completely neglected all the time. In this case, one may treat the contribution of H_{fast} as a first order perturbation. One refers to this coupling regimes as a strong coupling regime. Although, this regime implies stronger quantum-dot-phonon couplings comparing to the weak coupling case, note that one will further consider only moderate strong coupling constants that allows one to apply a perturbative treatment. Within the strong coupling regime, the first-order contribution of the fast rotating terms H^{eff}_{fast} is estimated as [188, 189]:

$$H^{eff}_{fast} = -\frac{i}{\hbar} H_{fast}(t) \int dt'\, H_{fast}(t') = H_0 - \hbar\bar{\Delta}R_z + \hbar\beta b^\dagger b R_z, \qquad (3.9)$$

where

$$\bar{\Delta} = \frac{g^2}{2}\left(\frac{\cos(2\theta)}{\omega_{ph}} - \frac{\sin^2(2\theta)}{4(\omega_{ph} + 2\bar{\Omega})}\right) \qquad (3.10)$$

and

$$\beta = g^2 \frac{\sin^2(2\theta)}{4(\omega_{ph} + 2\bar{\Omega})}. \qquad (3.11)$$

Here, H_0 is a constant and can be dropped as it does not contribute to the system's dynamics. The perturbative treatment of eq.(3.9) is completely compatible with the weak coupling regime as for smalls values of g, $\{\bar{\Delta}, \beta\} = 0$ and the contribution of the fast terms vanishes as in the case of the secular approximation. Moreover, the transition from one regime to other does not simply refers to the magnitude of g, but is related to the order of $\bar{\Delta}$ and β which are proportional to g^2. Therefore, one will further investigate the cases where a usual secular approximation is sufficient to fully describe the dynamics and the cases where the perturbative treatment is required, i.e., when the fast terms are introducing a change to the dynamics of the system and the secular approximation is no longer justified. One will refer to the last case as the beyond the secular approximation case.

The final Hamiltonian is defined as the sum of H_{slow} and H^{eff}_{fast}, and its expression is given back into the Schrödinger representation as:

$$\begin{aligned} H &= H_{slow} + H^{eff}_{fast} \\ &= \hbar(\omega_{ph} - 2\bar{\Omega})b^\dagger b - \hbar\bar{\Delta}R_z + \hbar\beta b^\dagger b R_z - \hbar g \frac{\sin(2\theta)}{2}\left(b^\dagger R^- + R^+ b\right). \end{aligned} \tag{3.12}$$

The previous transformations are also applied to the master equation of eq.(2.47). The dressed-state form of the master equation is given as:

$$\begin{aligned} \frac{\partial \rho}{\partial t} &= -\frac{i}{\hbar}[H, \rho] + \kappa(1+\bar{n})\mathcal{L}(b) + \kappa\bar{n}\mathcal{L}(b^\dagger) \\ &+ \gamma_+\mathcal{L}(R^-) + \gamma_-\mathcal{L}(R^+) + \gamma_0\mathcal{L}(R_z), \end{aligned} \tag{3.13}$$

where within the interaction picture, one has kept only the non-oscillating atomic damping terms and have neglected all other terms rotating at frequencies $\pm 2\bar{\Omega}$ via a secular approximation. This approximation is justified as long as $2\bar{\Omega} \gg \gamma$. Within the new basis, the spontaneous emission processes are described by three terms [190] determined by the quantum-dot's dressed-state decay rates:

$$\begin{aligned} \gamma_+ &= \gamma\cos^4\theta + \frac{1}{4}\gamma_c\sin^2(2\theta), \\ \gamma_- &= \gamma\sin^4\theta + \frac{1}{4}\gamma_c\sin^2(2\theta), \\ \gamma_0 &= \frac{1}{4}[\gamma\sin^2(2\theta) + \gamma_c\cos^2(2\theta)]. \end{aligned} \tag{3.14}$$

3.2 The master equation projection

In its current form, the master equation of eq.(3.13) with the Hamiltonian of eq.(3.12) may be solved by projecting it into the system basis. The projection of the density operator gives the elements of the density matrix. Therefore, the projection of the master equation leads to a system of differential equations given by the equations of motion of the density matrix elements. It is a system of coupled first order linear differential equation of dimension determined by the number of the quantum-dot states multiplied by the number of all possible phonon states. As the phonon field is defined within a basis of infinite states, the system is defined by $2 \times \infty$ variables. One shall further adapt the solving method to the properties of the phonon state basis in order to obtain a system of equation that may be truncated.

The phonon field basis, as the basis of any other single-mode boson field, is defined via the eigenfunctions of the Hamiltonian of the free field given within the second quantization of eq.(2.35), i.e., the Fock states. The phonon probability distribution is given via the diagonal elements of the reduced density matrix of the phonon field. The entire system is described within the Hilbert space defined by the quantum-dot-phonon state basis $\{|i, n\rangle\} \equiv \{|i\rangle \otimes |n\rangle\}$ which is a vectorial product of the atom dressed-state basis $\{|i\rangle, i \in \{|+\rangle, |-\rangle\}\}$ and phonon Fock state basis $\{|n\rangle, n \in \mathcal{N}\}$. In the Hilbert space, the phonon field represents a vectorial sub-space of the system, so its reduced density matrix is determined by tracing the system density matrix over the quantum-dot state basis, i.e., $\rho_{phonon} = Tr_{QD}[\rho]$. As the mechanical resonator is treated as a quantum field with a limited average number of phonons, its quanta probability distribution decreases asymptotically to zero when $n \to \infty$. In other words, the phonon probability to occupy a certain Fock state decreases to zero for high enough Fock states.

The model's dynamics is solved by using the asymptotic behaviour of the phonon distribution in order to truncate the system of equations of motion of the reduced density matrix elements. This criterion may be applied only to the diagonal matrix elements and the quantities related to them. However, a direct projection of the diagonal elements would require the use of off-diagonal elements that may not vanish for $n \to \infty$. The solving method consists in rearranging and combining those off-diagonal elements in order to form a closed system of equations of motion containing only the quantities that obey an asymptotic behaviour, instead of directly projecting all the involved matrix elements.

A first projection of the master equation of eq.(3.13) into the quantum-dot's dressed-state basis, defines the four equations of motion of the elements of the reduced quantum-dot density matrix

$\rho_{i,j} = \langle i|\rho|j\rangle$, where $\{i, j \in |+\rangle, |-\rangle\}$. The projection within the quantum-dot basis have eliminated the atomic operators from the equations of motion of $\rho_{i,j}$ that are defined only via the field's operators. A next projection within the phonon basis, will lead to a system of equations defined only via the scalar values of the projected quantities. One combines the off-diagonal matrix elements appearing in the equations of motion of $\dot{\rho}_{++}$ and $\dot{\rho}_{--}$ by forming Hermitian variables that contain the cross-correlation terms of the quantum-dot-phonon interaction [191]. The new set of variables is thus defined as:

$$\begin{aligned}
\rho^{(1)} &= \rho_{++} + \rho_{--}, \\
\rho^{(2)} &= \rho_{++} - \rho_{--}, \\
\rho^{(3)} &= b^{\dagger}\rho_{+-} - \rho_{-+}b, \\
\rho^{(4)} &= b^{\dagger}\rho_{+-} + \rho_{-+}b, \\
\rho^{(5)} &= \rho_{+-}b^{\dagger} - b\rho_{-+}, \\
\rho^{(6)} &= \rho_{+-}b^{\dagger} + b\rho_{-+}.
\end{aligned} \tag{3.15}$$

By forming the new set of Hermitian variables, one has eliminated the oscillating part of the off-diagonal elements that do not vanish asymptotically. Therefore, a further projection within the phonon basis will lead to a system that may be numerically solved. One continues to project within the quantum-dot basis the equations of motion of the new quantities, until the system of equation closes and finally obtain a set of six equations of motion, one for each of the new variables. The expressions of their equations of motion may be also deduced directly from the derivatives of $\rho_{i,j}$. A next projection within the phonon Fock basis $\{|n\rangle\}$ defines a new infinite system of differential equations where the variables are given by the scalar values $P_n^{(i)} = \langle n|\rho^{(i)}|n\rangle$:

$$\begin{aligned}
\dot{P}_n^{(1)} &= ig\frac{\sin(2\theta)}{2}\left(P_n^{(3)} - P_n^{(5)}\right) - 2\kappa(1+\bar{n})\left(nP_n^{(1)} - (n+1)P_{n+1}^{(1)}\right) \\
&- 2\kappa\bar{n}\left((n+1)P_n^{(1)} - nP_{n-1}^{(1)}\right),
\end{aligned}$$

$$\begin{aligned}
\dot{P}_n^{(2)} &= -ig\frac{\sin(2\theta)}{2}\left(P_n^{(3)} + P_n^{(5)}\right) 2(\gamma_+ - \gamma_-)P_n^{(1)} - 2(\gamma_+ + \gamma_-)P_n^{(2)} \\
&- 2\kappa(1+\bar{n})\left(nP_n^{(2)} - (n+1)P_{n+1}^{(2)}\right) - 2\kappa\bar{n}\left((n+1)P_n^{(2)} - nP_{n-1}^{(2)}\right),
\end{aligned}$$

$$
\begin{aligned}
\dot{P}_n^{(3)} &= ign\frac{\sin(2\theta)}{2}\left(P_n^{(1)} - P_n^{(2)} - P_{n-1}^{(1)} - P_{n-1}^{(2)}\right) - i\left(\beta(2n-1)-\delta\right)P_n^{(4)} \\
&- (\gamma_+ + \gamma_- + 4\gamma_0)P_n^{(3)} - \kappa(1+\bar{n})\left((2n-1)P_n^{(3)} - 2(n+1)P_{n+1}^{(3)} + 2P_n^{(5)}\right) \\
&- \kappa\bar{n}\left((2n+1)P_n^{(3)} - 2nP_{n-1}^{(3)}\right),
\end{aligned}
$$

$$
\begin{aligned}
\dot{P}_n^{(4)} &= -i\left(\beta(2n-1)-\delta\right)P_n^{(3)} - (\gamma_+ + \gamma_- + 4\gamma_0)P_n^{(4)} \\
&- \kappa(1+\bar{n})\left((2n-1)P_n^{(4)} - 2(n+1)P_{n+1}^{(4)} + 2P_n^{(6)}\right) \\
&- \kappa\bar{n}\left((2n+1)P_n^{(4)} - 2nP_{n-1}^{(4)}\right),
\end{aligned}
$$

$$
\begin{aligned}
\dot{P}_n^{(5)} &= -ig(n+1)\frac{\sin(2\theta)}{2}\left(P_n^{(1)} + P_n^{(2)} - P_{n+1}^{(1)} + P_{n+1}^{(2)}\right) - i\left(\beta(2n+1)-\delta\right)P_n^{(6)} \\
&- (\gamma_+ + \gamma_- + 4\gamma_0)P_n^{(5)} - \kappa(1+\bar{n})\left((2n+1)P_n^{(5)} - 2(n+1)P_{n+1}^{(5)}\right) \\
&- \kappa\bar{n}\left((2n+3)P_n^{(5)} - 2nP_{n-1}^{(5)} - 2P_n^{(3)}\right),
\end{aligned}
$$

$$
\begin{aligned}
\dot{P}_n^{(6)} &= -i\left(\beta(2n+1)-\delta\right)P_n^{(5)} - (\gamma_+ + \gamma_- + 4\gamma_0)P_n^{(6)} \\
&- \kappa(1+\bar{n})\left((2n+1)P_n^{(6)} - 2(n+1)P_{n+1}^{(6)}\right) \\
&- \kappa\bar{n}\left((2n+3)P_n^{(6)} - 2nP_{n-1}^{(6)} - 2P_n^{(4)}\right),
\end{aligned}
\tag{3.16}
$$

where $\delta = \omega_{ph} - 2\bar{\Omega} + 2\bar{\Delta}$. The dimension of the new system of equations is $6 \times \infty$, where the infinite dimension is introduced after the second projection by the infinite amount of the Fock states. When one uses the previously discussed truncation criterion, only a certain amount of first n_{max} Fock states is considered and the dimension of the system used for numerical calculation becomes $6 \times n_{max}$. The current projection method gives an important advantage over a direct projection mechanism, not only in terms of analytical accuracy of the approximations applied for its truncation, but also in terms of computational performance of the numerical calculations. From algorithmic point of view, the direct projection method leads to a system of dimension $\infty \times \infty$, that after truncation leads to an algorithm using a set of n_{max}^2 equations. This is a severe numerical limitation in number of elementary operations, comparing to the method of eqs.(3.15-3.16) which uses a system of only $6 \times n_{max}$ dimension.

The truncation threshold n_{max} depends of the mean number of the field bosons and their distribution. The applied threshold is validated empirically, by checking if a higher threshold will not introduce a significant change within the estimated statistics. The following results uses thresholds that give incertitudes of orders $10^{-5} - 10^{-4}$ if comparing to the results obtained with a higher threshold like, e.g., $2n_{max}$. The influence of a further increase of the threshold, may be monitored in order to verify the asymptotic behaviour. However, any increase of the threshold also increases the number of the numerical operation and, thus, decreases the computational power of the algorithm. Further, the thresholds are set for incertitudes of a few orders smaller than the value ranges of the investigated results. It is to note, that most of the plots are estimated by varying some of the system parameters and, at some point, it may drastically change the boson mean number or the field distribution. Therefore, a permanent evaluation of the validity of the applied threshold is recommended in order to validate the results.

The numerical algorithm was built in two different languages by using different numerical solving methods, in order to validate the numerical calculations. As one focuses on the steady-state behaviour of the statistics, the temporal derivates of the system variables are cancelled. This is possible to be done, as the system variables were built by eliminating the oscillatory elements of the off-diagonal terms. Within the steady-state regime, the differential system of equations is reduced to a simple linear system of coupled equations. It has been solved by using a C code for a solving method of linear matrix equations like $A \cdot X = B$ and also by using the Wolfram Mathematica's numerical solving methods like the NSolve[...] commands. As both algorithms lead to the same numerical results, the solving technique have been considered valid.

Once the equations of motion are solved, the system dynamics is found by combining the density matrix diagonal elements. The mechanical resonator's statistics are described via the mean phonon number $\langle n\rangle$ and the phonon-phonon second-order correlation function $g^{(2)}(0) = \langle b^\dagger b^\dagger b b\rangle / \langle b^\dagger b\rangle^2$. Both quantities are expressed only by field operators and may be deduced from the resonator's reduced density matrix. Let us consider a system made of two sub-systems A and B, and an operator $\mathcal{O}$ of the sub-system A. In the general case, the statistical value of any operator is found via the density matrix operator as $\langle\mathcal{O}\rangle = Tr[\rho\mathcal{O}]$. But as the operator $\mathcal{O}$ applies only to the sub-system A, it may be carried out from the tracing over the states of the sub-system B, i.e., $\langle\mathcal{O}\rangle = Tr[\rho\mathcal{O}] = Tr_B[Tr_A[\rho\mathcal{O}]]$. If one consider the case of the current model and the operator $\mathcal{O}$ as a field operator, then its statistical average is deduced as

$$\langle\mathcal{O}\rangle = Tr_{QD}[Tr_{phonon}[\rho\mathcal{O}]] = Tr_{QD}[\sum_{n=0}^{\infty}\langle n|\rho\mathcal{O}|n\rangle]. \tag{3.17}$$

The resonator's mean phonon number $\langle n\rangle$ is expressed from eq.(3.17) as:

$$\langle n\rangle \;\; = \;\; \langle b^\dagger b\rangle = Tr_{QD}\left[\sum_{n=0}^{\infty}\langle n|\rho\, b^\dagger b\,|n\rangle\right] = Tr_{QD}\left[\sum_{n=0}^{\infty} n\langle n|\rho|n\rangle\right], \tag{3.18}$$

where one has applied the field operators to the ket as $b^\dagger b\,|n\rangle = n|n\rangle$. Next, one develops the trace summation over the system states as:

$$\langle n\rangle = \sum_{i=\{+,-\}}\sum_{n=0}^{\infty} n\langle n,i|\rho|n,i\rangle = \sum_{n=0}^{\infty} n\langle n|\rho_{++}+\rho_{--}|n\rangle = \sum_{n=0}^{\infty} n\langle n|\rho^{(1)}|n\rangle, \tag{3.19}$$

where one has swapped the sums over the system states in order to perform the tracing over the quantum-dot's states first. Finally one may introduce in the last equality, the variables used in the system of equations (3.16), i.e., $P_n^{(1)}$ and truncate the sum over the infinite Fock states for the numerical calculus:

$$\langle n\rangle = \sum_{n=0}^{\infty} nP_n^{(1)} \simeq \sum_{n=0}^{n_{max}} nP_n^{(1)}. \tag{3.20}$$

In a similar way, the phonon-phonon second-order correlation function is estimated as:

$$\begin{aligned} g^{(2)}(0) &= \frac{\langle b^\dagger b^\dagger b\, b\rangle}{\langle b^\dagger b\rangle^2} = \frac{1}{\langle n\rangle^2} Tr_{QD}\left[\sum_{n=0}^{\infty}\langle n|\rho\, b^\dagger b^\dagger b\, b|n\rangle\right] = \frac{1}{\langle n\rangle^2} Tr_{QD}\left[\sum_{n=0}^{\infty} n(n-1)\langle n|\rho|n\rangle\right] \\ &= \frac{1}{\langle n\rangle^2}\sum_{i=\{+,-\}}\sum_{n=0}^{\infty} n(n-1)\langle n,i|\rho|n,i\rangle = \frac{1}{\langle n\rangle^2}\sum_{n=0}^{\infty} n(n-1)\langle n|\rho^{(1)}|n\rangle \\ &= \frac{1}{\langle n\rangle^2}\sum_{n=0}^{\infty} n(n-1)P_n^{(1)} \simeq \frac{1}{\langle n\rangle^2}\sum_{n=0}^{n_{max}} n(n-1)P_n^{(1)}, \end{aligned} \tag{3.21}$$

where one has applied the relation $b^\dagger b^\dagger bb\,|n\rangle = n(n-1)|n\rangle$.

Both of these parameters serve to the description of the quanta distribution of the resonator's vibrational motion. In terms of statistical distribution, the mean phonon number gives the information on the field intensity and gives the basic distribution parameter. The second-order correlation functions describes what kind of distribution one obtains. For coherent fields, described by Poissonian distributions, one obtains $g^{(2)}(0) = 1$. For more narrow distributions, the field's second-order correlation function decreases and has a minimum value $g^{(2)}(0) = 1/n$ for a completely narrow distribution like the Dirac delta function centred at n. The fields with narrower distributions are called sub-Poissonian distributed fields, while the Dirac peak corresponds to fields prepared in a pure Fock state. On the other side, broader distributions than the Poissonian ones, correspond to values $g^{(2)}(0) > 1$ and the case when $g^{(2)}(0) = 2$ represents a thermal distributed field with an exponential distribution. Fields with distributions of higher values of $g^{(2)}(0) > 2$ are called super-Poissonian fields and have a more prominent exponential-like behaviour than the thermal fields. Note, that the analysis of the second-order correlation function does not expand to the investigation of bunching or anti-bunching behaviours as one estimates here only the particular value $g^{(2)}(\tau = 0)$

of the general second-order correlation function $g^{(2)}(\tau) = \langle b^\dagger(t) b^\dagger(t+\tau) b(t+\tau)\, b(t)\rangle / \langle n\rangle^2$ [179].

In what follows, we shall study the system in the steady-state regime, i.e., $\dot{P}_n^{(i)} = 0$ for $\{i = 1 \cdots 6\}$. The second-order correlation function given by Eq. (3.21) and the average phonon number in Eq. (3.18) are used to describe the phonon field behaviors in the acoustical cavity mode [33]. The system of coupled equations (3.16) is completed with an additional equation describing the conservation of probability of the system wave function, that in the terms of density matrix operator is given as $Tr[\rho] = 1$, and once truncated the system is solved by setting the model's parameters $\{\gamma, \gamma_c, g, \omega_{ph}, \kappa, \bar{n}, \Omega, \Delta\}$.

3.3 Generation of sub-Poissonian distributed phonon fields

The main focus of the current investigation is the generation of phonon fields. As discussed at the beginning of the chapter, this is achieved within blue-laser configurations, i.e., when the laser frequency is set higher than the quantum-dot's transition frequency. Moreover, the possibility to generate coherent phonon fields in similar opto-mechanical devices has been reported in [18], together with a diverse palette of recent remarkable experimental achievements on the phonon laser analog obtained with piezoelectrically excited electromechanical resonators [15], laser driven compound microcavities [16] and trapped ions [17]. Therefore, the study of the fields statistics would allow one to understand the nature of the generated phonons and the possibility to confine a certain type of quantum fields.

As previously discussed, the coherent fields have a Poissonian distribution of quanta with a corresponding value of the second-order correlation function $g^{(2)}(0) = 1$. The sub-Poissonian distributed fields have their second-order correlation function values below unity and possess quantum features as they cannot be generated from classical sources and need some quantum setups and manipulations in order to be obtained. In this context, the coherent fields represent the edge between quantum sub-Poissonian fields and classical fields with $g^{(2)}(0) > 1$ like the thermal ones. In what follows, one will focus on the possibility to obtain a phonon laser analog with sub-Poissonian quantum features, by studying the required laser parameters as well as the influence of the thermal environment.

The influence of the pumping laser on the opto-mechanical setup within the steady-state regime is given in the Fig.3.3 where different mesh styles where used to differentiate the regions corre-

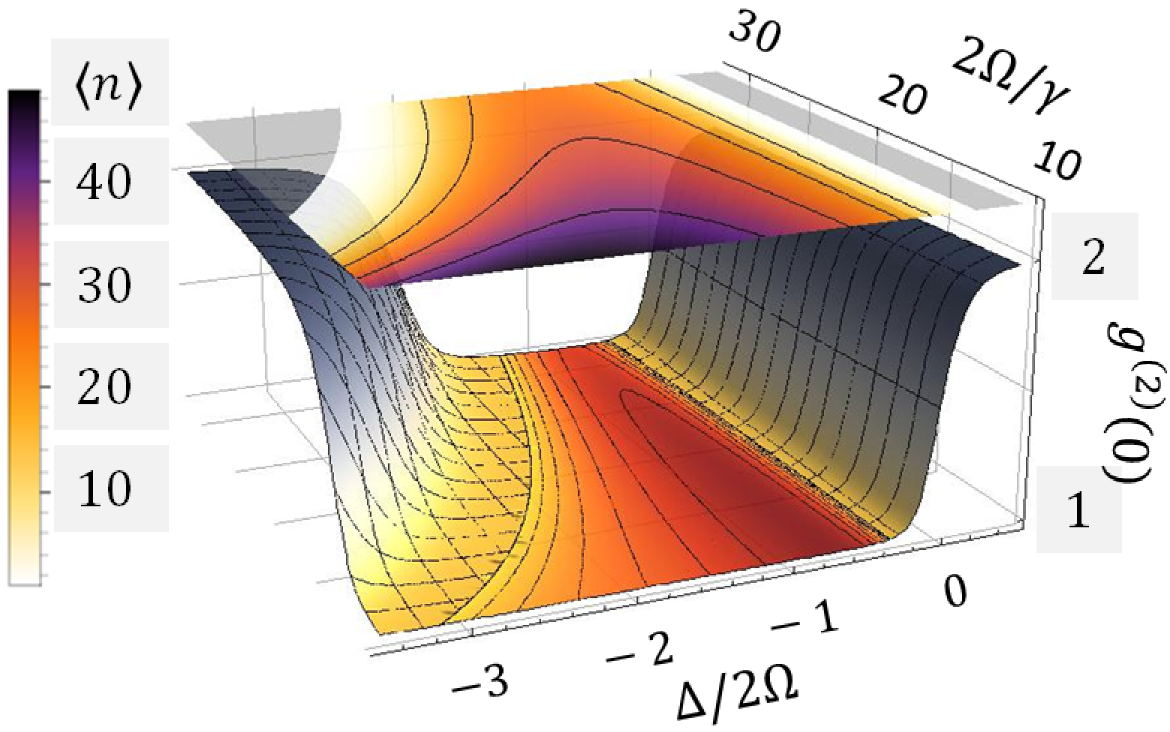

Fig. 3.3: The second-order phonon-phonon correlation function $g^{(2)}(0)$ (3D surface) and the mechanical resonator's mean phonon number $\langle n \rangle$ (2D density plot) as functions of the Rabi frequency 2Ω normalized by the quantum-dot spontaneous emission rate γ and the quantum-dot-laser detuning Δ normalized by the Rabi frequency. The figure is published in [151].

sponding to classical and quantum fields, i.e., the regions where $g^{(2)}(0)$ goes below or above unit. The system parameters were set to $\bar{n} = 0.01$, $\kappa/\gamma = 5 \times 10^{-3}$, $\gamma_c/\gamma = 0.1$, $g/\gamma = 15$ and $\omega_{ph}/\gamma = 30$. The gray transparent regions of the two-dimensional density plot are related to mean phonon numbers smaller than unity, i.e., $\langle n \rangle < 1$.

At quantum-dot-laser resonance, i.e., $\Delta = 0$, the laser excitations of the quantum-dot lead to no annihilation or creation of phonons. As expected, the mechanical resonator is found in equilibrium with its surroundings, whereas the mean phonon number corresponds to the thermal bath mean phonon number, i.e., $\langle n \rangle = \bar{n}$, while the phonon field is thermally distributed, i.e., $g^{(2)}(0) = 2$. A similar resonator-reservoir bath equilibrium is found for large detunings. Although for this case anti-Stokes type transition occurs, the quantum-dot-laser detuning is too high comparing to the resonator's frequency so that the transition probability converges to zero and, therefore, $\langle n \rangle \to \bar{n}$. Moreover, high enough laser frequencies could excite higher energetic levels so that the two-level model of the quantum-dot energetic structure would no longer be justified.

The relevant part of the results of the Fig.3.3 are found within the limits of the two-level model, i.e., for reasonable detuning values. The second-order correlation function region where sub-Poissonian distributed fields are generated is represented with a different mesh style and it overlaps with the region of the density plot where higher phonon numbers are generated. The model predicts quite intense phonon fields with quantum features. Lower laser intensity allows one to generate higher phonon numbers. This case corresponds to lower values of the Rabi frequency and weaker dynamic Stark splitting of the dressed-state energy levels, which allows more phonons to be generated when the spontaneous emission occurs. However, note that the current model is limited at lower values of Rabi frequencies by the requirements of the perturbative treatment of eq.(3.9).

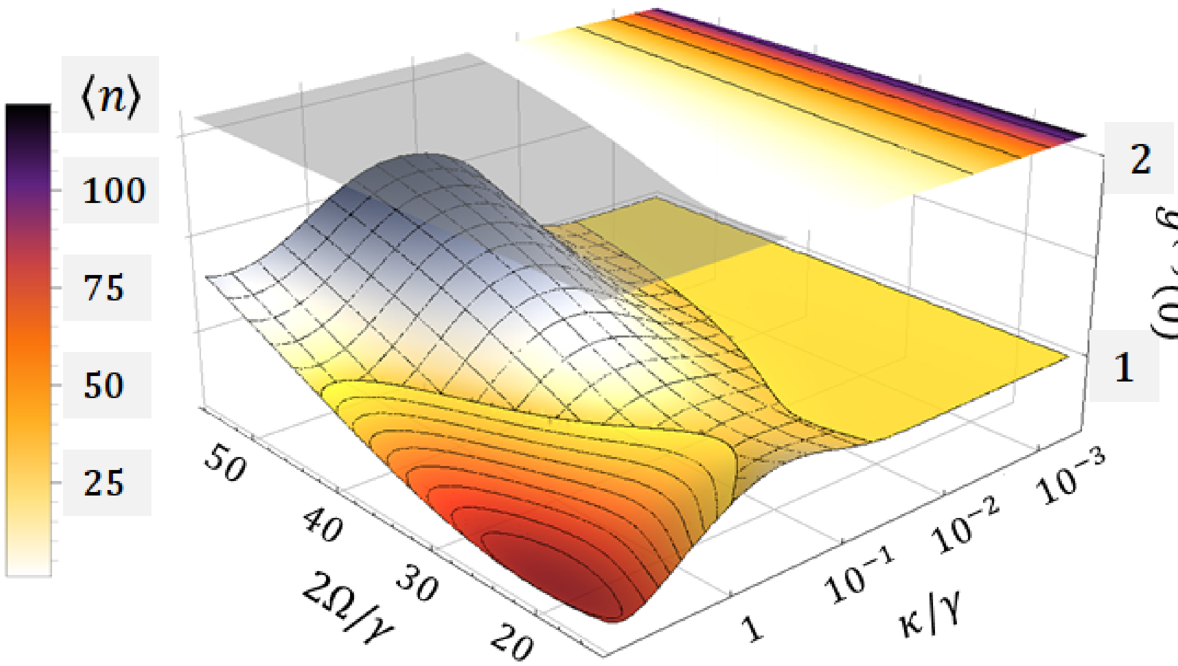

Fig. 3.4: The second-order phonon-phonon correlation function $g^{(2)}(0)$ (3D surface) and the mechanical resonator's mean phonon number $\langle n \rangle$ (2D density plot) as functions of the Rabi frequency 2Ω and the mechanical resonator damping rate κ, both normalized by the quantum-dot spontaneous emission rate γ.

The interaction of the system with the thermal surroundings is described in Fig.3.4, where one represents the previous quantities, i.e., the second-order correlation function and the mean phonon number, as functions of the Rabi frequency Ω and the resonator damping rate κ of its interaction with the thermal bath. The other system parameters are $\bar{n} = 0.01$, $\Delta/2\Omega = -0.7$, $\gamma_c/\gamma = 0.1$, $g/\gamma = 15$ and $\omega_{ph}/\gamma = 30$. Similarly to the previous figure, different mesh styles were used for the $g^{(2)}(0) < 1$ and $g^{(2)}(0) > 1$ plot regions. The choice of the laser-quantum-dot detuning Δ, was made from the Fig.3.3 where the plot region of $g^{(2)}(0) < 1$ with stronger sub-Poissonian behaviour have been selected. The second-order correlation function admits two separate plot regions where the vibrational quanta are sub-Poissonian distributed. These plot regions are represented in a different mesh style in Fig.3.4. As for the case of phonon generation small mean phonon numbers are irrelevant, the region of the density plot corresponding to $\langle n \rangle < 1$ is represented in transparent grey colour. Therefore, one observes that the plot region of sub-Poissonian distributed quanta corresponding to strong reservoir-resonator couplings, i.e., higher orders of magnitude of the thermal damping rate of $\kappa/\gamma \sim 1 - 10$ are not of interest to the study of phonon emission as the generated mean phonon number is small due to strong phonon leaking into the thermal bath.

The relevant plot region corresponds to weak reservoir-resonator interactions which reduces the phonon losses. The small values of the thermal damping rate κ can be also determined by the chosen mechanical resonator, able to capture a single phonon mode with a high quality factor $Q = \omega_{ph}/\kappa$. In Fig.3.4 the plot region where the phonon losses are small, i.e., $\kappa/\gamma < 10^{-2}$, allows sub-Poissonian distributions to be obtained for a high mean phonon number generated in the mechanical resonator. And the mean phonon number $\langle n \rangle$ within the steady-state regime is increasing when the damping rate κ is decreasing.

The phonon distribution $P_n \equiv P_n^{(1)}$ for a system with two different damping rates is represented in Fig.3.5. One considers here a system described by $2\Omega/\gamma = 20$, $\Delta/2\Omega = -0.8$, $\gamma_c/\gamma = 0.1$, $g/\gamma = 10$, $\omega_{ph}/\gamma = 20$ and a thermal bath with $\bar{n} = 0.1$. The strong damping case is given when the system interacts with the bath at a damping rate of $\kappa/\gamma = 25$ and the corresponding phonon distribution is represented in red bars. The weak damping case is given for $\kappa/\gamma = 4 * 10^{-3}$ and the corresponding phonon distribution is represented in blue bars.

When the system is strongly damped, the steady-state regime represents an equilibrium of the mechanical resonator with the thermal reservoir. In Fig.3.5 one has treated the case when the mean phonon number decreases to $\langle n \rangle \simeq 0.111$, close to the bath mean phonon occupation number of $\bar{n} = 0.1$. The second-order correlation function reaches the value of $g^{(2)}(0) \simeq 1.98$ close to the value of a pure thermal field $g^{(2)}(0) = 2$. In this case the phonon distribution is well fitted by a pure thermal distribution given via the distribution function [179]:

$$P_n = \frac{\langle n \rangle^n}{(\langle n \rangle + 1)^{n+1}}. \tag{3.22}$$

The case of a weaker damping of the mechanical resonator leads to a quasi-coherent phonon field with a significant increase of the mean phonon number $\langle n \rangle \simeq 29$. The mean phonon number may be further increased by decreasing the resonator's damping rate or by increasing the phonon-coupling constant. However, the increase of the coupling constant is strongly restricted by the considered theoretical model and, more precisely, by the first order perturbation treatment applied

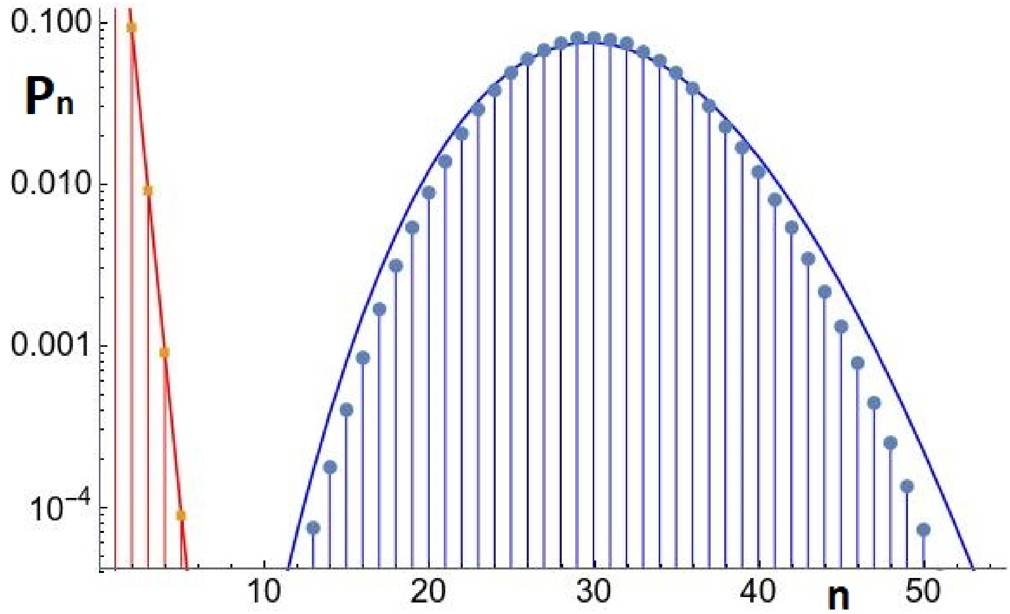

Fig. 3.5: The phonon probability distribution for different thermal damping rates. On the left side, the red bars represent the case of strong thermal damping. On the right side, a weak damping case is represented in blue bars.

to the fast rotating terms of the system Hamiltonian in the dressed-state interaction picture. A coupling strength g higher then the orders of magnitude of ω_{ph} or $\bar{\Omega}$ would no longer justify the applied approach and would require to consider higher orders of the perturbation development of eq.(3.9). Still, the current literature report experimental realization of nano-mechanical resonators and acoustic cavities with quality factors of higher than 10^4 order, therefore even higher phonon numbers than the ones reported in Fig.3.5 may be considered.

In Fig.3.5 one also compares the observed quanta distribution of the steady-state phonon field with a coherent field distribution defined as a Poissonian distribution given as:

$$P_n = \frac{\langle n\rangle^n e^{\langle n\rangle}}{n!}, \tag{3.23}$$

where one has used the observed value of $\langle n\rangle \simeq 29$. The second order correlation function of a coherent field is $g^{(2)}(0) = 1$, while for the observed one obtains $g^{(2)}(0) \simeq 0.99$. The difference between the theoretical distribution and the observed one is about 1% in terms of $g^{(2)}(0)$. It is similar to the thermal equilibrium case of the strong damping regime, where this difference was in the same vicinity of 1%. However, the theoretical fit does not match so well the expected quasi-coherent distribution. The obtained phonon field has a visibly narrower distribution, although the small difference in $g^{(2)}(0)$ terms. This feature of a narrower distribution represents a sub-Poissonian distributed phonon field, which is defined for correlation function values in the range of $g^{(2)}(0) < 1$. Sub-Poissonian quanta distributions represent a pure quantum feature of a field as classical field sources do not allow one to obtain this type of fields and quantum manipulations are required.

Another parameter which influences the phonon damping phenomena is the temperatures of the surrounding reservoir, which is related to the mean phonon number of the thermal bath $\bar{n}$. The temperature effect on the damping mechanics is represented in Fig.3.6, where different orders of magnitude of $\bar{n}$ were considered. Here, the phonon statistics evolution as function of normalized damping rate κ was plotted for different bath phonon numbers. The system parameters are the same as in Fig.3.5.

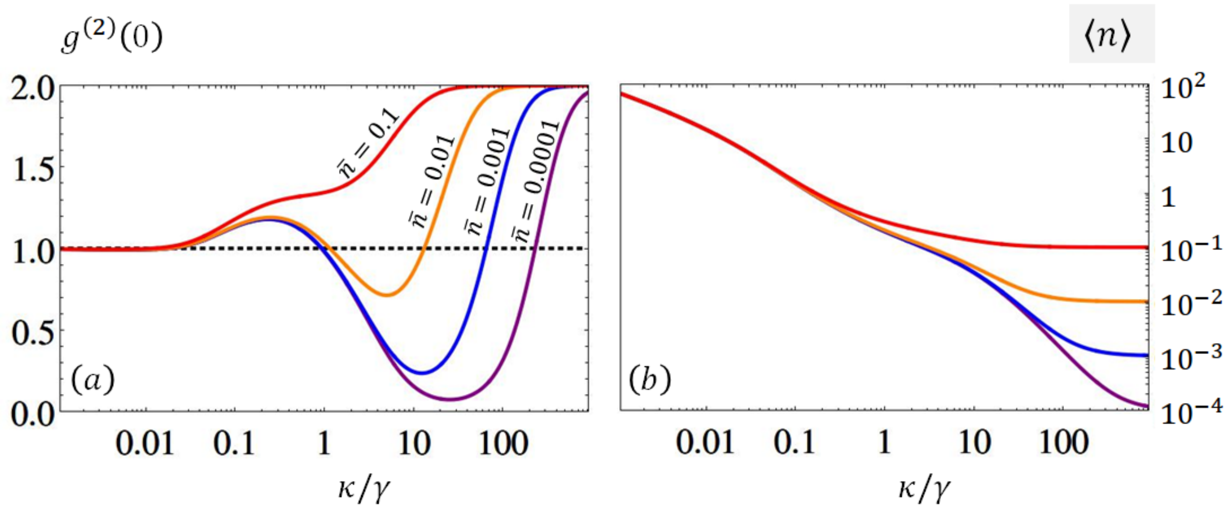

Fig. 3.6: (a) The phonon second-order correlation function $g^{(2)}(0)$ and (b) the mean phonon number $\langle n \rangle$ as function of normalized damping rate κ for different surrounding temperatures.

The previously discussed weak damping regimes are not affected by the considered change of the surrounding temperatures. All curves converge when decreasing the damping rate κ. However, higher temperatures, i.e., higher values of $\bar{n}$, allow the thermal equilibrium to be reached at considerably lower damping rates. Therefore, the definition of weak damping regime where quasi-coherent phonon field are obtained and strong damping regimes corresponding to a quasi-equilibrium with the thermal surrounding is related not only to the damping rate, but also to the temperature of the thermal bath.

It is to note, that for strong damping regimes, the decrease in temperature leads to prominent sub-Poissonian phonon distributions. This suggests that one is able to obtain narrower distributions of quantum states by decreasing the temperature of the surrounding environment. Within this condition, the phonons of the mechanical resonator are more likely to be found in some specific quantum states, as the probability distribution becomes more centred around the value of the mean phonon number. This effect could be explored to improve the discreteness of the phonon states in order to prepare the mechanical oscillator as a superposition of only a few Fock states or in a pure

Fock state. However, the regions with prominent sub-Poissonian distributions of Fig.3.6, does not allow one to obtain significantly high values of the mean phonon number at low temperatures.

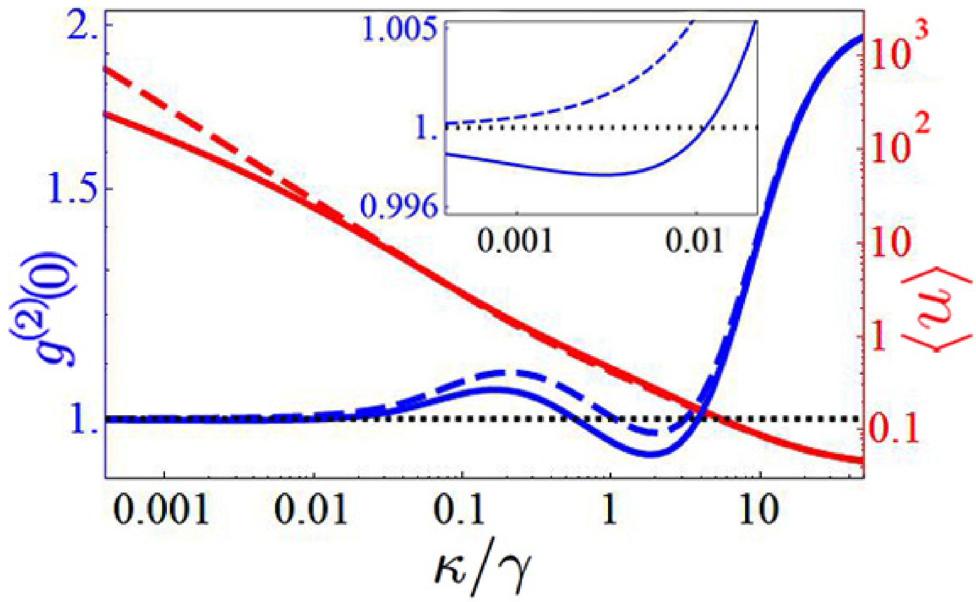

Fig. 3.7: The phonon statistics, i.e., $g^{(2)}(0)$ represented in blue curves and $\langle n \rangle$ plotted in red curves, as functions of the normalized cavity damping rate κ. The beyond the secular approximation treatment is given in continuous curves, whereas the dashed curves represent the treatment within the secular approximation. The figure is published in [151].

One of the most distinctive aspect of the current theoretical model consists in the implementation of a perturbation treatment to the fast rotating Hamiltonian terms within the dressed-state basis and interaction picture. As previously discussed in eq.(3.9), this method allows one to go beyond a traditional secular approximation and consider the regime of moderate strong couplings where the fast terms may be treated as a perturbation of the system Hamiltonian, instead of being definitively neglected. In order to highlight the contribution of the fast terms to the system dynamics, the current model is compared to a similar model where a secular approximation was applied. In Fig.3.7 one presents the phonon statistics for two different models, i.e., the one that goes beyond the secular approximation (continuous curves) and the other treated within the secular approximation (dashed curves). The second order correlation function is represented in blue lines and the mean phonon number in red lines. The other system parameters are $2\Omega/\gamma = 25$, $\Delta/(2\Omega) = -0.7$, $\bar{n} = 0.04$, $\gamma_c/\gamma = 0.1$, $g/\gamma = 15$ and $\omega_{ph}/\gamma = 35$.

One observes that the estimated second-order correlation functions in both cases converges for higher and smaller cavity damping rates. Although both models predict $g^{(2)}(0) \simeq 1$ for lower values of κ/γ, the quantum features are proper only beyond the secular approximation. The inset of Fig.3.7 gives a close look on how the second-order correlation function converges to a a quasi-coherent field in the weak damping regime, in the region around $10^{-3} \leq \kappa/\gamma \leq 10^{-2}$. The secular approximation model predicts a classical field as its distribution is always a bit larger than the Poissonian, i.e., one observes $g^{(2)}(0) > 1$ while asymptotically converging. On the contrary, the treatment beyond the secular approximation predicts a similar quasi-coherent phonon distribution, but with $g^{(2)}(0) < 1$. Thus, only the beyond the secular approximation model may reveal to quantum features of the phonon field. Moreover, for the weak damping regime, a significant change in the estimation of the mean phonon number $\langle n \rangle$ is introduced by the model beyond the secular approximation.

The perturbation terms become more important for the second-order correlation function in the region of stronger damping rates, i.e., in the region about $0.1 \leq \kappa/\gamma \leq 1$. Although, in this region, the overall behaviour of the system dynamics is the same for both models, the beyond the secular approximation model predicts a more prominent sub-Poissonian distribution.

3.4 Quantum cooling and phonon assisted population inversion

The contribution of the fast rotating terms to the system dynamics have shown some significant contribution to the estimation and understanding of the process of phonon generation scheme. One has used a blue-detuned pumping laser, i.e., $\omega_{qd} < \omega_L$, which leads to a phonon generation process. Stronger quantum-dot-phonon coupling regimes were considered where the contribution of the fast-rotating terms of the system "dressed" Hamiltonian can be treated as a perturbation. In this paragraph, one proposes to switch the pumping laser detuning to the red-detuned region,, i.e., $\Delta = \omega_{qd} - \omega_L > 0$, where quantum cooling effect can be achieved, and to investigate the consequences of the perturbation treatment on this effect.

The quantum dynamics of the system is investigated in the steady-state regime via the cavity mean phonon number $\langle n \rangle$ and its second-order phonon-phonon correlation function $g^{(2)}(0)$ presented in Fig.3.8 as functions of the detuning Δ divided by the Rabi frequency Ω. The other system parameters are $\kappa/\gamma = 10^{-3}$, $\bar{n} = 30$, $2\Omega/\gamma = 40$, $g/\gamma = 30$, $\gamma_c/\gamma = 0.1$ and $\omega_{ph}/\gamma = 35$. The negative laser-quantum-dot detuning, i.e., a blue-detuned laser, corresponds to anti-Stokes transitions that leads to the generation of phonons and thus to values of $\langle n \rangle$ considerably higher than than the thermal bath mean phonon number $\langle n \rangle \gg \bar{n}$. The quantum-dot-laser resonant case, i.e., $\Delta = 0$, does not contribute to the phonon statistics as there does not occur any Raman-type interactions and the cavity is in equilibrium with the thermal reservoir. Consequently, the mean phonon number is given by $\langle n \rangle = \bar{n}$ and the phonons are thermally distributed, i.e., $g^{(2)}(0) = 2$.

The quantum cooling regime is reached for red-detuned laser, i.e., in the region $\Delta > 0$. The cooling mechanics is based on Stokes transitions among the laser driven quantum-dot and phonons combined with the spontaneous emission effect, as discussed at the beginning of this chapter. The mean phonon number $\langle n \rangle$ first decreases to the near-ground state. However, the Raman type transitions are less probable to occur for very high quantum-dot-laser detuning values compared to the mechanical vibration frequency, leading to a less prominent cooling effect. As the cooling effect weakens, the mechanic resonator rests in quasi-equilibrium state with the thermal bath, i.e., $\langle n \rangle \simeq \bar{n}$ and $g^{(2)}(0) \simeq 2$, for $\Delta \gg \omega_{ph}$.

Within the strong coupling regime, the model beyond the secular approximation expressed via continuous lines, predicts an enhanced maximum cooling effect if comparing to the secular approximation treatment expressed via dashed lines. Although being small, the main contribution of the fast-rotating terms becomes significant in the region where the mean phonon number is decreased as well. The predicted mean phonon number is cooled down to the minimum value $\langle n \rangle_{min} \simeq 0.12$

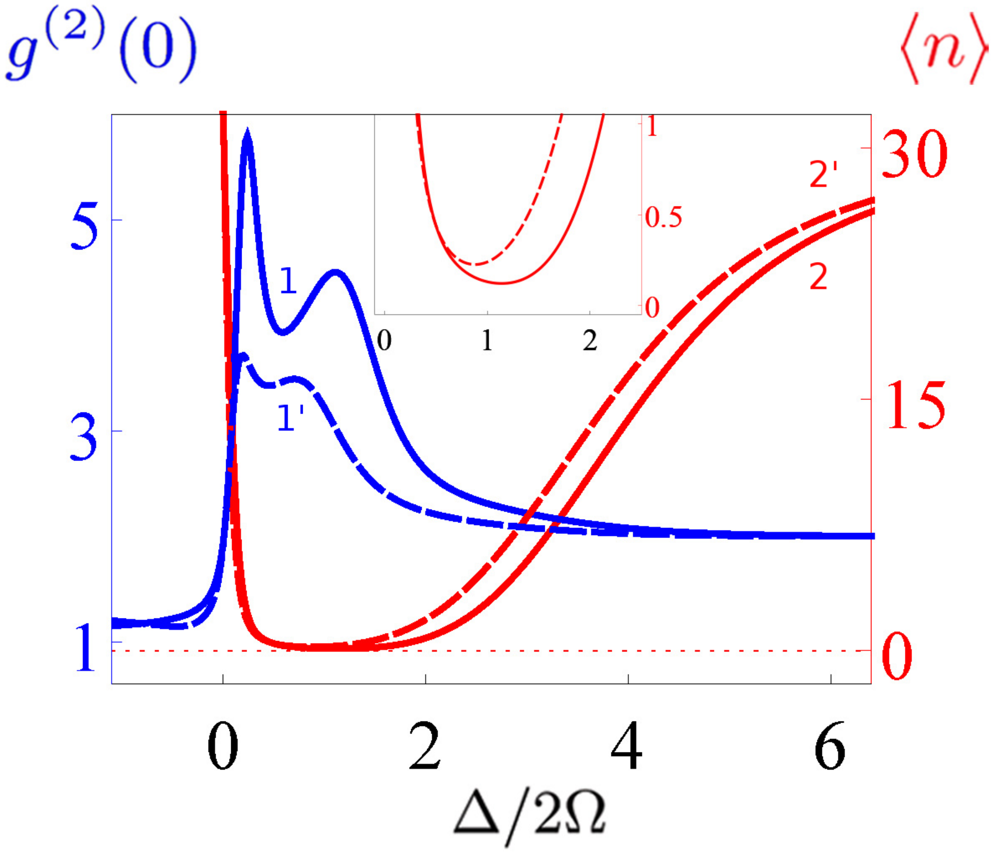

Fig. 3.8: The second-order phonon-phonon correlation function $g^{(2)}(0)$ (blue curves 1 and 1') and the mechanical resonator mean phonon number $\langle n \rangle$ (red curves 2 and 2') as functions of the ratio of detuning Δ and Rabi frequency Ω, within the secular approximation (dashed lines 1' and 2') and beyond the secular approximation, i.e., considering the fast rotating terms (continuous lines 1 and 2). The inset represents a close look at the mean phonon number when maximum cooling effect occurs. The figure is published in [137].

for the beyond the secular approximation case, which is approximatively a twice better result comparing to the secular approximation treatment which predicts a minimum of $\langle n \rangle_{min} \simeq 0.23$.

Another improvement brought by the beyond the secular approximation treatment consists in the shifting of the predicted detuning position when maximum cooling is achieved and in a wider range of the possible laser detunings which can be applied for cooling the mechanical resonator in its ground-state vicinity. Note that the cooling scheme is considered in the good cavity limit of the phonon fields, i.e., $\kappa \gg \gamma$. One also requires high damping rates κ comparing to the temperature of the environmental reservoir, in order to sufficiently reduce the pumping effect of the thermal bath and, thus, reach the near-ground-state of the mechanical resonator.

As expected, one observes super-Poissonian behaviour of the vibrational quanta during the cooling effect. This behaviour is also affected in the strong coupling regime and the fast-rotating terms give a more accurate description of it. An analogy may be made with the phonon laser effect, where these terms changes the distribution of the phonon emission from a coherent to a sub-Poissonian one [151].

The focus of the study of phonon assisted population inversion is made on the statistics of the created steady-state phonon fields of the quantum mechanical resonator and, furthermore, one investigates how the created phonon field influences the artificial atom's state in the steady-state regime. The entire process is controlled by the laser's parameters and various acoustic nano-cavities or nano-beams with different damping rates are considered in order to obtain the weak and strong damping regimes. The quantum-dot's behaviour is described by the population inversion W term, which has negative values when the quantum-dot is more likely to be in the ground state and positive values for the quantum-dot more probably to be found in the excited state.

The population inversion represents the quantity $\sigma_z = |e\rangle\langle e| - |g\rangle\langle g|$ which may be expressed through the atomic operators as $\sigma_z = 2S_z$. Within the dressed-state transformation of eqs.(3.3), S_z is defined as:

$$S_z = \frac{cos(2\theta)}{2} R_z. \tag{3.24}$$

The statistical average of σ_z, $W = \langle \sigma_z \rangle$, is deduced by tracing over the quantum-dot-phonon system states, the quantity $R_z\rho$ as discussed in eq.(3.17). Namely:

$$W = \langle (|e\rangle\langle e| - |g\rangle\langle g|)\rho\rangle = \cos(2\theta)\langle R_z\rho\rangle = \cos(2\theta) Tr_{phonon}[Tr_{QD}[R_z\rho]]. \tag{3.25}$$

Within the dressed-state basis, the population inversion may be estimated from the numerical system of eqs.(3.16), similarly to the calculus applied with eqs.(3.18-3.21):

$$\begin{aligned} W &= \cos(2\theta) Tr_{phonon}[Tr_{QD}[R_z\rho]] = \cos(2\theta) Tr_{phonon}[\sum_{i=\{+,-\}} \langle i|R_z\rho|i\rangle] \\ &= \cos(2\theta) Tr_{phonon}[\rho_{++} - \rho_{--}] = \cos(2\theta) Tr_{phonon}[\rho^{(2)}] \\ &= \cos(2\theta) \sum_{n=0}^{\infty} \langle n|\rho^{(2)}|n\rangle = \cos(2\theta) \sum_{n=0}^{\infty} P_n^{(2)} \simeq \cos(2\theta) \sum_{n=0}^{n_{max}} P_n^{(2)}, \end{aligned} \tag{3.26}$$

where in the first line, one has traced over the atomic dressed-states. In the second line, one has inserted the quantity $\rho^{(2)}$ defined the eq.(3.15), which have allowed one to introduce the variables $P_n^{(2)}$ in the last line of eq.(3.26) after tracing over the phonon infinite Fock states. Within the last equality, one has truncated the sum of the infinite phonon states at a certain n_{max} of considered Fock states as discussed in eq.(3.20).

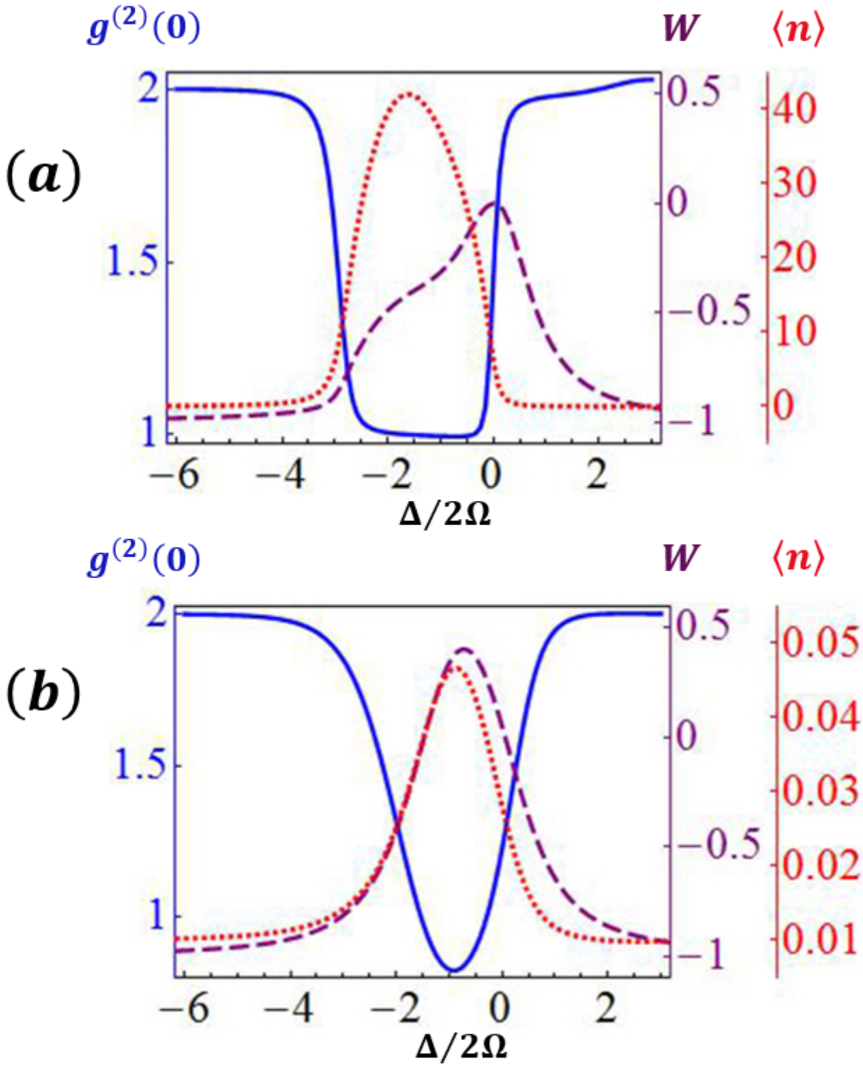

Fig. 3.9: The second-order correlation function $g^{(2)}(0)$ (continuous blue curve), the mean phonon number $\langle n \rangle$ (dotted red curve) and the quantum-dot's population inversion W (dashed purple curve) as functions of the laser's normalized detuning Δ. (a) For a weak damping regime with $\kappa/\gamma = 10^{-3}$ and (b) for a strong damping regime with $\kappa/\gamma = 15$. .

Two different damping regimes of the studied model are represented in Fig.3.9, corresponding to low and high damping rates, with $\kappa/\gamma = 10^{-3}$ and $\kappa/\gamma = 15$ respectively. The phonon field statistics is given by the second-order correlation function represented in blue continuous curves and the mean phonon number represented in red dotted lines, while the quantum-dot statistics is given by the population inversion W represented in purple dashed curves. The other model's parameters are: $\bar{n} = 0.01$,$\Omega/\gamma = 25$, $\gamma_c/\gamma = 0.1$, $\omega_{ph}/\gamma = 35$, $g/\gamma = 25$.

In the first case shown in Fig.3.9(a), for low damping rates of the order of $\kappa/\gamma \sim 10^{-3}$, the acoustical field's statistics are modified to a less prominent sub-Poissonian behaviour but a higher mean phonon number in the cavity. The population inversion is always negative, so that this regime is of no interest for monitoring the quantum-dot's state. However, for the studies of the phonon fields' statistics only, one has previously shown that quite strong fields with quantum statistics may be obtained in an enough realistic case (see Fig.3.3 and Fig.3.4). Actually in both cases of Fig.3.9, the phonon field statistics is similar to what has been discussed in the previous section on the investigation of the phonon generation model.

The second case shown in Fig.3.9(b), corresponding to high damping rates of the order of $\kappa/\gamma \sim 10$, is described for a well-chosen detuning, by weak phonon fields with a prominent sub-Poissonian distribution. This quantum feature is obtained for similar detuning range as in the weak damping case. Under the phonon field's action, the quantum-dot's population is inverted in the region where the field is more intense and reaches the maximum level in the region of sub-Poissonian fields. Thus, an information about the quantum-dot's state can be obtained by monitoring the phonon fields' statistics and vice versa.

3.5 Conclusions of Chapter 3

In this chapter, one has investigated the phonon quantum statistics of a mechanical resonator strongly coupled to a pumped two-level quantum-dot in the steady-state regime. Various laser-quantum-dot detunings have been considered in order to reach the phonon generation regime or the quantum cooling regime. Different damping rates of the mechanical resonator, have been considered as well.

The particularity of the current model consists in evaluating the contribution of the fast-rotating terms of the "dressed" quantum-dot-phonon interaction as a first order perturbation of the system dynamics, instead of completely neglecting them. This condition is achieved by considering stronger qubit-phonon couplings than an usual secular approximation requires, but not very strong so that the first order perturbation treatment remains valid. One has compared the current model, which goes beyond the secular approximation treatment to the case when this approximation is applied. One has shown, that although the contribution is small or completely negligible most of the time, it may introduce significant correction to the obtained results and interpretation in different scenarios.

Within the phonon generation regime, i.e., when a blue-detuned laser is applied, the current model gives a better interpretation of the generation process. One has shown, that the mechanical resonator possess quantum features as the sub-Poissonian distributed vibrational quanta. Although, in any case one observes quasi-coherent generated phonon fields for small phonon damping rates, only the beyond the secular approximation case shows that this fields has a sub-Poissonian distribution. Moreover, ignoring the fast-rotation terms contribution would lead to an erroneous estimation of the phonon field strength, i.e., the mean phonon number of the mechanical resonator. This investigation predicts that the phonon lasing effect that may be achieved via the current optomechanical setup, has a quantum feature.

Within the cooling regime,i.e., for a red-detuned laser pumping, a different laser-quantum-dot detuning for a maximal quantum cooling effect have been estimated when the beyond the secular approximation treatment had been applied. Also, stronger cooling had been predicted, by obtaining a twice lower minimum phonon number. In this configuration, the fast terms play an essential role in the behaviour of the phonon statistics, describing a more prominent super-Poissonian statistics during the cooling process.

Finally, regimes related to high damping rates, correspond to the case where the quantum-dot's population is inverted by the created phonon fields. Moreover, one shows that for this regime the maximum of the population inversion is located in the region were the phonon field is more intense and possesses a more prominent sub-Poissonian distributions.

4 AN ARTIFICIAL ATOM PLACED IN AN OPTICAL RESONATOR

In this chapter, one investigates the case when a three-level equidistant ladder-type quantum-well is placed in an optical cavity. The quantum-well is pumped via two lasers with different phases. Each laser is applied resonantly on one of the two quantum-well transitions. Under the laser driving, the energetic levels of the quantum-well are subject to the dynamical Stark splitting effect, as shown in Fig.4.1. Various transitions with different transition frequencies appear among the split energy levels. In the case of driven two-level emitter, one observes three different transitions in the emitter's emission spectra called the Mollow triplet. The Mollow triplet is made of a central peak corresponding to the free emitter transition energy and two sidebands equally shifted on both sides of the central peak. In the case of a driven three-level emitter even more sidebands appear. In this research, one has considered an equidistant three-level emitter. As both transitions occur at same frequency, the emission spectra of the laser driven quantum-well is made of a central peak and two pairs of sidebands.

As the quantum-well architecture has equidistant energy levels and orthogonal transition dipoles, the optical cavity couples to both emitter's transitions in the good cavity limit. As under the laser pumping the quantum-well is prepared in a superposition of states, the cavity indistinguishably interacts with the upper and lower transitions. These indistinguishable amplitudes of the cavity interaction with different quantum-well transitions lead to the interference effect. In order to solve the system dynamics, one was able to significantly reduce the complexity of the quantum dynamics without loosing much of generality of the problem by successively tuning the cavity in resonance with one of the frequencies of the emitter's spectra.

As the interaction amplitudes may be influenced by laser intensities and phases, one is able to achieve strong destructive quantum interferences. Therefore, the cavity field may be emptied for a well-chosen laser phase difference as the laser phases are transferred to the interactional amplitudes. In this case, the pumped quantum-well spontaneously decays in all directions except the cavity. Furthermore, this behaviour of the interfering the quantum-well-cavity system is associated with a quantum switch, where the income laser signals may switch the cavity field on and off by varying their phase difference and intensity.

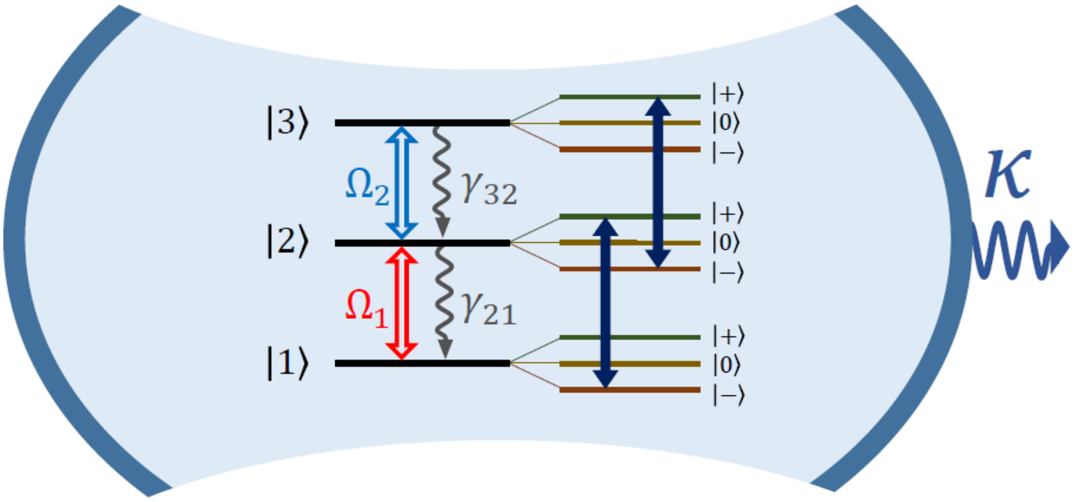

Fig. 4.1: Schematic of the model. A three-level atom, placed in a leaking optical cavity, interacts with external coherent fields with $\Omega_{2,1}$ being the corresponding Rabi frequencies. γ_{32} and γ_{21} are the respective spontaneous emission decay rates. The full arrows depict the dressed-state transitions in resonance with the cavity mode frequency leading to cavity quantum interference phenomena.

4.1 The model

The quantum-well is described by its bare-states $|i\rangle$, $\{i = 1, 2, 3\}$ and their corresponding energies $\hbar\omega_i$. The quantum-well free Hamiltonian is expressed from the eq.(2.3). The only difference with the two-level case, is that this time summation is performed over all the three atomic eigenenergies. The atomic operators of the three-level emitter are defined as $S_{ij} = |i\rangle\langle j|$, $\{i, j = 1, 2, 3\}$ and obey the commutation rule:

$$[S_{\alpha,\beta}, S_{\beta',\alpha'}] = \delta_{\beta,\beta'}S_{\alpha,\alpha'} - \delta_{\alpha',\alpha}S_{\beta',\beta}. \tag{4.1}$$

The most energetic level $|3\rangle$ may spontaneously decay to the intermediate level $|2\rangle$ with a emission rate γ_{32}, while the last one decays to the ground level $|1\rangle$ with a rate γ_{21}.

The laser pumping of the quantum-well is obtained by applying different lasers for each atomic transition. The laser driving the lower transition is described by its frequency ω_{L1} and phase ϕ_1, while the laser applied on the upper transition is given by ω_{L2} and ϕ_2. The quantum-well pumping is described via semi-classical interactions given by the Rabi frequencies Ω_1 and Ω_2 for the lower and upper transitions, respectively. The corresponding interaction Hamiltonian is given by two separate terms defined in eq.(2.10), adapted for each of the atomic transition.

The cavity-quantum-well interaction is also expressed via two separate Hamiltonian terms, one for each of the transitions. The two corresponding terms are given by the interaction part of the Jaynes-Cummings model of eq.(2.24) and are described by the coupling constants g_1 and g_2. The first coupling constant represents the quantum interaction of the optical resonator with the lower transition, while the second one - with the upper transition.

The quantized cavity field is defined by its frequency ω_c and the bosonic creation operator $a^\dagger$ and annihilation operator a, defined in eq.(2.12). The bosonic operators commute as $[a, a^\dagger] = 1$. The optical cavity is dumped by an environmental electromagnetic vacuum reservoir at a leaking rate κ.

The system Hamiltonian, in its general form, is defined as:

$$\begin{aligned} H &= \hbar\omega_c a^\dagger a + \hbar\sum_{i=1}^{3}\omega_i S_{ii} + i\hbar g_1(a^\dagger S_{12} - S_{21}a) + i\hbar g_2(a^\dagger S_{23} - S_{32}a) \\ &+ \hbar\Omega_1(S_{21}e^{-i(\omega_{L1}t+\phi_1)} + S_{12}e^{i(\omega_{L1}t+\phi_1)}) \\ &+ \hbar\Omega_2(S_{32}e^{-i(\omega_{L2}t+\phi_2)} + S_{23}e^{i(\omega_{L2}t+\phi_2)}), \end{aligned} \tag{4.2}$$

where the first two terms in Eq. (4.2) describe the single mode free cavity field and the quantum-well free Hamiltonians. As mentioned previously, the external laser fields and the cavity field interact with both transitions of the quantum-well and every interaction is defined via separate terms according to each transition. Thus, the next two terms of the Hamiltonian represent the interaction of the quantized cavity with the atom whereas the last two terms describe the laser-atom semi-classical interaction.

The system's quantum dynamics is given by the master equation for the density operator ρ as:

$$\frac{\partial\rho}{\partial t} = -\frac{i}{\hbar}[H,\rho] + \frac{\kappa}{2}\mathcal{L}(a) + \frac{\gamma_{32}}{2}\mathcal{L}(S_{23}) + \frac{\gamma_{21}}{2}\mathcal{L}(S_{12}), \tag{4.3}$$

where, on the right-hand side of the equation, the first term represents the coherent part based on the von-Neumann equation of eq.(2.47), while the other terms describe the damping phenomena. The second term of the equation represents the cavity photon leaking term of eq.(2.62), which appears due to the interaction of the optical resonator with the environmental electromagnetic vacuum. The last two terms represent the spontaneous emission of the two excited states, with two different rates corresponding to each of the quantum-well's transitions. In the case of a multi-level atomic structure, as in our case, the reservoir theory may be applied to each transition separately. Therefore, the spontaneous decay dynamics will be defined by separate damping terms of eq.(2.64) adapted for each of the possible decay transitions. The damping effects are expressed by the Liouville superoperator $\mathcal{L}$, which acts on a given operator $\mathcal{O}$ as: $\mathcal{L}(\mathcal{O}) = 2\mathcal{O}\rho\mathcal{O}^\dagger - \mathcal{O}^\dagger\mathcal{O}\rho - \rho\mathcal{O}^\dagger\mathcal{O}$.

Note that the thermal cavity pumping term is not introduced in the master equation of eq.(4.3). This term vanishes when one considers the electromagnetic vacuum as environmental reservoir. This condition is equivalent to the case of an empty thermal reservoir treated in Chapter 2, i.e., when the mean photon number of the thermal reservoir becomes $\bar{n} = 0$. This condition is valid as long as one operates the cavity at optical or higher frequencies. For frequencies such as THz or microwave, the thermal cavity pumping effect should be considered for the current model, especially in scenarios where the cavity field vanishes and there are no photons emitted in the cavity. In such cases, the cavity mean photon number should equilibrate with the mean photon number of the thermal reservoir due to the pumping effect.

As in the previous chapter, a direct implementation of system Hamiltonian of eq.(4.2) into the master equation of eq.(4.3) does not allow one to accurately solve it without adopting drastic approximation to the system dynamics. In this paragraph, a set of various transformations shall be applied to the system dynamics in order to obtain a solvable master equation, without loosing much of the generality of the problem.

A first step consists in setting the pumping laser frequencies in resonance with the two transitions of the equidistant three-level emitter, i.e., $\omega_{L1} = \omega_2 - \omega_1$ and $\omega_{L2} = \omega_3 - \omega_2$. As the transition frequencies of the quantum-well are equal, i.e., $\omega_3 - \omega_2 = \omega_2 - \omega_1$, one may further note $\omega_L = \omega_{L1} = \omega_{L2}$. This allows the free quantum-well Hamiltonian term to vanish when one goes in the frame rotating with ω_L, via the unitary transformation $U(t) = exp(-iH_1 t/\hbar)$ with $H_1 = \hbar\omega_L S_z$ and $S_z = S_{++} - S_{--} = |+\rangle\langle+| - |-\rangle\langle-|$. In this frame, one obtains the following system Hamiltonian:

$$\begin{aligned} H &= \hbar\omega_c a^\dagger a + i\hbar g_1(a^\dagger S_{12}e^{-i\omega_L t} - e^{i\omega_L t}S_{21}a) + i\hbar g_2(a^\dagger S_{23}e^{-i\omega_L t} - e^{i\omega_L t}S_{32}a) \\ &+ \hbar\Omega_1(S_{21}e^{-i\phi_1} + S_{12}e^{i\phi_1}) + \hbar\Omega_2(S_{32}e^{-i\phi_2} + S_{23}e^{i\phi_2}), \end{aligned} \tag{4.4}$$

Next, one transfers the phase term from the laser-quantum-well interaction terms to the cavity-quantum-well interaction terms, by applying the following transformation to the atomic operators:

$$\begin{aligned} S_{12}e^{i\phi_1} &\rightarrow S_{12}, \\ S_{21}e^{-i\phi_1} &\rightarrow S_{12}, \\ S_{23}e^{i\phi_2} &\rightarrow S_{23}, \\ S_{32}e^{-i\phi_1} &\rightarrow S_{32}, \end{aligned} \tag{4.5}$$

which leads to the system Hamiltonian:

$$
\begin{aligned}
H &= \hbar\omega_c a^\dagger a + i\hbar g_1(a^\dagger S_{12}e^{-i(\omega_L t+\phi_1)} - e^{i(\omega_L t+\phi_1)}S_{21}a) \\
&+ i\hbar g_2(a^\dagger S_{23}e^{-i(\omega_L t+\phi_2)} - e^{i(\omega_{L2} t+\phi_2)}S_{32}a) \\
&+ \hbar\Omega_1(S_{21}+S_{12}) + \hbar\Omega_2(S_{32}+S_{23}).
\end{aligned} \tag{4.6}
$$

The Hamiltonian is brought to an easy diagonalizable form of the quantum-well-lasers subsystem terms. But before diagonalising it, one goes in a frame rotating with the frequency ω_L by applying the unitary transformation $U(t) = exp(-iH_2 t/\hbar)$ with $H_2 = \hbar\omega_L a^\dagger a$. Within this frame, the cavity-quantum-well interaction terms do not rotate any longer and the system Hamiltonian is expressed as:

$$
\begin{aligned}
H &= \hbar(\omega_c-\omega_L)a^\dagger a + \hbar\Omega_1(S_{21}+S_{12}) + \hbar\Omega_2(S_{32}+S_{23}) \\
&+ i\hbar g_1(a^\dagger S_{12}e^{-i\phi_1} - e^{i\phi_1}S_{21}a) + i\hbar g_2(a^\dagger S_{23}e^{-i\phi_2} - e^{i\phi_2}S_{32}a).
\end{aligned} \tag{4.7}
$$

Within this form, one adopts the semi-classical dressed-state transformation according to the dynamical Stark splitting effect of the quantum-well under the laser pumping [100]. The new Hermitian base is defined considering the pumped quantum-well subsystem eigenfunctions. The new atomic wave function basis vectors, i.e., the dressed-states, are defined as [102]:

$$
\begin{aligned}
|1\rangle &= -\frac{1}{\sqrt{2}}\cos\theta\,|-\rangle - \sin\theta\,|0\rangle + \frac{1}{\sqrt{2}}\cos\theta\,|+\rangle, \\
|2\rangle &= \frac{1}{\sqrt{2}}|-\rangle + \frac{1}{\sqrt{2}}|+\rangle, \\
|3\rangle &= -\frac{1}{\sqrt{2}}\sin\theta\,|-\rangle + \cos\theta\,|0\rangle + \frac{1}{\sqrt{2}}\sin\theta\,|+\rangle,
\end{aligned} \tag{4.8}
$$

where $\theta = \tan^{-1}(\Omega_2/\Omega_1)$ and $\Omega = \sqrt{\Omega_1^2+\Omega_2^2}$. Similarly to the bare-state operators, the new atomic operators are defined as $R_{ij} = |i\rangle\langle j|$, $\{i,j = -,0,+\}$ and $R_z = R_{++} - R_{--}$, and obey the same commutation rules of eq.(4.1).

The system Hamiltonian in the dressed-state picture is expressed as:

$$
\begin{aligned}
H &= \hbar(\omega_c-\omega_L)a^\dagger a + \hbar\Omega R_z + \Bigg\{\frac{i}{2}(g_1e^{-i\phi_1}\cos\theta + g_2e^{-i\phi_2}\sin\theta)a^\dagger R_z \\
&+ \frac{i}{2}(g_1e^{-i\phi_1}\cos\theta - g_2e^{-i\phi_2}\sin\theta)a^\dagger\Big(R_{+-} - R_{-+}\Big) \\
&- \frac{i}{\sqrt{2}}g_1e^{-i\phi_1}\sin\theta\,a^\dagger\Big(R_{0-}+R_{0+}\Big) + \frac{i}{\sqrt{2}}g_2e^{-i\phi_2}\cos\theta\,a^\dagger\Big(R_{-0}+R_{+0}\Big) \\
&+ \text{H.c.}\Bigg\}.
\end{aligned} \tag{4.9}
$$

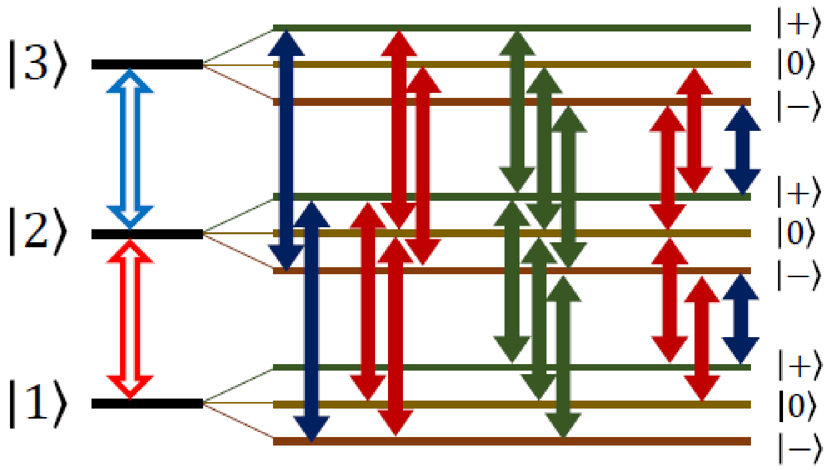

Fig. 4.2: The dynamic Stark splitting of the quantum-well energy levels under the laser pumping effect. Various transition among the "dressed" atomic level are represented in different colours. The external sidebands are shown in purple bold arrows, the internal sidebands in red bold arrows and the central frequency in green bold arrows.

Finally, one goes in the interaction picture of the "dressed" system Hamiltonian by performing the unitary transformation: $U(t) = \exp\{itH_3/\hbar\}$ where $H_3 = \hbar(\omega_c - \omega_L)a^\dagger a + \hbar\Omega R_z$. In this picture, the system Hamiltonian becomes:

$$
\begin{aligned}
H &= \frac{i}{2}(g_1 e^{-i\phi_1}\cos\theta - g_2 e^{-i\phi_2}\sin\theta)a^\dagger e^{i(\omega_c-\omega_L)t}\Big(R_{+-}e^{2i\Omega t} - R_{-+}e^{-2i\Omega t}\Big) \\
&- \frac{i}{\sqrt{2}}g_1 e^{-i\phi_1}\sin\theta\, a^\dagger e^{i(\omega_c-\omega_L)t}\Big(R_{0-}e^{i\Omega t} + R_{0+}e^{-i\Omega t}\Big) \\
&+ \frac{i}{\sqrt{2}}g_2 e^{-i\phi_2}\cos\theta\, a^\dagger e^{i(\omega_c-\omega_L)t}\Big(R_{-0}e^{-i\Omega t} + R_{+0}e^{i\Omega t}\Big) \\
&+ \frac{i}{2}(g_1 e^{-i\phi_1}\cos\theta + g_2 e^{-i\phi_2}\sin\theta)a^\dagger e^{i(\omega_c-\omega_L)t}R_z + \text{H.c.}. \qquad (4.10)
\end{aligned}
$$

Within the interaction picture, the Hamiltonian terms oscillates at five distinct frequencies $\omega_c - \omega_L \pm \Omega$, $\omega_c - \omega_L \pm 2\Omega$ and $\omega_c - \omega_L$. This terms corresponds to the interaction of the optical cavity with the sidebands and the central frequency of the quantum-well which appear under the laser pumping effect. The dynamical Stark splitting effect which appear due to the laser-quantum-well interactions leads to five transition frequencies among the split atomic states as shown in Fig.4.2. The quantum-well resonance fluorescence spectra of each transition is formed of degenerate sidebands centred at $\omega_L \pm \Omega$ and $\omega_L \pm 2\Omega$ as well as a central peak around ω_L.

The system Hamiltonian of eq.(4.10) may be significantly simplified if tuning the optical cavity in resonance with one of the possible transitions of the pumped quantum-well. The resonance case would allow one to keep only the resonant interaction term and neglect other interactions via a secular approximation. The simplified Hamiltonian shall accurately describe the quantum dynamics within the adopted approximations as long as $g_{1,2}/\Omega \ll 1$. In what follows one will study separately each of the possible resonant cases.

In the next paragraph 4.2, one shall first discuss the case of the cavity tuned in resonance with one of the external sidebands represented in purple bold arrows in Fig.4.2. Here, the dynamics and the results are similar when the cavity is tuned with either the most or the less energetic external sideband, i.e., when $\omega_c = \omega_L + 2\Omega$ or $\omega_c = \omega_L - 2\Omega$, respectively. When tuning the cavity as $\omega_c = \omega_L + 2\Omega$, the dressed-state Hamiltonian is reduced to:

$$H \;=\; i|g|\left(a^\dagger R_{-+}e^{i\psi} - e^{-i\psi}R_{+-}a\right), \tag{4.11}$$

where

$$g \;=\; \frac{1}{2}(g_2 e^{-i\phi_2}\sin\theta - g_1 e^{-i\phi_1}\cos\theta) \tag{4.12}$$

and $\psi = \arg(g)$. The obtained Hamiltonian has a similar form to the Hamiltonian of a two-level atom interacting with a cavity with an effective coupling g. This effective coupling originates from the quantum interference of the two dressed-state transition amplitudes, contributing to the quantum-well pumping of the cavity mode. As it will be shown later, it is possible to configure the two Rabi frequencies in order to effectively decouple the atom from the cavity, i.e., the effective coupling g vanishes when $g_1/g_2 = \Omega_2/\Omega_1$ and the lasers are in-phase. This point corresponds to the case where the interfering interaction amplitudes of the upper and lower transitions become equal.

In the last study of the paragraph 4.2, the investigation is focused on the system dynamics when the cavity is tuned in resonance with one of the internal sidebands, i.e., when $\omega_c = \omega_L \pm \Omega$. All the possible transitions that may occur at this frequencies are represented in red bold arrays in Fig.4.2. Again, the system dynamics shows a similar behaviour when the cavity is tuned either to the most or less energetic internal sideband, i.e., when $\omega_c = \omega_L + \Omega$ or $\omega_c = \omega_L - \Omega$, respectively. Therefore, the further study is considering only the case when $\omega_c = \omega_L + \Omega$. The resonant Hamiltonian is expressed for this case as:

$$H \;= i\bar{g}_2\left(a^\dagger R_{-0}e^{-i\phi_2} - e^{i\phi_2}R_{0-}a\right) - i\bar{g}_1\left(a^\dagger R_{0+}e^{-i\phi_1} - e^{i\phi_1}R_{+0}a\right), \tag{4.13}$$

where

$$\bar{g}_1 \;=\; \frac{g_1\sin\theta}{\sqrt{2}} \quad \text{and} \quad \bar{g}_2 = \frac{g_2\cos\theta}{\sqrt{2}}. \tag{4.14}$$

Within this case, one does not observe any analytic expression of an effective coupling as in the previous case and the coupling of the optical resonator with the artificial atom is expressed via two separate terms.

In the paragraph 4.3, the last studied configuration corresponds to the case when the cavity is tuned with the central peak of the pumped quantum-well, i.e., when $\omega_c = \omega_L$. In Fig.4.2 the corresponding transitions are represented in green bold arrows. Note that although one sets here the cavity in resonance with the free quantum-well transition, the model still requires the laser pumping to be applied. For this case, the resonant Hamiltonian is obtained after neglecting the fast-terms as:

$$H = i|g|\left(a^{\dagger}e^{i\psi} - e^{-i\psi}a\right)R_z, \tag{4.15}$$

where

$$g = \frac{1}{2}(g_1 e^{-i\phi_1}\cos\theta + g_2 e^{-i\phi_2}\sin\theta) \tag{4.16}$$

and $\psi = \arg(g)$. As in the case of eq.(4.12), an effective coupling constant appears in the term of the resonant Hamiltonian and the nature of the interference phenomena can be interpreted analytically. The difference with the previous case is that the laser phases have to be offset by π in order to obtain destructive interference phenomena. However, the system dynamics should be solved in order to estimate if these interferences can be quantitatively observed.

As in the previous chapter, all transformations applied to the system Hamiltonian have to be applied to the entire master equation of eq.(4.3). Within the dressed-state basis defined in eqs.(4.8) and within the "dressed" interaction picture applied to the Hamiltonian of eq.(4.10), the system's dynamics is described by the following dressed-state master equation:

$$\begin{aligned}\frac{\partial\rho}{\partial t} &= -\frac{i}{\hbar}[H,\rho] + \frac{\kappa}{2}\mathcal{L}(a) + \frac{\gamma_{32}\cos^2\theta}{4}\left(\mathcal{L}(R_{-0}) + \mathcal{L}(R_{+0})\right) \\ &+ \frac{\gamma_{32}\sin^2\theta + \gamma_{21}\cos^2\theta}{8}\left(\mathcal{L}(R_z) + \mathcal{L}(R_{+-}) + \mathcal{L}(R_{-+})\right) \\ &+ \frac{\gamma_{21}\sin^2\theta}{4}\left(\mathcal{L}(R_{0-}) + \mathcal{L}(R_{0+})\right). \end{aligned}\tag{4.17}$$

Here, the secular approximation was performed in the spontaneous emission terms by neglecting the time-dependent rapidly oscillating terms - an approximation valid as long as $\gamma_{32(21)}/\Omega \ll 1$. The dressed-state atomic operators $R_{ij} = |i\rangle\langle j|$, $\{i,j\} \in \{-,0,+\}$, and $R_z = R_{++} - R_{--}$, obey the same commutation relations of eq.(4.1) as the operators expressed in the bare-state basis.

4.2 The cavity in resonance with sidebands

The master equation (4.17), with the Hamiltonian (4.11), is solved by projecting it into the system's states basis [191]. The solving technique is similar to the method applied in paragraph 3.2 of the previous chapter. The Hamiltonian (4.11) is similar to the case of a two-level emitter of the Jaynes-Cummings model and involves only the states $|+\rangle$ and $|-\rangle$. However, the spontaneous emission terms of the master equation (4.17) involves all of the quantum-well dressed-states. Therefore, the method [191] requires to define some additional variables to the system in order to adapt it to the case of a three-level emitter. As previously, the master equation is first projected into the atomic basis and, after some rearrangements of the elements of the reduced density matrix, their equation of motion are projected into the field basis. One defines the following Hermitian quantities as variables for the system:

$$\begin{aligned}
\rho^{(0)} &= \rho_{--} + \rho_{00} + \rho_{++}, \\
\rho^{(1)} &= \rho_{++} + \rho_{--}, \\
\rho^{(2)} &= \rho_{++} - \rho_{--}, \\
\rho^{(3)} &= (a^{\dagger}\rho_{+-} + \rho_{-+}a)/2, \\
\rho^{(4)} &= (\rho_{+-}a^{\dagger} + a\rho_{-+})/2,
\end{aligned} \tag{4.18}$$

where the elements of the reduced density matrix are defined as $\rho_{ij} = \langle i|\rho|j\rangle$, $\{i, j \in -, 0, +\}$. The projection into the quantum-well dressed-state basis leads to a set of five linearly coupled differential equations. The obtained system of equations of motion is expressed as:

$$\begin{aligned}
\dot{\rho}^{(0)} &= -2|g|\left(\rho^{(4)} - \rho^{(3)}\right) + \frac{\kappa}{2}\mathcal{L}_0(a), \\
\dot{\rho}^{(1)} &= -2|g|\left(\rho^{(4)} - \rho^{(3)}\right) + \frac{\kappa}{2}\mathcal{L}_1(a) - \frac{\alpha}{2}\rho^{(1)} + \gamma_{32}\cos^2\theta\rho^{(0)}, \\
\dot{\rho}^{(2)} &= -2|g|\left(\rho^{(4)} + \rho^{(3)}\right) + \frac{\kappa}{2}\mathcal{L}_2(a) - \frac{\beta}{2}\rho^{(2)}, \\
\dot{\rho}^{(3)} &= \frac{|g|}{4}\left(2a^{\dagger}(\rho^{(2)} + \rho^{(1)})a + a^{\dagger}a(\rho^{(2)} - \rho^{(1)}) + (\rho^{(2)} - \rho^{(1)})a^{\dagger}a\right) - \zeta\rho^{(3)} \\
&\quad + \frac{\kappa}{2}(\mathcal{L}_3(a) + \rho^{(3)} - 2\rho^{(4)}), \\
\dot{\rho}^{(4)} &= \frac{|g|}{4}\left(2a(\rho^{(2)} - \rho^{(1)})a^{\dagger} + aa^{\dagger}(\rho^{(2)} + \rho^{(1)}) + (\rho^{(2)} + \rho^{(1)})aa^{\dagger}\right) - \zeta\rho^{(4)} \\
&\quad + \frac{\kappa}{2}(\mathcal{L}_4(a) - \rho^{(4)}).
\end{aligned} \tag{4.19}$$

Here $\alpha = \gamma_{21}\sin^2\theta + 2\gamma_{32}\cos^2\theta$, $\beta = \gamma_{21} + \gamma_{32}\sin^2\theta$ and $\zeta = (\gamma_{21}(2+\cos^2\theta) + 3\gamma_{32}\sin^2\theta)/4$. The next projection in the field's basis leads to a set of infinite equations corresponding to the infinite Fock states $\{|n\rangle, n \in \mathcal{N}\}$, that is,

$$
\begin{aligned}
\dot{P}_n^{(0)} &= -2|g|\left(P_n^{(4)} - P_n^{(3)}\right) + \kappa(n+1)P_{n+1}^{(0)} - \kappa n P_n^{(0)}, \\
\dot{P}_n^{(1)} &= -2|g|\left(P_n^{(4)} - P_n^{(3)}\right) + \kappa(n+1)P_{n+1}^{(1)} - (\kappa n + \alpha/2)P_n^{(1)} + \gamma_{32}\cos^2\theta P_n^{(0)}, \\
\dot{P}_n^{(2)} &= -2|g|\left(P_n^{(4)} + P_n^{(3)}\right) + \kappa(n+1)P_{n+1}^{(2)} - (\kappa n + \beta/2)P_n^{(2)}, \\
\dot{P}_n^{(3)} &= |g|n\left(P_{n-1}^{(1)} - P_n^{(1)} + P_{n-1}^{(2)} + P_n^{(2)}\right)/2 - \kappa P_n^{(4)} \\
&\quad + \kappa(n+1)P_{n+1}^{(3)} - (\kappa(n-1/2) + \zeta)P_n^{(3)}, \\
\dot{P}_n^{(4)} &= |g|(n+1)\left(P_{n+1}^{(2)} + P_n^{(2)} - P_{n+1}^{(1)} + P_n^{(1)}\right)/2 \\
&\quad + \kappa(n+1)P_{n+1}^{(4)} - (\kappa(n+1/2) + \zeta)P_n^{(4)},
\end{aligned} \tag{4.20}
$$

where $P_n^{(i)} = \langle n|\rho^{(i)}|n\rangle$. Interestingly, $P_n^{(0)}$ are the diagonal elements of the field's reduced density matrix, i.e., it contains the trace over the atom's dressed-states: $P_n^{(0)} = \langle n|Tr_{atom}[\rho]|n\rangle$. Hence, it is possible to deduce the cavity field's mean photon number $\langle n\rangle$ by tracing over the field's states as discussed in eqs.(3.18-3.20):

$$
\langle n\rangle = \langle a^\dagger a\rangle = \sum_{n=0}^{\infty} n P_n^{(0)}. \tag{4.21}
$$

Similarly to the calculus of eq.(3.21), the second order photon-photon correlation function $g^{(2)}(0)$ is given by:

$$
g^{(2)}(0) = \frac{\langle a^\dagger a^\dagger a a\rangle}{\langle n\rangle^2} = \frac{\sum_{n=0}^{\infty} n(n-1)P_n^{(0)}}{\langle n\rangle^2}. \tag{4.22}
$$

Finally, in order to solve the infinite system of eqs. (4.20), we truncate it at a certain maximum value $n = N_{max}$ of considered Fock states. The photon distribution of the field converges to zero for larger N_{max}, and thus, N_{max} is selected such that a further increase of its value does not modify the obtained results.

A first investigation is performed when the two lasers are set in-phase, i.e., $\phi_1 = \phi_2 = 0$. For this case, the effective coupling of the atom vanishes. This is achieved by varying the ratio of the Rabi frequencies of the two lasers Ω_2/Ω_1. The variation of Ω_2/Ω_1 changes the meanings of $\sin\theta$ and $\cos\theta$ within the expression of the cavity-quantum-well interaction amplitudes of eq.(4.12).

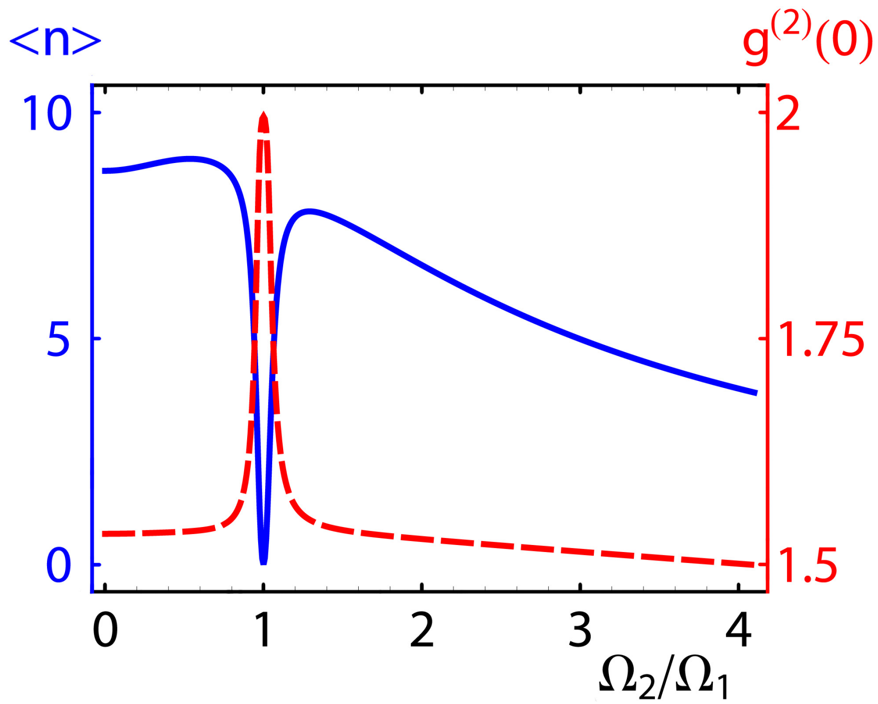

Fig. 4.3: The steady-state cavity mean photon number $\langle n \rangle$ (solid curve) and the second-order photon-photon correlation function $g^{(2)}(0)$ (dashed line) as a function of the ratio of the two Rabi frequencies Ω_2/Ω_1. The figure is published in [102].

The steady-state behaviour of the mean cavity photon number as well as their quantum statistics are shown in Fig.4.3, for a system defined by $\gamma_{32} = \gamma_{21} \equiv \gamma$, $g_1/\gamma = 5.001$, $g_2/\gamma = 5$ and $\kappa/\gamma = 10^{-3}$. A dip in the photon number is clearly visible when $g_1/g_2 = \Omega_2/\Omega_1$. It is due to quantum interference effects having a destructive nature on the cavity field photons. The interference occurs because both dressed-state transitions of the atom are coupled to the cavity mode leading to indistinguishable interaction amplitudes. When the interaction amplitudes of this two couplings become equal, the cavity field completely vanishes. Respectively, the atom decouples from the cavity field in this particular case as discussed in eqs.(4.11-4.12). Thus, the zero cavity photon detection in this scheme is directly related to quantum interference phenomena. Although, the atom is pumped and spontaneously emits photons in all other directions, there is no photon emission on the axis of the optical cavity.

A second investigation consists in observing the effect of the laser phases on the system dynamics. The cavity field behaviour shows a good evidence of quantum interferences, as presented in Fig.4.4. One has fixed the phase of the laser pumping the lower frequency at $\phi_1 = \pi/4$ and have varied the phase of the laser pumping the upper transition ϕ_2. The other system parameters are $g_1/\gamma_1 = 6$, $g_2/\gamma_1 = 4$, $\gamma_2/\gamma_1 = 2$ and $\kappa/\gamma = 10^{-3}$. One observes that for a certain configuration of laser phases and Rabi frequencies ratio, the mean photon number is strongly decreased

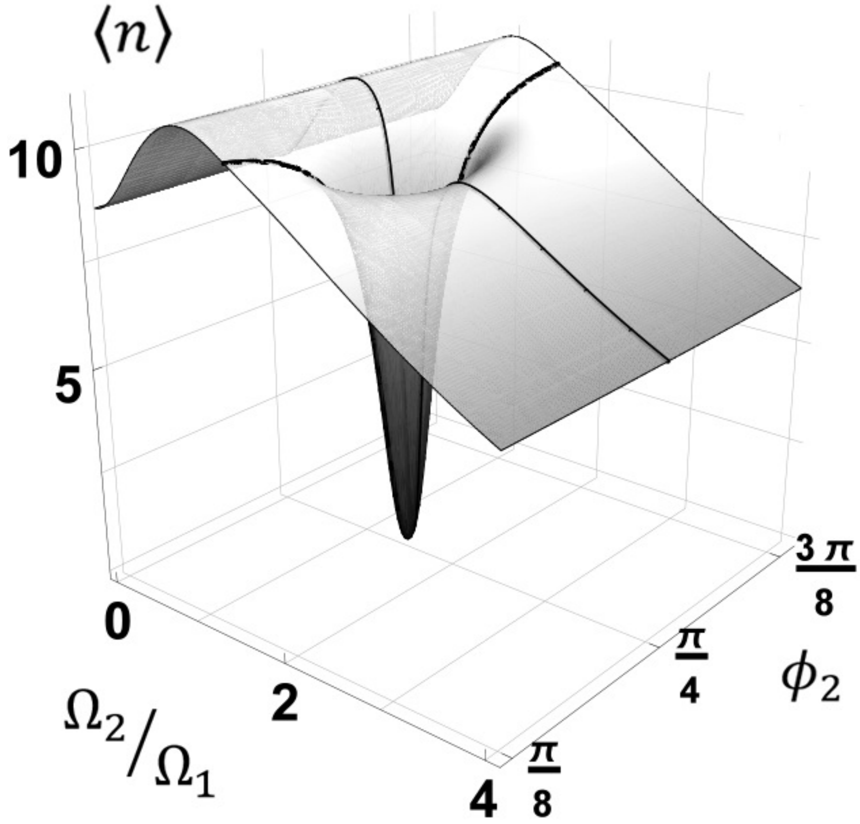

Fig. 4.4: The cavity mean photon number $\langle n \rangle$ as function of Rabi frequencies ratio Ω_2/Ω_1 and the laser phase ϕ_2 whereas the other laser frequency is fixed at $\phi_1 = \pi/4$. The figure is published in [103].

down to the zero value. As mentioned previously, this minimum describes a complete cancellation of the cavity field and corresponds to the case when the two indistinguishable amplitudes of the quantum-well-cavity interaction are equal and in-phase.

The phase difference of the input lasers plays a crucial role in the control of the quantum interference. The interaction amplitudes phases are related to the laser phases as suggested by the expression of the coupling constant g of the Hamiltonian form of equation (4.11) at cavity-quantum-well resonance and within the secular approximation. Therefore, a destructive superposition is obtained when the interaction amplitudes are in-phase, i.e., $\phi_2 = \phi_1 + 2\pi m, m \in \mathcal{Z}$, as shown in Fig.4.4. Under this condition, the system behaves similarly to the case when no laser phase was considered in Fig.4.3, where the field cancels simply for $g_1/g_2 = \Omega_2/\Omega_1$.

The system of equation of motions of eqs.(4.20) carries not only the information on the field dynamics, but also the information on the dynamics of the quantum-well. Therefore, another investigation has been carried on the dynamics of the atomic population of the quantum-well. Namely, one shall further discuss the behaviour of the population of the most excited energetic level $\langle S_{33}\rangle$. From the definition of the dressed-state basis of eq.(4.8), the bare state operator S_{33} may be defined as:

$$
\begin{aligned}
S_{33} &= |3\rangle\langle 3| = \Big(-\frac{1}{\sqrt{2}}\sin\theta\,|-\rangle + \cos\theta\,|0\rangle + \frac{1}{\sqrt{2}}\sin\theta|-\rangle\Big) \\
&\quad \times\Big(-\frac{1}{\sqrt{2}}\sin\theta\,\langle -| + \cos\theta\,\langle 0| + \frac{1}{\sqrt{2}}\sin\theta\langle +|\Big) \\
&= \frac{1}{2}\sin^2\theta\Big(R_{++} + R_{--}\Big) + \cos^2\theta R_{00} - \frac{1}{2}\sin^2\theta\Big(R_{+-} + R_{-+}\Big) \\
&\quad + \frac{1}{\sqrt{2}}\sin^2\theta\Big(R_{0+} + R_{+0} - R_{-0} - R_{0-}\Big). \qquad (4.23)
\end{aligned}
$$

When going into the interaction picture as discussed in eq.(4.10), the expression of S_{33} becomes:

$$
\begin{aligned}
S_{33} &= \frac{1}{2}\sin^2\theta\Big(R_{++} + R_{--}\Big) + \cos^2\theta R_{00} - \frac{1}{2}\sin^2\theta\Big(R_{+-}e^{2i\Omega t} + R_{-+}e^{-2i\Omega t}\Big) \\
&\quad + \frac{1}{\sqrt{2}}\sin^2\theta\Big(R_{0+}e^{-i\Omega t} + R_{+0}e^{i\Omega t} - R_{-0}e^{-i\Omega t} - R_{0-}e^{i\Omega t}\Big). \qquad (4.24)
\end{aligned}
$$

Here, a secular approximation is performed by neglecting the rotating terms. This terms are neglected by assuming the condition $\Omega \gg 1$, where one has used the trigonometric relations $\sin\theta, \cos\theta < 1$. The simplified expression of S_{33} is obtained as:

$$
S_{33} = \cos^2\theta + \frac{1}{2}(1 - 3\cos^2\theta)\Big(R_{++} + R_{--}\Big), \qquad (4.25)
$$

where one has applied the identity operator $1 = R_{++} + R_{00} + R_{--}$.

The calculus of the upper bare-state population of the quantum-well $\langle S_{33}\rangle$ is related to the quantity $\langle R_{++} + R_{--}\rangle$. The average value of a system operator $\mathcal{O}$ had been discussed in eq.(3.17) and is given as:

$$
\langle \mathcal{O}\rangle = Tr_{phonon}[Tr_{QD}[\rho\mathcal{O}]] = Tr_{phonon}[\sum_{i=\{+,0,-\}} \langle i|\rho\mathcal{O}|i\rangle], \qquad (4.26)
$$

where, this time, one traces first over the elements of the quantum-well reduced density matrix. Inserting the quantity $R_{++} + R_{--}$ into this expression, allows one to implement the variables of the solved system of equations (4.20) as follows:

$$\begin{aligned}\langle R_{++} + R_{--}\rangle &= Tr_{ph}\Big[\sum_{i=\{+,0,-\}} \langle i|\rho\big(R_{++} + R_{--}\big)|i\rangle\Big] = Tr_{ph}\Big[\rho_{++} + \rho_{--}\Big] \\ &= Tr_{ph}[\rho^{(1)}] = \sum_{n=0}^{\infty}\langle n|\rho^{(1)}|n\rangle = \sum_{n=0}^{\infty} P_n^{(1)}. \end{aligned} \tag{4.27}$$

Finally, the population of the upper bare state of eq.(4.25) is calculated as:

$$\langle S_{33}\rangle = \cos^2\theta + (1 - 3\cos^2\theta)\sum_{n=0}^{\infty} P_n^{(1)}/2. \tag{4.28}$$

As a concrete atomic system, for this particular configuration, one may consider He atoms, $\{3^1S, 2^1P_1, 1^1S_0\}$ [192]. The spontaneous decay rates ratio is approximately $\gamma_{32}/\gamma_{21} \approx 10^{-2}$. The corresponding transition wavelengths are $\lambda_{32} = 728.3$nm and $\lambda_{21} = 58.4$nm. This atomic system differs from what was considered previously, however the current analytical model fits well the case when the optical cavity couples only with the upper transition and thus $g_1 = 0$. Instead of a continuous wave laser on the high-frequency transition one may consider a long pulse laser wave. Potential applications here may be related to entangled photon pair emissions [179] in optical and EUV (or even higher) frequency ranges.

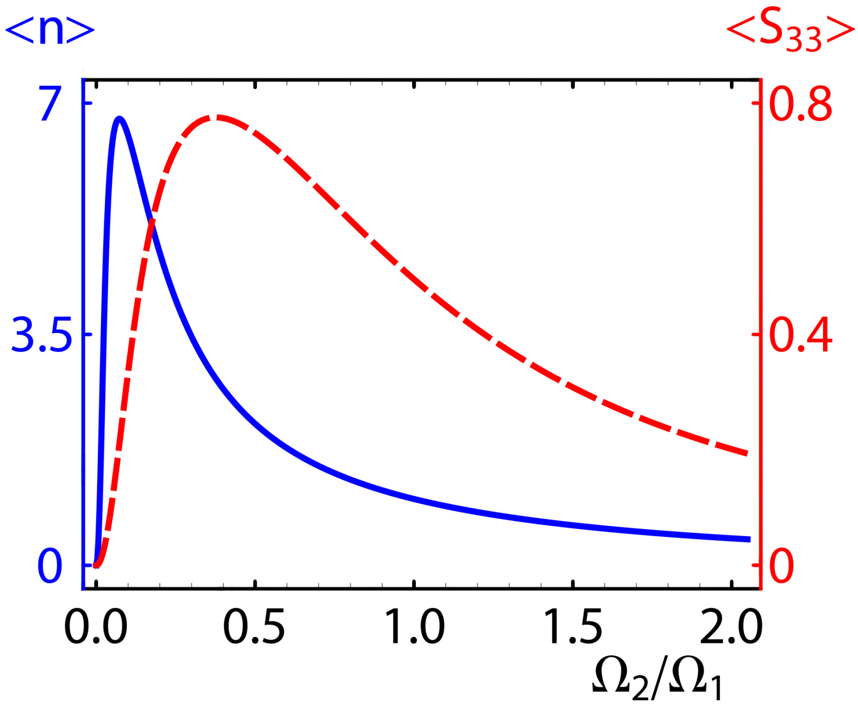

Fig. 4.5: The steady-state evolution of the cavity mean photon number $\langle n\rangle$ (solid line) and the upper bare-state population $\langle S_{33}\rangle$ (dashed curve) as a function of Ω_2/Ω_1. The figure is published in [102].

Fig.4.5 shows the bare-state population of the upper state $|3\rangle$ as well as the cavity mean-photon number when $\gamma_{32} \ll \gamma_{21}$ while $\omega_{32} = \omega_{L2}$ and $\omega_{21} = \omega_{L1}$ with $\omega_{L1} \neq \omega_{L2}$. The other system parameters are $\gamma_{32}/\gamma_{21} = 10^{-2}$, $g_2/\gamma_{21} = 5$, $\kappa/\gamma_{21} = 10^{-3}$. The cavity mode resonantly couples with the upper atomic transition $|3\rangle \leftrightarrow |2\rangle$ only, i.e. $g_1 = 0$. This situation is described as well by the analytical formalism developed here via setting $g_1 = 0$ in Eqs. (4.20). Reasonable population inversion is achieved. We have found that the inversion is a signature of the coherent population trapping phenomenon [193], i.e., the atom is trapped in the dressed-state $|0\rangle = \cos\theta|3\rangle - \sin\theta|1\rangle$. Then with a suitable chose of the ratio Ω_2/Ω_1 one can transfer the populations among the state $|3\rangle \leftrightarrow |1\rangle$. Furthermore, the cavity field does not affect the bare-state population dynamics in the adopted approximations.

A less fruitful investigation have been performed to the case when the optical cavity is tuned in resonance with one of the internal sidebands, namely when $\omega_c = \omega_L + \Omega$. For this case, the system dynamics is expressed via the Hamiltonian term of eq.(4.13). As mentioned previously, there is no analytical effective coupling term which would indicate to a interference case. Instead, the coupling of the cavity with the quantum-well is expressed via two separate Hamiltonian terms, one for each atomic transition.

As in the previous case when the cavity is tuned with the external sidebands, the numerical method [191] used to solve the system dynamics shall be adapted to the particular case of Hamiltonian of eq.(4.13). In order to solve the corresponding master equation, a new set of variables is defined as:

$$\begin{aligned}
\rho^{(0)} &= \rho_{--} + \rho_{00} + \rho_{++}, \\
\rho^{(1)} &= \rho_{++} + \rho_{--}, \\
\rho^{(2)} &= \rho_{++} - \rho_{--}, \\
\rho^{(3)} &= a^{\dagger}\rho_{0-} + \rho_{-0}a, \\
\rho^{(4)} &= \rho_{0-}a^{\dagger} + a\rho_{-0}, \\
\rho^{(5)} &= a^{\dagger}\rho_{+0} + \rho_{0+}a, \\
\rho^{(6)} &= \rho_{+0}a^{\dagger} + a\rho_{0+}, \\
\rho^{(7)} &= a^{\dagger}\rho_{+-}a^{\dagger} + a\rho_{-+}a, \\
\rho^{(8)} &= a^{\dagger}a^{\dagger}\rho_{+-} + \rho_{-+}aa, \\
\rho^{(9)} &= \rho_{+-}a^{\dagger}a^{\dagger} + aa\rho_{-+},
\end{aligned} \tag{4.29}$$

where $\rho_{ij} = \langle i|\rho|j\rangle$, $\{i, j \in -, 0, +\}$, are the elements of the quantum-well reduced density matrix.

The next projection in the field's basis leads to a set of infinite equations corresponding to the infinite Fock states $\{|n\rangle, n \in \mathcal{N}\}$, that is,

$$
\begin{aligned}
\dot{P}_n^{(0)} &= \bar{g}_1(P_n^{(6)} - P_n^{(5)}) + \bar{g}_2(P_n^{(3)} - P_n^{(4)}) + \kappa(n+1)P_{n+1}^{(0)} - \kappa n P_n^{(0)}, \\
\dot{P}_n^{(1)} &= \bar{g}_1 P_n^{(6)} + \bar{g}_2 P_n^{(3)} + \kappa(n+1)P_{n+1}^{(1)} - (\kappa n + \alpha/2)P_n^{(1)} + \gamma_{32}\cos^2\theta P_n^{(0)}, \\
\dot{P}_n^{(2)} &= \bar{g}_1 P_n^{(6)} - \bar{g}_2 P_n^{(3)} + \kappa(n+1)P_{n+1}^{(2)} - (\kappa n + \beta/2)P_n^{(2)}, \\
\dot{P}_n^{(3)} &= -\bar{g}_1 P_n^{(8)} + \bar{g}_2 n\Big(2P_{n-1}^{(0)} - 2P_{n-1}^{(1)} + P_n^{(2)} - P_n^{(1)}\Big) - \kappa P_n^{(4)} \\
&\quad +\kappa(n+1)P_{n+1}^{(3)} - \Big(\kappa(n-1/2) + \beta/4\Big)P_n^{(3)}, \\
\dot{P}_n^{(4)} &= -\bar{g}_1 P_n^{(7)} + \bar{g}_2(n+1)\Big(2P_n^{(0)} - 2P_n^{(1)} + P_{n+1}^{(2)} - P_{n+1}^{(1)}\Big) \\
&\quad +\kappa(n+1)P_{n+1}^{(4)} - \Big(\kappa(n+1/2) + \beta/4\Big)P_n^{(4)}, \\
\dot{P}_n^{(5)} &= -\bar{g}_2 P_n^{(7)} + \bar{g}_1 n\Big(2P_n^{(0)} - 2P_n^{(1)} - P_{n-1}^{(2)} - P_{n-1}^{(1)}\Big) - \kappa P_n^{(6)} \\
&\quad +\kappa(n+1)P_{n+1}^{(5)} - \Big(\kappa(n-1/2) + \beta/4\Big)P_n^{(5)}, \\
\dot{P}_n^{(6)} &= -\bar{g}_2 P_n^{(9)} + \bar{g}_1(n+1)\Big(2P_{n+1}^{(0)} - 2P_{n+1}^{(1)} - P_n^{(2)} - P_n^{(1)}\Big) \\
&\quad +\kappa(n+1)P_{n+1}^{(6)} - \Big(\kappa(n+1/2) + \beta/4\Big)P_n^{(6)}, \\
\dot{P}_n^{(7)} &= \bar{g}_1\Big((n+1)P_{n+1}^{(3)} - P_n^{(4)}\Big) + \bar{g}_2\Big(nP_{n-1}^{(6)} + P_n^{(5)}\Big) - \kappa P_n^{(9)} \\
&\quad +\kappa(n+1)P_{n+1}^{(7)} - (\kappa n + \zeta)P_n^{(7)}, \\
\dot{P}_n^{(8)} &= \bar{g}_2 n P_{n-1}^{(5)} + \bar{g}_1\Big((2n-1)P_n^{(3)} - nP_{n-1}^{(4)}\Big) - 2\kappa P_n^{(7)} \\
&\quad +\kappa(n+1)P_{n+1}^{(8)} - \Big(\kappa(n-1) + \zeta\Big)P_n^{(8)}, \\
\dot{P}_n^{(9)} &= \bar{g}_1(n+1)P_{n+1}^{(4)} + \bar{g}_2\Big((2n+3)P_n^{(6)} - (n+1)P_{n+1}^{(5)}\Big) \\
&\quad +\kappa(n+1)P_{n+1}^{(9)} - \Big(\kappa(n+1) + \zeta\Big)P_n^{(9)}. \qquad (4.30)
\end{aligned}
$$

Here $\alpha = \gamma_{21}\sin^2\theta + 2\gamma_{32}\cos^2\theta$, $\beta = \gamma_{21} + \gamma_{32}\sin^2\theta$ and $\zeta = (\gamma_{21}(2+\cos^2\theta) + 3\gamma_{32}\sin^2\theta)/4$.

The field quantum statistics are evaluated from eq.(4.21). Their steady-state behaviour is represented in Fig.4.6, where one has evaluated the cavity mean phonon number $\langle n\rangle$ as a function of the Rabi frequencies ratio and cavity-quantum-well cavity coupling with the upper transition g_2/γ normalized by the spontaneous rate γ, while keeping the value of the cavity-quantum-well coupling with the lower transition fixed at $g_1/\gamma = 5$. For the sake of simplicity, one has considered the two

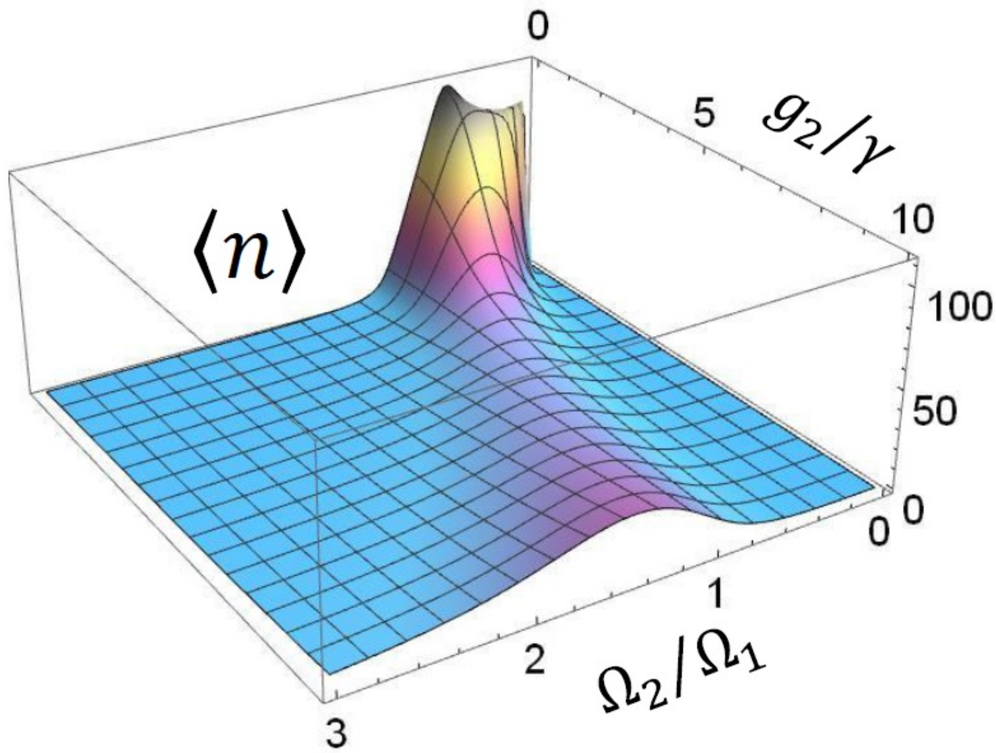

Fig. 4.6: The cavity mean photon number $\langle n \rangle$ as function of the Rabi frequencies ratio Ω_2/Ω_1 and cavity-quantum-well cavity coupling g_2/γ, for a fixed value of $g_1/\gamma = 5$.

spontaneous emission rates being equal, i.e., $\gamma_{32} = \gamma_{21} = \gamma$. The cavity damping rate have been set as $\kappa/\gamma = 10^{-3}$.

One observes a maximum of photons in the cavity when the coupling with the lower transition is dominant, i.e., $g_1 \gg g_2$, and most of the pumping is on the lower transition as well. By increasing g_2, one increases the amplitude of the cavity coupling with the upper transition and the maximum value of the mean photon number in the cavity decreases. While the two amplitudes cancels each other, one cannot determine an analytical or numerical point when a complete destructive quantum interference effect occurs.

4.3 The cavity in resonance with the central frequency

In this paragraph one investigates the system dynamics of the case when the optical cavity is tuned in resonance with the quantum-well central transition frequency, i.e., $\omega_c = \omega_L$. The numerical method applied in paragraph 4.2 is no longer usable in this case due to the form of the resonant Hamiltonian term of eq.(4.15). When projecting the master equation of eq.(4.3) into the dressed-state basis, one cannot close the system and, therefore, the numerical method [191] cannot be accurately applied.

Instead, one is able to solve the system dynamics by building the equation of motion of the quantities of interest, namely the mean cavity photon number $\langle n\rangle$ and the second-order correlation function $g^{(2)}(0)$. This is done by using the relation for a system operator Q:

$$\frac{\partial\langle Q\rangle}{\partial t} = Tr[\rho\frac{\partial Q}{\partial t}] = Tr[Q\frac{\partial \rho}{\partial t}] \tag{4.31}$$

into the system master equation. This allows one to define the general form of the equation of motion for a system operator as:

$$\begin{aligned}\frac{\partial\langle Q\rangle}{\partial t} &= \frac{i}{\hbar}\langle[H,Q]\rangle - \frac{\kappa}{2}\Big\{\langle a^\dagger[a,Q]\rangle + \langle[Q,a^\dagger]a\rangle\Big\} \\ &- \frac{\gamma_c}{2}\Big\{\langle R_{0-}[R_{-0},Q]\rangle + \langle[Q,R_{0-}]R_{-0}\rangle + \langle R_{0+}[R_{+0},Q]\rangle + \langle[Q,R_{0+}]R_{+0}\rangle\Big\} \\ &- \frac{\gamma_d}{2}\Big\{\langle R_{-0}[R_{0-},Q]\rangle + \langle[Q,R_{-0}]R_{0-}\rangle + \langle R_{+0}[R_{0+},Q]\rangle + \langle[Q,R_{+0}]R_{0+}\rangle\Big\} \\ &- \frac{\gamma_a}{2}\Big\{\langle R_{+-}[R_{-+},Q]\rangle + \langle[Q,R_{+-}]R_{-+}\rangle + \langle R_{-+}[R_{+-},Q]\rangle + \langle[Q,R_{-+}]R_{+-}\rangle \\ &\quad + \langle R_z[R_z,Q]\rangle + \langle[Q,R_z]R_z\rangle\Big\}.\end{aligned} \tag{4.32}$$

The system of equations of motion required to define the dynamics of the field statistics is made of a closed system of first-order linear coupled differential equations deduced from eq.(4.32). Namely, the full system is defined as:

$$\begin{aligned}\frac{\partial\langle R_z\rangle}{\partial t} &= -(2\gamma_a+\gamma_b)\langle R_z\rangle, \\ \frac{\partial\langle a^\dagger a\rangle}{\partial t} &= |g|\Big(\langle a^\dagger R_z\rangle + \langle aR_z\rangle\Big) - \kappa\langle a^\dagger a\rangle, \\ \frac{\partial\langle a^\dagger R_z\rangle}{\partial t} &= |g|\langle R_z^2\rangle - (\frac{\kappa}{2}+2\gamma_a+\gamma_d)\langle a^\dagger R_z\rangle, \\ \frac{\partial\langle R_z^2\rangle}{\partial t} &= -(2\gamma_c+\gamma_d)\langle R_z^2\rangle + 2\gamma_c,\end{aligned}$$

$$
\begin{aligned}
\frac{\partial\langle a^\dagger a^\dagger aa\rangle}{\partial t} &= 2|g|\Big(\langle a^\dagger a^\dagger aR_z\rangle + \langle R_z a^\dagger aa\rangle\Big) - 2\kappa\langle a^\dagger a^\dagger aa\rangle,\\
\frac{\partial\langle a^\dagger a^\dagger aR_z\rangle}{\partial t} &= |g|\Big(\langle a^\dagger a^\dagger R_z^2\rangle + 2\langle a^\dagger aR_z^2\rangle\Big) - (\frac{3\kappa}{2} + 2\gamma_a + \gamma_d)\langle a^\dagger a^\dagger aR_z\rangle,\\
\frac{\partial\langle a^\dagger aR_z^2\rangle}{\partial t} &= |g|\Big(\langle a^\dagger R_z\rangle + \langle R_z a\rangle\Big) - (\kappa + 2\gamma_c + \gamma_d)\langle a^\dagger aR_z^2\rangle + 2\gamma_c\langle a^\dagger a\rangle,\\
\frac{\partial\langle a^\dagger a^\dagger R_z^2\rangle}{\partial t} &= 2|g|\langle a^\dagger R_z\rangle - (\kappa + 2\gamma_c + \gamma_d)\langle a^\dagger a^\dagger R_z^2\rangle + 2\gamma_c\langle a^\dagger a^\dagger\rangle,\\
\frac{\partial\langle a^\dagger a^\dagger\rangle}{\partial t} &= 2|g|\langle a^\dagger R_z\rangle - \kappa\langle a^\dagger a^\dagger\rangle,
\end{aligned}
\tag{4.33}
$$

together with the conjugates equations, which allows one to define the analytical solution of the parameters describing the cavity field dynamics. Here $\gamma_a = (\gamma_{32}\sin^2\theta + \gamma_{21}\cos^2\theta)/4$, $\gamma_b = (\gamma_{21} + \gamma_{32} - 3\gamma_{32}\cos^2\theta)/4$, $\gamma_c = \gamma_{32}\cos^2\theta/2$ and $\gamma_d = \gamma_{21}\sin^2\theta/2$.. Within the steady-state regime the previous system of equations leads to the expressions:

$$
\langle n\rangle = \langle a^\dagger a\rangle = \frac{4|g|^2\gamma_c}{\kappa(\kappa/2 + 2\gamma_a + \gamma_d)(2\gamma_c + \gamma_d)} \tag{4.34}
$$

and

$$
g^{(2)}(0) = \frac{\langle a^\dagger a^\dagger aa\rangle}{\langle a^\dagger a\rangle^2} = \frac{3(\kappa + 2\gamma_c)(\kappa/2 + 2\gamma_a + \gamma_d)(2\gamma_c + \gamma_d)}{2\gamma_c(3\kappa/2 + 2\gamma_a + \gamma_d)(\kappa + 2\gamma_c + \gamma_d)}. \tag{4.35}
$$

Notice, that the second-order correlation function is unaffected by the effective coupling constant g and, therefore, by laser phases.

Similarly to the case when the cavity is set in resonance with the external sidebands of paragraph 4.2, an effective coupling among the quantum-well and the cavity appears for the current case. The destructive nature of these interferences is expressed in the analytical form of the effective coupling constant $g = (g_1 e^{-i\phi_1}\cos\theta + g_2 e^{-i\phi_2}\sin\theta)/2$ of eq.(4.35), when one interaction amplitude cancels the other. This condition is achieved when the amplitudes are equal, i.e., $g_1/g_2 = \Omega_2/\Omega_1$, and interfere destructively, i.e., $\phi_2 = \phi_1 + (2m+1)\pi, m \in \mathcal{Z}$. This condition is verified in Fig.4.7, where one shows the cavity mean photon number $\langle n\rangle$ as function of the Rabi frequencies ratio Ω_2/Ω_1 and laser phase ϕ_2, while keeping the phase of the laser pumping the lower transition at a fixed value of $\phi_1 = 0$. The other system parameters are $\gamma_{32} = \gamma_{21} = \gamma$, $g_1/\gamma = 4$, $g_2/\gamma = 2$ and $\kappa/\gamma = 10^{-3}$. The two deeps in the surface of $\langle n\rangle$ corresponds well to the previously mentioned interference condition with $g_1/g_2 = \Omega_2/\Omega_1 = 2$ and $\phi_2 = \phi_1 + \pi$ or $\phi_2 = \phi_1 + 3\pi$. In these particular points, similarly to the deep of Fig.4.4, one observes an effective decoupling of the quantum-well from the optical cavity. The cavity is empty, although the atom is pumped and spontaneously emits photons in all other directions except the cavity.

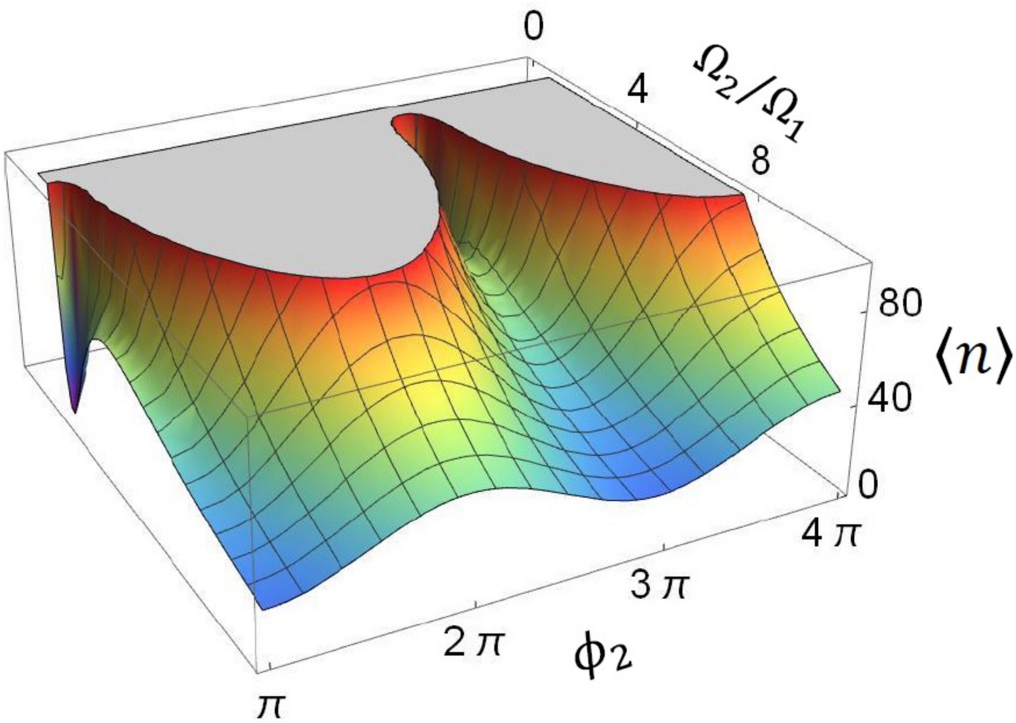

Fig. 4.7: The cavity mean photon number $\langle n \rangle$ as function of Rabi frequencies ratio Ω_2/Ω_1 and laser phase ϕ_2, for a fixed value of $\phi_1 = 0$. The figure is published in [194].

4.4 Conclusions to Chapter 4

The model of a pumped equidistant three-level ladder-type quantum-well placed in an optical cavity had been investigated in the good cavity limit. The emitter has perpendicular transition dipoles and the cavity couples to both of the quantum-well transitions. Two intense lasers with different phases are used to resonantly drive the emitter and each laser couples semi-classically to a different transition. It has been shown that the laser phases are transferred to the quantum-well-cavity interaction amplitudes. Therefore, the superposition of the indistinguishable amplitudes is phase dependent, so that the resulting destructive quantum interferences effect on the cavity field becomes sensitive to the phase difference of the input lasers.

In order to solve the system dynamics, one has tuned the cavity resonantly with the different transition frequencies which appear as a consequence of the dynamical Stark splitting of the quantum-well energetic levels. Each of the resonant case have been treated separately via different solving approaches. One has identified quantum interference effect in situations where the optical resonator is tuned in resonance either with one of the external sideband or with the central peak frequency. All of these interference cases have been interpreted via an effective coupling among the quantum-well and the cavity composed from the superposition of different interaction amplitudes. One has analytically described the effective coupling constant, what have allowed one to tune the laser parameters in order to obtain a destructive superposition case. After solving the system dynamics, one was able to observe the effect of quantum interferences. As a consequence, the cavity mean photon number goes to zero. Photon vanishing is due to quantum interference effects involving two possible dressed-state atomic transitions. Particularly, $\langle n \rangle \to 0$ when $\Omega_2/\Omega_1 = g_1/g_2$ and the laser phases are tuned destructively. Here, the involved parameters or their ratios can be determined when the cavity mean photon number vanishes.

The possibility to control and turn-off the cavity field via quantum interferences suggests a potential application of the studied quantum-well-cavity system for quantum network circuits [3, 195], where tools for controlling the involved processes are highly required. The model is sensitive to phase and intensity variations of the input lasers and acts as quantum switch, because, the mean-photon number abruptly changes from zero to a particular value depending on the atom-cavity coupling. Both input parameters are largely confined in experimental conditions. Moreover, artificial-atom-based systems could be relevant candidates for on-chip quantum circuits [48].

5 MULTIPLE ARTIFICIAL ATOMS PLACED ON A MECHANICAL RESONATOR

In this chapter, one considers a setup where collective radiative effects and nanomechanical motion are brought together. In particular, one envisions a model of a collection of initially excited two-level quantum-dots which are embedded on a nanomechanical resonator. The quantum-dots are spatially arranged to allow for a superradiant collective decay. The nanomechanical vibrations couple to the quantum-dots excited states, leading to a modified phonon dynamics.

The system quantum dynamics is solved by considering a large number of emitters embedded on the mechanical resonator. This allow one to neglect some statistical fluctuations of high order correlation in phonon-quantum-dot interactions.

The decay of the excited quantum-dots contribute to phonon emission into the mechanical resonator. One of the features of the superradiant behaviour, is the fast dynamics of the emitters' decay. One shows here that this feature is transferred to the mechanical resonator. Therefore, one observes that the resulting dynamics of the mechanical resonator has superradiant features in both the phonon emission time scales and the intensity of the generated phonon field. However, the intensity of the phonon emission is also subject to damping phenomena which appear due to the interaction of the resonator with the environmental temperature reservoir. In consequence, the superradiant behaviour of the intensity of the photon emission cannot be equivalenced with its phonon counterpart.

One also investigates the model of two identical two-level quantum-dots embedded on a quantum mechanical resonator, such as a vibrating membrane or a nanomechanical resonator. The artificial atoms interact with the surrounding electromagnetic field, as well as with the nano-resonator's single-mode phonon field. The aim of this study is to explain the mechanics of the phonon field behaviour within the superradiant regime. This regime is reached when the emitters are spaced closer to each other comparing to their transition wavelength. Therefore, this two-emitter system allows an analytical treatment for inside dynamics of the collective interaction within the superradiant regime and shows a significant enhancement of the phonon signal of the quantum mechanical resonator.

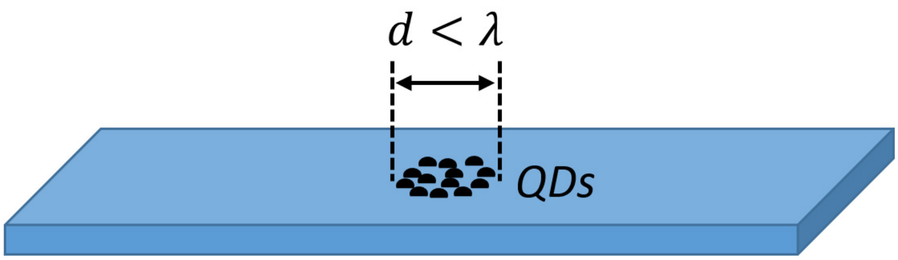

Fig. 5.1: Schematic of the model: An initially excited ensemble of two-level quantum-dots (QDs) are fixed on a vibrating nanomechanical resonator. The linear dimension d of the sample is smaller than the relevant transition photon wavelength λ, *i.e.,* $d < \lambda$.

5.1 The model

One considers a collection of N initially excited two-level quantum-dots fixed on a vibrating membrane as shown in Fig.5.1. The membrane acts as a quantum harmonic oscillator vibrating at a frequency ω. It is damped by an environmental thermal reservoir of temperature T. The mechanical oscillator couples to each quantum-dot of the sample in an equal manner, with a coupling constant η. At lower environmental temperatures one can consider the fundamental mechanical mode only. Therefore, one may treat the oscillator in the single-mode approximation, whereas other modes at different frequencies contribute weakly to the whole quantum dynamics. This is the case if the length L of the nanomechanical resonator is considerably bigger than its width l and thickness a [124], i.e., $L \gg l \gg a$. For $L \sim 10^3$nm, $a \sim 30$nm and $l \sim 100$nm one can still have a sufficient number of quantum-dots fixed on the nanomechanical resonator in order to the superradiance effect to occur, considering that the sizes of quantum-dots are approximately within few to several nanometres.

The system Hamiltonian is built as:

$$H = \hbar\omega b^\dagger b + \sum_{j=1}^{N} \hbar\omega_{\rm qd} S_z^{(j)} + \sum_{j=1}^{N} \hbar\eta|e\rangle_{jj}\langle e|(b + b^\dagger). \tag{5.1}$$

The first term of H is the membrane's free single-mode Hamiltonian of eq.(2.35), expressed via the phonon annihilation and creation operators b and $b^\dagger$, respectively, that obey the usual bosonic commutation relations $[b, b^\dagger] = 1$ and $[b, b] = [b^\dagger, b^\dagger] = 0$.

The second term represents the free Hamiltonian of the quantum-dot sample, given by the eq.(2.3), where $\omega_{\rm qd}$ denotes the quantum-dot's transition frequency. In the second term, one has considered that all the quantum-dots are identical. Which allows one to represent the sum over all of the free individual quantum-dot Hamiltonian terms via the collective inversion operator of the quantum-dot sample expressed as $S_z = \sum_{j=1}^{N} S_z^{(j)}$. Here, the j^{th} quantum-dot is described by its excited $|e\rangle_j$ and ground $|g\rangle_j$ levels. The corresponding single quantum-dot operators are $S_j^+ = |e\rangle_{jj}\langle g|$, $S_j^- = |g\rangle_{jj}\langle e|$ and $S_z^{(j)} = \big(|e\rangle_{jj}\langle e| - |g\rangle_{jj}\langle g|\big)/2$.

Finally, the last interactional term in Hamiltonian of eq.(5.1) represents the interaction of the quantum-dot sample with the phonon field. One has considered that the membrane's spatial scale is larger than the extent of the quantum-dot sample. Consequently, the coupling strengths of each quantum-dot with the vibrational degrees of freedom are identical and have the same magnitude η. This allows one to express the sum of each individual quantum-dot-membrane interaction given by eq.(2.46) via the collective operator for the quantum-dots' upper state defined as $S_{22} = \sum_{j=1}^{N} |e\rangle_{jj}\langle e|$.

After introducing the atomic collective operators in eq.(5.1), the system Hamiltonian is expressed as:

$$H = \hbar\omega b^\dagger b + \hbar\omega_{\text{qd}} S_z + \hbar\eta S_{22}(b + b^\dagger). \tag{5.2}$$

The system dynamics is described by the master equation for the density matrix operator ρ. One is able to introduce the collective operators into the system master equation, as well [76]. The quantum dynamics equation is defined as:

$$\frac{\partial\rho}{\partial t} = -\frac{i}{\hbar}[H,\rho] + \kappa\bar{n}\mathcal{L}(b^\dagger) + \kappa(1+\bar{n})\mathcal{L}(b) + \gamma\mathcal{L}(S^-). \tag{5.3}$$

As in the previous chapters, the damping terms are expressed by the Liouville superoperator $\mathcal{L}$, which, for a given operator $\mathcal{O}$, is defined as $\mathcal{L}(\mathcal{O}) = 2\mathcal{O}\rho\mathcal{O}^\dagger - \mathcal{O}^\dagger\mathcal{O}\rho - \rho\mathcal{O}^\dagger\mathcal{O}$. Here, as usually, the first term of the master equation represents the coherent evolution as given by the Liouville-von Neumann equation of eq.(2.47) and the Hamiltonian of eq.(5.2), whereas the second and the third terms, respectively, denote the pumping and the damping of the mechanical resonator via the environmental thermal reservoir expressed by the damping term of eq.(2.61). The reservoir is described by the mean phonon number:

$$\bar{n} = 1/\big[\exp\left(\hbar\omega/k_B T\right) - 1\big] \tag{5.4}$$

and the damping rate κ. Here, k_B is the Boltzmann constant and T denotes the reservoir's temperature.

The last damping term characterizes the collective spontaneous emission from the sample of quantum-dots as a result for the interaction of the sample with the environmental electromagnetic vacuum field modes. This term is characterized by the single-quantum-dot spontaneous decay rate γ and is expressed via the collective operator $S^{\pm} = \sum_{j=1}^{N} S_j^{\pm}$. By expanding the Liouville super-operator $\mathcal{L}(S^{-})$ term, one observes that the collective spontaneous emission term does not simply contain the sum of the separate independent atomic spontaneous emission terms. It also contains the cross-atomic interactions which occur if one assumes that the spatial separation between different quantum-dots in the sample is much smaller than the quantum-dots' transition wavelength, i.e., a small-volume sample.

The system dynamics is solved by using the method applied in the paragraph 4.3 of the previous chapter. There, one has applied the following property of the system density operator ρ, given for a system operator Q:

$$\frac{\partial\langle Q\rangle}{\partial t} = Tr[\rho\frac{\partial Q}{\partial t}] = Tr[Q\frac{\partial \rho}{\partial t}], \tag{5.5}$$

which is used to build the equation of motion of the corresponding operator. Therefore, by applying this property to the master equation of eq.(5.3), the equation of motion of Q is defined as:

$$\begin{aligned}\frac{\partial\langle Q\rangle}{\partial t} &= i\omega\langle[b^{\dagger}b, Q]\rangle + i\omega_{qd}\langle[S_z, Q]\rangle + i\eta\langle[S_{22}b^{\dagger}, Q]\rangle + i\eta\langle[S_{22}b, Q]\rangle \\ &+ \kappa(1+\bar{n})\Big\{2\langle b^{\dagger}Qb\rangle - \langle b^{\dagger}bQ\rangle - \langle Qb^{\dagger}b\rangle\Big\} + \kappa\bar{n}\Big\{2\langle bQb^{\dagger}\rangle - \langle bb^{\dagger}Q\rangle - \langle Qbb^{\dagger}\rangle\Big\} \\ &+ \gamma\Big\{2\langle S^{+}QS^{-}\rangle - \langle S^{+}S^{-}Q\rangle - \langle QS^{+}S^{-}\rangle\Big\}. \end{aligned} \tag{5.6}$$

The equations of motion of the parameter of interest, i.e., the mean phonon number $\langle b^{\dagger}b\rangle$ and the population inversion $\langle S_z\rangle$, are built from the eq.(5.6). The expressions of the derivatives of parameters of interest introduce a new set of quantities $\langle S_z b^{\dagger}\rangle$, $\langle S_z b\rangle$, $\langle S_z^2 b^{\dagger}\rangle$, $\langle S_z^2 b\rangle$, $\langle b^{\dagger}\rangle$, $\langle b\rangle$ and $\langle S_z^2\rangle$. This results in a system of coupled linear first order differential equation, given as:

$$\begin{aligned}\frac{\partial\langle b^{\dagger}b\rangle}{\partial t} &= i\eta\{\langle S_z b\rangle - \langle S_z b^{\dagger}\rangle + j\langle b\rangle - j\langle b^{\dagger}\rangle\} - 2\kappa\langle b^{\dagger}b\rangle + 2\kappa\bar{n}, \\ \frac{\partial\langle S_z b\rangle}{\partial t} &= -(\kappa + 2\gamma + i\omega)\langle S_z b\rangle + 2\gamma\langle S_z^2 b\rangle \\ &- i\eta\{\langle S_z^2\rangle + j\langle S_z\rangle\} - 2\gamma j(j+1)\langle b\rangle, \\ \frac{\partial\langle S_z b^{\dagger}\rangle}{\partial t} &= -(\kappa + 2\gamma - i\omega)\langle S_z b^{\dagger}\rangle + 2\gamma\langle S_z^2 b^{\dagger}\rangle \\ &+ i\eta\{\langle S_z^2\rangle + j\langle S_z\rangle\} - 2\gamma j(j+1)\langle b^{\dagger}\rangle, \\ \frac{\partial\langle b\rangle}{\partial t} &= -(\kappa + i\omega)\langle b\rangle - i\eta\{\langle S_z\rangle + j\},\end{aligned}$$

$$
\begin{aligned}
\frac{\partial\langle b^\dagger\rangle}{\partial t} &= -(\kappa - i\omega)\langle b^\dagger\rangle + i\eta\{\langle S_z\rangle + j\},\\
\frac{\partial\langle S_z\rangle}{\partial t} &= -2\gamma\{\langle S_z\rangle - \langle S_z^2\rangle + j(j+1)\}.
\end{aligned}
\tag{5.7}
$$

In deriving these equations, one has used $j \equiv N/2$ and the relations

$$
\begin{aligned}
&S_z = S_{22} - j,\\
&S_z^2 + (S^+S^- + S^-S^+)/2 = j(j+1),
\end{aligned}
\tag{5.8}
$$

as well as the commutation relations of collective operators:

$$
\begin{aligned}
&\left[S^+, S^-\right] = 2S_z,\\
&\left[S_z, S^\pm\right] = \pm S^\pm.
\end{aligned}
\tag{5.9}
$$

The system of equations of motions of eqs.(5.7) has not been closed, because a further derivation of the S_z^2 dependent correlations will introduce higher order correlations. If continuing building the equations of motion for those higher order correlations, new even higher order correlation will appear and so on. Therefore, the current system is an infinite system and cannot be closed by further building the equations of the new appearing quantities. Instead, one is able to close this system for some particular situations. Either one may consider a small amount of quantum-dots and explicitly develop S_z^2 as shown in the next paragraph 5.2 or one may consider a large amount of quantum-dots placed on the sample and therefore neglect some of the fluctuations of the higher order correlations as presented in paragraph 5.3.

5.2 Small number of quantum-dots

For only a few quantum-dots, it is possible to solve the system by using the explicit expression of the S_z^2 depending terms, *i.e.*, by considering the equations of motion of every $S_z^{(i)}S_z^{(j)}$ term. Here, one will consider the simplest cases of a single quantum-dot, i.e., $N = 1$ and the case of a pair of collectively interacting quantum-dots placed on the membrane, i.e., $N = 2$. In the first case when $N = 1$, $S_z^2 = 1/4$ and, hence, the system is closed and analytically solvable. Considering that the quantum-dot is initially excited while the membrane is in thermal equilibrium with the reservoir, the temporal behaviour of the mean phonon number is given by

$$\langle b^\dagger b\rangle \;=\; \bar{n} + \bar{a}e^{-2\gamma t} - (\bar{a} + \bar{b}\bar{c})e^{-2\kappa t} + \bar{b}e^{-(2\gamma+\kappa)t}\left(\bar{c}\cos\omega t - \bar{d}\sin\omega t\right), \tag{5.10}$$

where the equation coefficients are defined as:

$$\begin{aligned}
\bar{a} &= \kappa\eta^2/\left[(\kappa-\omega)(\kappa^2+\omega^2)\right],\\
\bar{b} &= 2\eta^2/(\bar{c}^2+\bar{d}^2),\\
\bar{c} &= 2\gamma\kappa - \kappa^2 - \omega^2,\\
\bar{d} &= 2\gamma\omega.
\end{aligned} \tag{5.11}$$

Likewise, the temporal evolution of the quantum-dot population inversion reads [76]:

$$\langle S_z(t)\rangle = -1/2 + e^{-2\gamma t}. \tag{5.12}$$

For initially excited $N = 2$ collectively interacting qubits, one solves the system of equations which is given for a pair of collectively interacting quantum-dots, $q1$ and $q2$ as:

$$\begin{aligned}
\frac{\partial\langle S_z\rangle}{\partial t} &= -2\gamma\langle S^+S^-\rangle,\\
\frac{\partial\langle S^+S^-\rangle}{\partial t} &= 8\gamma\{1 + \langle S_z\rangle - \langle S^+S^-\rangle\},\\
\frac{\partial\langle b^\dagger b\rangle}{\partial t} &= i\eta\{\langle S_z b\rangle - \langle S_z b^\dagger\rangle + \langle b\rangle - \langle b^\dagger\rangle\} - 2\kappa\langle b^\dagger b\rangle + 2\kappa\bar{n},\\
\frac{\partial\langle S_z b\rangle}{\partial t} &= -(\kappa + i\omega)\langle S_z b\rangle - 2\gamma\langle S^+S^-b\rangle - i\eta\{2 + 2\langle S_z\rangle - \langle S^+S^-\rangle\},\\
\frac{\partial\langle S^+S^-b\rangle}{\partial t} &= -(\kappa + 8\gamma + i\omega)\langle S^+S^-b\rangle - 2i\eta\{1 + \langle S_z\rangle\} + 8\gamma\{\langle b\rangle + \langle S_z b\rangle\},\\
\frac{\partial\langle b\rangle}{\partial t} &= -(\kappa + i\omega)\langle b\rangle - i\eta\{1 + \langle S_z\rangle\},
\end{aligned} \tag{5.13}$$

where $S_z = S_z^{(q1)} + S_z^{(q2)}$ and $S^\pm = S_{q1}^\pm + S_{q2}^\pm$. The missing equations of motion can be obtained via Hermitian conjugation of the last three equations in (5.13). This system of equations is solved numerically and the results are shown in Fig.5.2. One can observe that the vibrational mean phonon number is increased in comparison to single-qubit case. The initial condition for the involved variables are:

$$\begin{aligned}
\langle S_z \rangle_{t=0} &= 1, \\
\langle S^+ S^- \rangle_{t=0} &= 2, \\
\langle S_z b \rangle_{t=0} &= \langle S_z b^\dagger \rangle_{t=0} = \langle S^+ S^- \, b \rangle_{t=0} = \langle S^+ S^- \, b^\dagger \rangle_{t=0} = \langle b \rangle_{t=0} = \langle b^\dagger \rangle_{t=0} = 0, \\
\langle b^\dagger b \rangle_{t=0} &= \bar{n}.
\end{aligned} \tag{5.14}$$

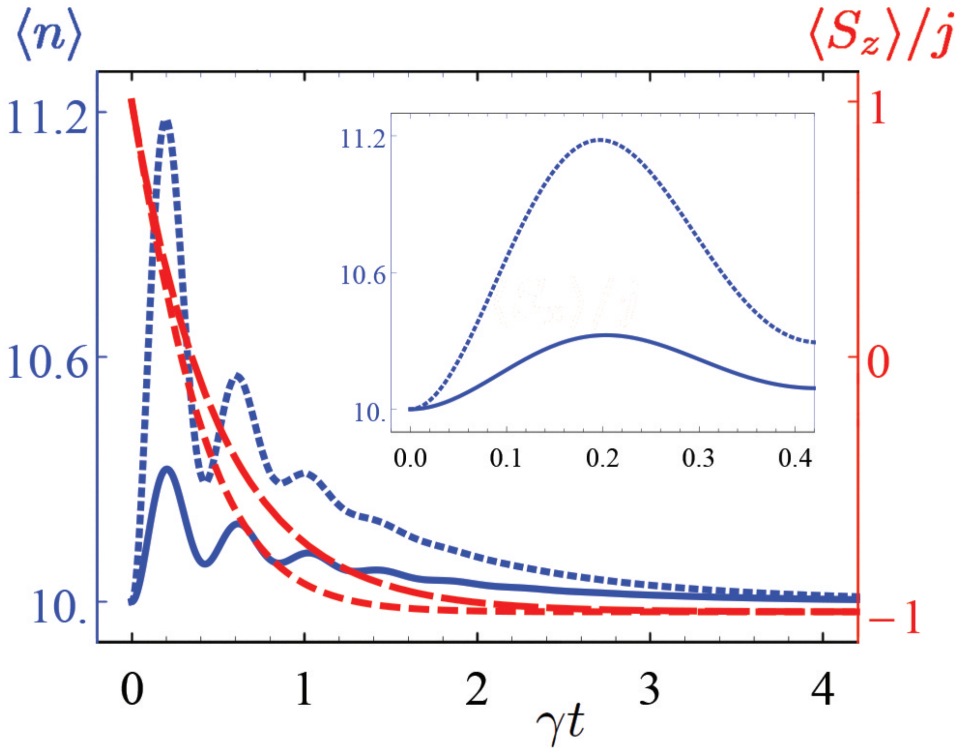

Fig. 5.2: Temporal evolution of the mean phonon number $\langle n \rangle$ and the population inversion $\langle S_z \rangle$ for a single-quantum-dot sample (solid and long-dashed lines, respectively) as well as for $N = 2$ (dotted and short-dashed curves, respectively). The inset shows the mean phonon number for $N = 1$ and $N = 2$ at the beginning of the time-evolution. The figure is published in [175].

In Fig.5.2, the dynamics of $\langle b^\dagger b \rangle$ and $\langle S_z \rangle$ is depicted for the case when a single quantum-dot or a pair of collectively interacting quantum-dots are placed on the membrane. The system parameters are defined as: $\omega/\gamma = 15$, $\eta/\gamma = 5$, $\kappa/\gamma = 0.5$ and $\bar{n} = 10$. One sees that the mean phonon number first slightly increases and oscillates as a result of the interaction between the quantum-dot sample and the mechanical vibrations. However, for $N = 2$ the mean vibrational phonon number is enhanced in comparison to single-qubit case although the dynamics is not faster (i.e., one needs larger ensembles to see a rapid evolution) in spite of the fact that the inversion decays faster for $N = 2$.

The increase in the decay dynamics is better represented in Fig.5.3, where one has used logarithmic coordinates for the same model as in Fig.5.2, in order to represent the expectational behaviour of the population decay dynamics. Here, one has represented in red dashed lines the single qubit case and in continuous blue line the two-qubit case. In the last case, a quasi-linear behaviour in logarithmic scale with a considerably increased slope, i.e., increased exponential damping rate, is observed in the decay dynamics.

After the quantum-dot's decay, the membrane returns back to thermal equilibrium since in the Hamiltonian (5.1) phonons only couple to the quantum-dots' excited states. Consequently, once the quantum-dot reaches its ground state, the phonon field is subject to damping due to the thermal reservoir. Another intrinsic property of the model is that the behaviour of the quantum-dot population decay and its fluorescence dynamics is not affected by the phonon activity in this model. This property is observed in the analytic expression of $\langle S_z \rangle$ and it is also valid for the following results obtained for a more numerous quantum-dot collection. This is the case if the preparation time, Δt, of the initial excited state is fast, *i.e.*, it takes place on a time-scale shorter than η^{-1}.

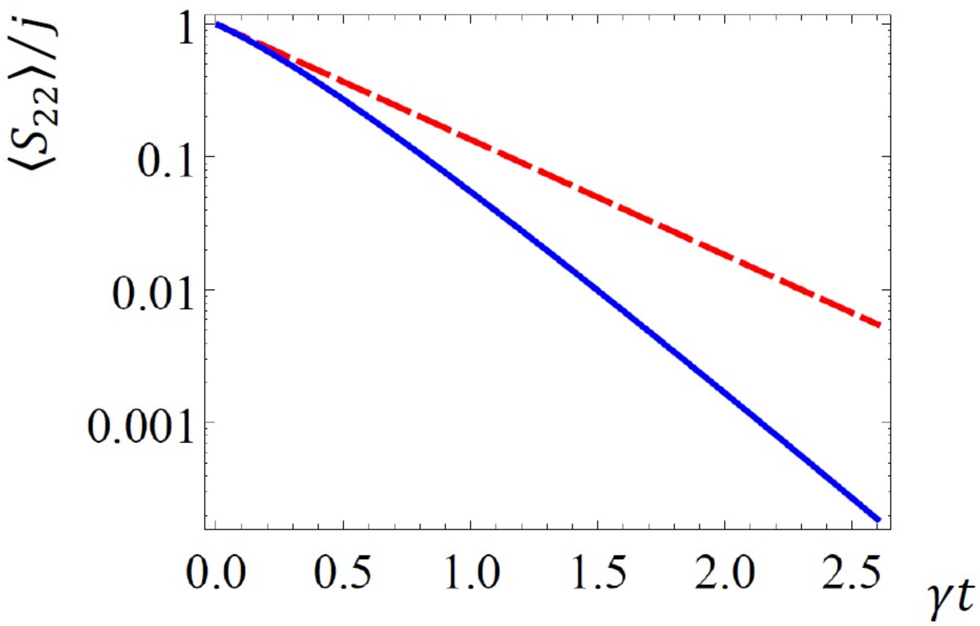

Fig. 5.3: The temporal evolution of the collective excited state population S_{22} in logarithmic scale for a single-quantum-dot case represented in red dashed line and $N = 2$ case represented in blue continuous line.

5.3 Large number of quantum-dots

For samples of $N \gg 1$ quantum-dots, the system of equations (5.7) can be closed by a factorization of the correlations $\langle S_z^2 \rangle$, $\langle S_z^2 b^\dagger \rangle$, and $\langle S_z^2 b \rangle$ according to [168].

One starts with $\langle S_z^2 \rangle \simeq \langle S_z \rangle^2$, which is equivalent to neglecting the fluctuations of the collective population inversion of the quantum-dot sample, reasonable as long as $N \gg 1$. This assumption does not break the symmetry of the system as there are no new variables introduced. In this context, the collective inversion operator $\langle S_z(t) \rangle$ simply becomes [168]:

$$\langle S_z(t) \rangle = -\frac{N}{2} \tanh\Big[\frac{1}{2\tau_R}(t - t_0)\Big], \tag{5.15}$$

where $\tau_R = 1/(2\gamma N)$ and $t_0 = \tau_R \log(N)$.

For higher order correlations, the symmetry of the system of equations is also maintained and one can choose either $\langle S_z^2 b \rangle \simeq \langle S_z \rangle \langle S_z b \rangle$ or $\langle S_z^2 b \rangle \simeq \langle S_z \rangle^2 \langle b \rangle$ for the decoupling scheme. Similarly, one proceeds with the $\langle S_z^2 b^\dagger \rangle$ term. Note that these two schemes are justified for larger quantum-dot ensembles and for larger phonon numbers. Under this conditions, one verifies that both of the decoupling schemes lead to a similar result in the system quantum dynamics.

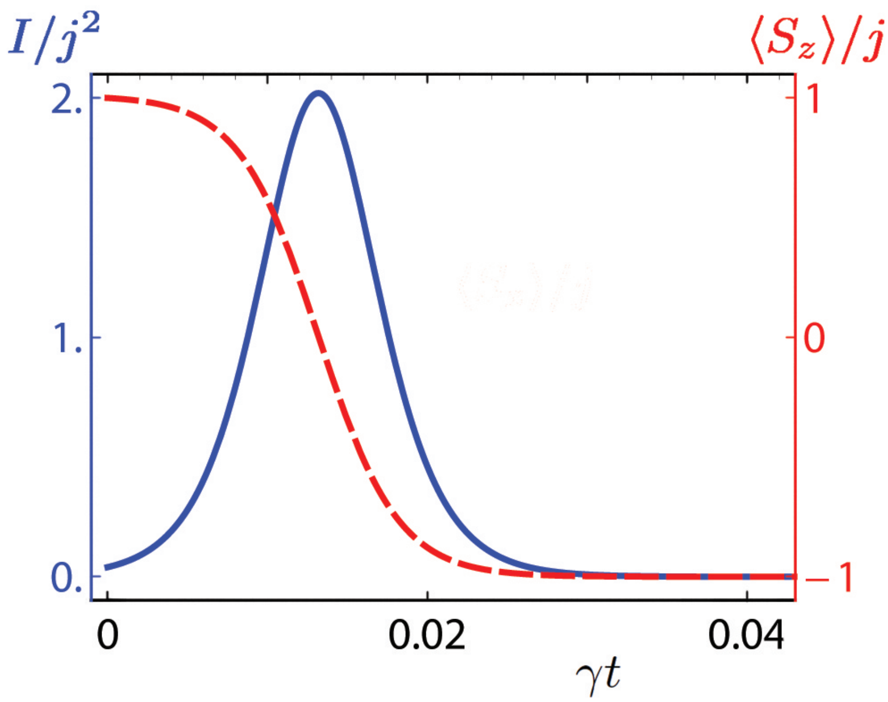

Fig. 5.4: Temporal evolution of the collective population inversion $\langle S_z(t) \rangle / j$ (dashed line) and the collective fluorescence intensity I/j^2 (solid line) for a sample of $N = 200$ quantum-dots. The figure is published in [175].

Using the numerical solution of the system of equations (5.7), one depicts in Fig.5.4 the dynamics of the collective population inversion of the quantum-dot sample $\langle S_z(t)\rangle/j$ represented in dashed red line and the corresponding fluorescence intensity $I(t)$ in blue continuous line. The fluorescence intensity expression is given as:

$$I(t) \propto -\partial\langle S_z\rangle/\partial t, \tag{5.16}$$

for which one has chosen the following initial conditions:

$$\begin{aligned}\langle S_z\rangle_{t=0} &= j,\\ \langle S_z b\rangle_{t=0} &= \langle S_z b^\dagger\rangle_{t=0} = \langle b\rangle_{t=0} = \langle b^\dagger\rangle_{t=0} = 0,\\ \langle b^\dagger b\rangle_{t=0} &= \bar{n}.\end{aligned} \tag{5.17}$$

Note that the two-level quantum-dot sample can be excited initially with a short laser pulse of duration $\Delta t < 1/\eta$ in order to avoid the influence of vibrational phonons on the preparation stage. Similar to the single-quantum-dot case, the vibrations of the membrane do not affect the behaviour of $\langle S_z(t)\rangle$ and $\partial\langle S_z(t)\rangle/\partial t$, resembling the classical superradiance effect of a small volume sample. Indeed, one obtains a decrease of the quantum-dots' lifetime which is inversely proportional to N, whereas the intensity increases proportional to N^2. Evidently, the maximum fluorescence intensity is reached for an equal number of quantum-dots in the excited and ground states, respectively (see Fig.5.4).

With an increased number of quantum-dots, the condition of having quasi-identical emitters becomes more difficult to achieve. This condition is validated as long as the variations in the frequencies of the quantum-dots do not exceed the bandwidth of the collective state of the quantum-dots $N\gamma$. More precisely, the resemblance of the ensemble of emitters is treated statistically by considering the frequency distribution of the quantum-dots. For a frequency distribution centred at ω_{ph} and a width $\Delta\omega_{ph}$, $\Delta\omega_{ph}$ should not exceed the bandwidth of the collective state $N\gamma$, in order to consider the emitters quasi-identical, i.e., $\Delta\omega_{ph} < N\gamma$.

On the other hand, the phonon dynamics is affected by the collective effect within the quantum-dot sample as shown in Fig. 5.5. For this plot, the system is defined via the parameters $\omega/\gamma = 50$, $\eta/\gamma = 5$, and $\bar{n} = 10$. Here, a superradiant behaviour is observed in both: a reduced lifetime and an enhanced mean phonon number. This can be explained as follows. The membrane's vibrations interact with the quantum-dots' excited states and, therefore, the time scale for when phonons are created is related to the decay rate of the atomic sample. Then, in analogy to the single-quantum-dot case, when the quantum-dot sample approaches its collective ground state, the phonon dynamics becomes dominated by damping phenomena due to the environmental reservoir. Hence, the mean phonon number decreases to its initial value $\bar{n}$, characterizing equilibrium with the thermal reservoir. Further, the superradiance effect exhibits a bell-like behaviour for the collective intensity. One can identify this behaviour in Fig. 5.5 together with faster dynamics in comparison to the single-qubit case. However, the intensity does not simply scale as N^2 although one has a clear enhancing of phonon emission.

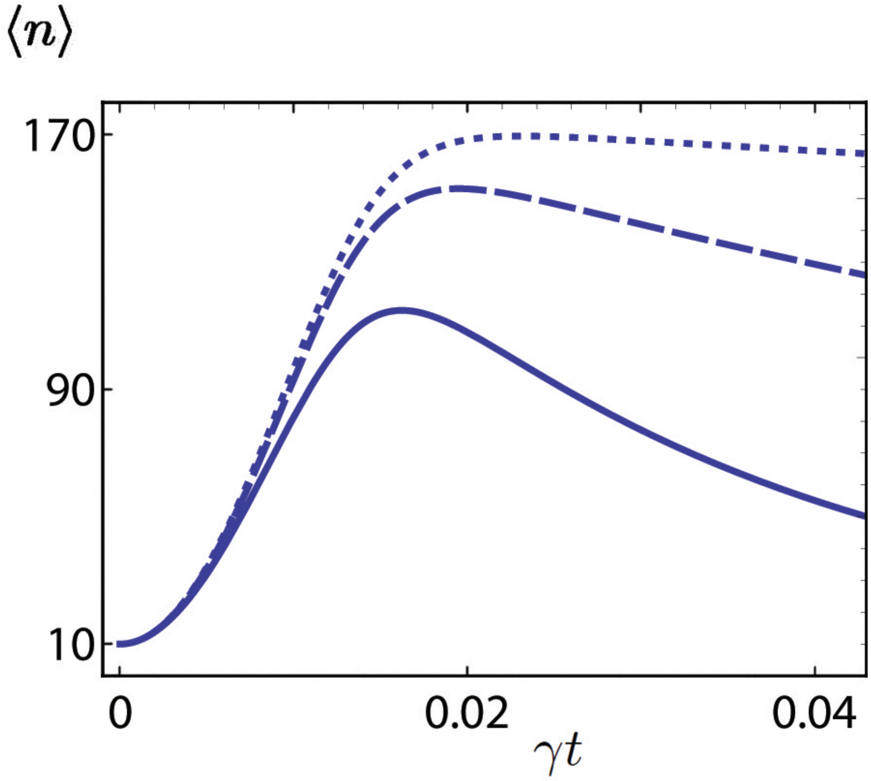

Fig. 5.5: Temporal evolution of the mechanical resonator's mean phonon number $\langle n \rangle$. Here, a collection of $N = 200$ quantum-dots is excited initially. The results are shown for different damping rates κ, *i.e.*, for $\kappa/\gamma = 1$ (dotted curve), $\kappa/\gamma = 5$ (dashed curve), and $\kappa/\gamma = 20$ (solid curve). The figure is published in [175].

In the absence of collective effects, one would have similar behaviours as shown in Fig. 5.2 for $N = 1$, i.e. no fast dynamics, however the phonon number will be enhanced as well because the coupling of qubits to phonons increases due to many independent emitters. A simplistic representation of this case is to consider a giant emitter with an effective coupling N times stronger than the individual couplings of independent emitters. In this case the phonon dynamics will be described via the eq.(5.10) given for a single quantum-dot sample, but with an effective coupling given by $\eta \to N\eta$. All the terms of eq.(5.10) are proportional to η^2 as given in eq.(5.11). Therefore, an increase in the coupling constant by N would lead to an increase in the resonator mean phonon number by N^2. Hence, the N^2 increase in the phonon number is not a feature of phonon superradiance, but an intrinsic property resulting from the nature of the phonon-quantum-dot coupling.

Note that although the phonon superradiance is interconnected to the collective effects within the quantum-dot sample and, therefore, to the number N of quantum-dots, the maximum mean phonon number is also determined by the damping rate κ. This can be seen in Fig. 5.5 as the superradiant phonon emission increases in width and maximum for weaker damping, i.e., for smaller κ, resembling a good or bad cavity limit, respectively.

5.4 Conclusions to Chapter 5

In conclusion, one has investigated the quantum dynamics of a coupled system composed of an ensemble of two-level quantum-dots that are fixed on a vibrating, nano-mechanical membrane. One has discussed the temporal evolution and the underlying equations of motion in detail, as well as their solving techniques. Two separate approaches have been used, in order to solve the system quantum dynamics. Considering small quantum-dot samples one was able to solve the dynamics without any approximations and, therefore, investigate the nature of the phonon-quantum-dot coupling. Considering large quantum-dot collections, one was able to neglect the fluctuations of high order correlations and, therefore, observe the collective dynamics influence on the mechanical resonator.

Two distinct features of the superradiant behaviour have been discussed. Namely, the faster phonon dynamics and the stronger intensity of emission. The fast phonon dynamics appears from the fast decaying mechanics of the collective quantum-dot sample. As the phonons couple only to the sample collective excited state, the faster decay of this state leads to shorter time of phonon generation. However, the phonon pulse width is not only dependent of the sample decay mechanics, but also of the rate of the damping phenomena of phonon leaking into its surroundings. A similar dependency has been observed for the phonon peak maximum, where stronger damping lead to lower peaks and vice-versa.

As the main result, it have been found that the quantum-dot sample exhibits superradiance features which are transferred to the vibrational degrees of freedom of the nanomechanical resonator, leading to phonon superradiance in a nanomechanical setup. Furthermore, the detection of photon superradiance ensures the existence of phonon superradiance. Thus, our scheme may serve as a vibrational phonon detector in case of superradiance effects. Therefore, phonon superradiance effect may improve the optical mass sensing scheme described in [196] or to enhance ultra-weak signal detections [197]. Notice that phonon superradiance phenomenon in a different context was investigated in [174, 176] and [198, 199], for instance.

CONCLUSIONS AND RECOMMENDATIONS

The objectives of the thesis have been fulfilled and various quantum effects had been identified when studying the scientific problem of artificial atoms interacting with optical or mechanical resonators. Following the objectives, three distinct models had been proposed and investigated, each requiring a separate solving approach in order to accurately estimate the quantum dynamics. Namely, the investigation of different emitter-resonator coupling schemes had allowed the identification of two distinct cases. In the first case, a special treatment for moderately strong optomechanical couplings has allowed to identify quantum distributed quanta in the vibrational motion of the mechanical resonator. In the second case, considering a three-level quantum-well where both transitions couple to an optical resonator, has allowed to identify a quantum interference phenomenon. The investigation of collective phenomena of a closely spaced ensemble of artificial atoms coupled to a nanomechanical resonator, has allowed to identify a superradiant-like behaviour of the mechanical motion.

The main scientific results presented in this thesis are summarized as follows:

1) The novel treatment applied to the model of a quantum-dot embedded on a quantum mechanical resonator has contributed to an improved description of the system quantum dynamics for strong optomechanical coupling regimes. For characteristic couplings strength of same order of magnitude as the mechanical frequency, a perturbation treatment introduces new fast-rotating terms into the Hamiltonian describing the system coherent dynamics. The observation of quantum features as sub-Poissonian distribution of the mechanical vibration quanta, becomes possible only when considering the new terms. Moreover, a different mean phonon number had been estimated comparing to the case when a secular approximation is applied in order to neglect the fast-rotating terms. The corresponding study is published in [151].

2) The model adapted for moderately strong optomechanical couplings, has been investigated in other possible scenarios such as quantum cooling regime and strong damping regimes. A stronger cooling effect has been predicted via the novel approach for strong coupling regimes. For strong damping regimes, phonon assisted population inversion has been observed as expected. The study on the quantum cooling effect is published in [137].

3) The investigation of the quantum dynamics of a three-level ladder-type quantum-well interacting with an optical resonator has been made possible by adapting the numerical solving technique to the case of a three-level emitter. The quantum interferences among different atomic transitions which appear from the splitting of the energetic levels of the quantum-well under the laser pumping have been investigated. Different interference schemes have been identified. The laser phase and intensity are used in order to tune the system to a completely destructive interference which leads to the cancellation of the cavity field. The first study on this model is published in [102], while the phase-dependence was lately described in [103].

4) Although the described quantum interference effect requires the implementation of an equidistant three-level emitter, the solved model may also be applied for emitters with different transition energies, e.g., He atoms with the upper transition in visible range and the lower one in extreme ultraviolet. In this case, the solved model has predicted a coherent population trapping where the emitter had been prepared in a dark state by well choosing the suitable intensities ratio of the pumping lasers.

5) Fast phonon dynamics was observed when a collection of quantum-dots embedded on a vibrating membrane had been considered. When the closely-spaced quantum-dots reach the superradiant condition, the collective behaviour of faster decay dynamics is transferred to the dynamics of the mechanical resonator. A superradiant characteristic of N times faster dynamics has been observed in the phonon emission dynamics of a sample of N quantum-dots. The system dynamics has been solved assuming a large number of emitters and a large number of vibrational quanta, which have allowed to split the high order correlations and define a closed system of equations of motion. The presented results are published in [175] and have been one of the firsts reports on the effect of phonon superradiance. These results have been cited since in remarkable reports on optomechanical superradiant effect [198, 199] and collective quantum cooling effect [200].

Considering the conclusions above, one would highlight the following recommendations:

1) The method applied to the theoretical treatment of the model of a quantum-dot placed on a mechanical resonator, has significantly improved the estimation of the quantum statistics of the mechanical resonator for specific optomechanical coupling strengths. Therefore, one would recommend further investigation of the validity of the secular approximation in other models based on optomechanical devices possessing quantum-dots in order to identify the cases where treatments beyond the secular approximation could improve the accuracy of the estimated results.

2) A strong destructive quantum interference phenomenon predicted in the model of a quantum-well placed in an optical resonator leads to a complete cancellation of the cavity field for a specific ration of laser intensities. This model can be implemented for measuring the coupling constants of the emitter, as their ratio is proportional to the ratio of laser intensities when the cavity field is completely cancelled. This case can be experimentally detected with ease.

3) A quantum switch where the cavity field is turned on and off via the input laser parameters is recommended as an application for the model of a quantum-well placed in an optical resonator. Moreover, a potential inclusion of other effects which could influence the interfering interaction amplitudes would suggest an application for sensing techniques. One would recommend the inclusion of optomechanical couplings to the current model which will affect only the excited states of the emitter.

4) The study of the collective phenomena of an ensemble of quantum-dots placed on a mechanical resonator has revealed a superradiant-like behaviour of fast phonon dynamics. One recommends the implementation of this effect to phonon based sensing techniques where short enhanced phonon pulses may be required.

5) One would also recommend a further investigation of the influence of phonon superradiant features on other optomechanical effects. For example, the increase of the decay dynamics due to the superradiant phenomenon could affect the dynamics of phonon cooling and generation processes described in Chapter 3, for a single emitter. One has predicted that the phonon lasing and quantum cooling effects via a detuned laser pumping are dependent of the spontaneous emission effect. Therefore, one would recommend the implementation of collective dynamics into these models due to the enhancement of the collective decay rate which occurs for superradiant conditions. For instance, the collective dynamics of the quantum cooling effect have been recently investigated in [200].

The limitation of presented results is related to the theoretic models disclosed in the previous chapters. In Chapter 2, one has presented the theoretical framework related to each element of the dynamics, where a series of assumptions has been applied in order to define the Hamiltonians describing various interactions as well as the damping phenomena. All these assumptions were strictly respected when solving the models. Moreover, further theoretical treatment presented in chapters 3, 4 and 5, has required the application of several approximations, e.g., the rotating wave approximation, the secular approximation. The validity of these approximations has been discussed and further respected when plotting the results. The numerical solving techniques applied in chapters 3 and 4, have required another series of approximations due to the infinite number of quantum states of the optical or mechanical resonator. These assumptions and approximations do not affect the generality of the studied problems and have been experimentally approved in different scenarios.

The personal contribution of the author to the presented results: The author had participated to the identification of the presented objectives, tasks and models; for each model slightly-advised he had solved the theoretical treatment applied to the quantum dynamics and had independently numerically solved the different systems of equations defining the quantum dynamics; he had written the firsts drafts of the publications related to the results presented in this thesis.

References

[1] REN, J.-G., XU, P., PAN, J.-W.. *et al.*. Ground-to-satellite quantum teleportation. In: *Nature*, 2017, vol. 549, pp. 70–73.

[2] BOARON, A., BOSO, G., RUSCA, D., VULLIEZ, C., AUTEBERT, C., CALOZ, M., PERRENOUD, M., GRAS, G., BUSSIERES, F., LI, M.-J., NOLAN, D., MARTIN, A., ZBINDEN, H.. Secure Quantum Key Distribution over 421 km of Optical Fiber. In: *Phys. Rev. Lett.*, 2018, vol. 121, pp. 190502/1-4.

[3] KIMBLE, H., J.. The quantum internet. In: *Nature (London)*, 2008, vol. 453, pp. 1023–1030.

[4] KNILL, E., LAFLAMME, R., MILBURN, G., J.. A scheme for efficient quantum computation with linear optics. In: *Nature*, 2000, vol. 409, pp. 46–52.

[5] SPRING, J. B., METCALF, B. J., HUMPHREYS, P. C., KOLTHAMMER, W. S., JIN, X.-M., BARBIERI, M., DATTA, A., THOMAS-PETER, N., LANGFORD, N. K., KUNDYS, D., GATES, J. C., SMITH, B. J., SMITH, P. G. R., WALMSLEY, I. A.. Boson Sampling on a Photonic Chip. In: *Science*, 2013, vol. 339, pp. 798–801.

[6] BEVERATOS, A., ABRAM, I., GERARD, J.-M., ROBERT-PHILIP, I.. Quantum optics with quantum dots. In: *Eur. Phys. J. D*, 2014, vol. 68, pp. 377/1-14.

[7] O'CONNELL, A. D., HOFHEINZ, M., ANSMANN, M., RADOSLAW, C., BIALCZAK LENANDER, M., LUCERO, E., NEELEY, M., SANK, D., WANG, H., WEIDES, M., WENNER, J., MARTINIS, J. M., CLELAND, A. N.. Quantum ground state and single-phonon control of a mechanical resonator. In: *Nature*, 2010, vol. 464, nr. 7289, pp. 697-703.

[8] ASPELMEYER, M., KIPPENBERG, T. J., MARQUARDT, F.. Cavity optomechanics. In: *Rev. Mod. Phys.*, 2014, vol. 86, nr. 4, pp. 1391-1452.

[9] ASPELMEYER, M., KIPPENBERG, T. J., MARQUARDT, F.. *Cavity Optomechanics.* Berlin Heidelberg: Springer-Verlag, 2014. 357 p.

[10] CARLIG, S., MACOVEI, M. A.. Long-time correlated quantum dynamics of phonon cooling. In: *Phys. Rev. A*, 2014, vol. 90, pp. 043411/1-4.

[11] ULHAQ, A., WEILER, S., ROY, C., ULRICH, S. M., JETTER, M., HUGHES, S., MICHLER, P.. Detuning-dependent Mollow triplet of a coherently-driven single quantum dot. In: *Optics Express*, 2013, vol. 21, pp. 4382-4395.

[12] HUGHES, S., CARMICHAEL, H. J.. Phonon-mediated population inversion in a semiconductor quantum-dot cavity system. In: *New J. Phys.*, 2013, vol. 15, pp. 053039/1-15.

[13] CECOI, E., CIORNEA, V., ISAR, A., MACOVEI, M. A.. Entanglement of a laser-driven pair of two-level qubits via its phonon environment. In. *J. Opt. Soc. Am. B*, 2018, vol. 35, pp. 1127-1132.

[14] WOLLMAN, E. E., LEI, C. U., WEINSTEIN, A. J., SUH, J., KRONWALD, A., MARQUARDT, F., CLERK, A. A., SCHWAB, K. C.. Quantum squeezing of motion in a mechanical resonator. In: *Science*, 2015, vol. 349, pp. 952-955.

[15] MAHBOOB, I., NISHIGUCHI, K., FUJIWARA, A., YAMAGUCHI, H.. Phonon Lasing in an Electromechanical Resonator. In: *Phys. Rev. Lett.*, 2013, vol. 110, nr. 12, pp. 127202/1-5.

[16] GRUDININ, I. S., LEE, H., PAINTER, O., VAHALA, K. J.. Phonon Laser Action in a Tunable Two-Level System. In: *Phys. Rev. Lett.*, 2010, vol. 104, nr. 8, pp. 083901/1-4.

[17] VAHALA, K., HERRMANN, M., KNÜNZ, S., BATTEIGER, V., SAATHOFF, G., HÄNSCH, T. W., UDEM, T.. A phonon laser. In: *Nat. Phys.*, 2009, vol. 5, pp. 682–686.

[18] KABUSS, J., CARMELE, A., BRANDES, T., KNORR, A.. Optically Driven Quantum Dots as Source of Coherent Cavity Phonons: A Proposal for a Phonon Laser Scheme. In: *Phys. Rev. Lett.*, 2012, vol. 109, nr. 5, pp. 054301/1-5.

[19] KABUSS, J., CARMELE, A., KNORR, A.. Threshold behavior and operating regimes of an optically driven phonon laser: Semiclassical theory. In: *Phys. Rev. B*, 2013, vol. 88, nr. 6, pp. 064305/1-6.

[20] OKUYAMA, R., ETO, M., BRANDES, T.. Lasing and antibunching of optical phonons in semiconductor double quantum dots. In: *New J. Phys.*, 2013, vol. 15, pp. 083032/1-27.

[21] QIAN, J., CLERK, A. A., HAMMERER, K., MARQUARDT, F.. Quantum Signatures of the Optomechanical Instability. In: *Phys. Rev. Lett.*, 2012, vol. 109, nr. 25, pp. 253601/1-5.

[22] NATION, P. D.. Nonclassical mechanical states in an optomechanical micromaser analog. In: *Phys. Rev. A*, 2013, vol. 88, pp. 053828/1-7.

[23] PATEL, R. B., BENNETT, A. J., FARRER, I., NICOLL, C. A., RITCHIE, D. A., SHIELDS, A. J.. Two-photon interference of the emission from electrically tunable remote quantum dots. In: *Nat. Photon.*, 2010, vol. 4, pp. 632–635.

[24] SCHEIBNER, M., SCHMIDT, T., WORSCHECH, L., FORCHEL, A., BACHER, G., PASSOW, T., HOMMEL, D.. Superradiance of quantum dots. In: *Nat. Phys.*, 2007, vol. 3, pp. 106–110.

[25] PLANCK, M.. On an Improvement of Wien's Equation for the Spectrum. In: *Verhandl. Dtsch. phys. Ges.*, 1900, vol. 2, nr. 2, pp. 202-204.

[26] PLANCK, M.. On the Theory of the Energy Distribution Law of the Normal Spectrum. In: *Verhandl. Dtsch. phys. Ges.*, 1900, vol. 2, pp. 237-245.

[27] EINSTEIN, A.. On the present status of the radiation problem. In: *Phys. Z.*, 1909, vol. 10, nr. 6, pp. 185-193.

[28] EINSTEIN, A.. On the development of our views concerning the nature and constitution of radiation. In: *Phys. Z.*, 1909, vol. 10, nr. 22, pp. 817-825.

[29] EINSTEIN, A.. Über einen die Erzeugung und Verwandlung des Lichtesbetreffendenheuristischen Gesichtspunkt. In: *Annalen der Physik*, 1905, vol. 6, nr. 17, pp. 132-148.

[30] GORDON, J. P., ZEICER, H. J., TOWNES, C. H.. The Maser New Type of Microwave Amplifier, Frequency Standard, and Spectrometer.In: *Phys. Rev.*, 1955, vol. 99, nr. 4, pp. 1264-1274.

[31] BASOV, N. G., PROKHOROV, A. M.. The use of molecular bundles for radiospectroscopic study of the band spectra of molecules. In: *Zh. Eksp. Teor. Fiz.*, 1954, vol.27, pp. 431-438.

[32] MAIMAN, T. H.. Stimulated Optical Radiation in Ruby. In: *Nature*, 1960, vol. 187, pp. 493-494.

[33] GLAUBER, R. J.. The Quantum Theory of Optical Coherence. In: *Phys. Rev.*, 1963, vol. 130, nr. 6, pp. 2529-2539.

[34] MANDEL, L., WOLF, E.. Coherence Properties of Optical Fields. In: *Rev. Mod. Phys.*, 1965, vol. 37, nr. 2, pp. 231-287.

[35] PURCELL, E. M.. Spontaneous emission probabilities at radio frequencies. In: *Phys. Rev.*, 1946, vol. 69, p. 681.

[36] DREXHAGE, K. H.. Interaction of light with monomolecular dye lasers. In: *Progress in Optics (E. Wolf, ed.)*, 1974, vol. 12, pp. XVII 165-229.

[37] DE MARTINI, F., INNOCENTI, G., JACOBOVITZ, G, MANTOLINI, P.. Anomalous Spontaneous Emission Time in a Microscopic Optical Cavity. In: *Phys. Rev. Lett.*, 1987, vol. 59, nr. 26, pp. 2955–2958.

[38] MESCHEDE, D., WALTHER, H., MULLER, G.. One-Atom Maser. In: *Phys. Rev. Lett.*, 1985, vol. 54, nr. 6, pp. 551–554.

[39] JAYNES, E. T., CUMMINGS, F. W.. Comparison of Quantum and Semiclassical Radiation Theories with Application to the Beam Maser. In: *Proc. IEEE*, 1963, vol. 51, nr. 1, pp. 89–109.

[40] REMPE, G., WALTHER, H., KLEIN, N., Observation of Quantum Collapse and Revival in a One-Atom Maser. In: *Phys. Rev. Lett.*, 1987, vol. 58, nr. 4, pp. 353–356.

[41] REMPE, G., SCHMIDT-KALER, F., WALTHER, H.. Observation of Sub-Poissonian Photon Statistics in a Micromaser. In: *Phys. Rev. Lett.*, 1990, vol. 64, nr. 23, pp. 2783–2786.

[42] HAGLEY, E., MAÎTRE, X., NOGUES, G., WUNDERLICH, C., BRUNE, M., RAIMOND, J. M., HAROCHE, S.. Generation of Einstein-Podolsky-Rosen Pairs of Atoms. In: *Phys. Rev. Lett.*, 1997, vol.79, nr. 1, pp. 1–5.

[43] WEIDINGER, M., VARCOE, B. T. H., HEERLEIN, R., WALTHER, H.. Trapping States in the Micromaser. In: *Phys. Rev. Lett.*, 1999, vol. 82, nr. 19, pp. 3795–3798.

[44] VARCOE, B. T. H., BRATTKE, S., WEIDINGER, M., WALTHER, H.. Preparing pure photon number states of the radiation field. In: *Nature*, 2000, vol. 403, pp. 743–746.

[45] ASPURU-GUZIK, A., WALTHER, Ph.. Photonic quantum simulators. In: *Nature Physics*, vol. 8, 2012, pp. 285–291.

[46] GISIN, N., THEW, R.. Quantum communication. In: *Nat. Photon.*, 2007, vol. 1, pp. 165–171.

[47] DIETRICH, C. P., FIORE, A., THOMPSON, M. G., KAMP, M., HÖFLING, S.. GaAs integrated quantum photonics: Towards compact and multi-functional quantum photonic integrated circuits. In: *Laser Photonics Rev.*, 2016, vol. 10, nr. 6, pp. 870–894.

[48] HOUCK, A. A., TÜRECI, H. E., KOCH, J.. On-chip quantum simulation with superconducting circuits. In: *Nat. Phys.*, 2012, vol. 8, pp. 292-299.

[49] HENNESSY, K., BADOLATO, A., WINGER, M., GERACE, D., ATATÜRE, M., GULDE, S., FÄLT, S., HU, E. L., IMAMOĞLU, A.. Quantum nature of a strongly coupled single quantum dot–cavity system. In: *Nature*, 2007, vol. 445, pp. 896–899.

[50] GURUDEV DUTT, M. V., CHILDRESS, L., JIANG, L., TOGAN, E., MAZE, J., JELEZKO, F., ZIBROV, A. S., HEMMER, P. R., LUKIN, M. D.. Quantum register based on individual electronic and nuclear spin qubits in diamond. In: *Science*, 2007, vol. 316, pp. 1312–1316.

[51] CLARKE, J., WILHELM, F. K.. Superconducting quantum bits. In: *Nature*, 2008, vol. 453, pp. 1031–1042.

[52] JOSEPHSON, B. D.. Possible new effects in superconductive tunnelling. In: *Phys. Lett.*, 1962, vol. 1, nr. 7, pp. 251-253.

[53] BULUTA, I., ASHHAB, S., NORI, F.. Natural and artificial atoms for quantum computation. In: *Rep. Prog. Phys.*, 2011, vol. 74, pp. 104401/1-16.

[54] NIEMCZYK, T., DEPPE, F., HUEBL, H., MENZEL, E. P., HOCKE, F., SCHWARZ, M. J., GARCIA-RIPOLL, J. J., ZUECO, D., HÜMMER, T., SOLANO, E., MARX, A., GROSS, R.. Circuit quantum electrodynamics in the ultrastrong-coupling regime. In: *Nat. Phys.*, 2010, vol. 6, pp. 772–776.

[55] LOUNIS, B., BECHTEL, H. A., GERION, D., ALIVISATOS, P., MOERNER, W. E.. Photon antibunching in single CdSe/ZnS quantum dot fluorescence. In: *Chem. Phys. Lett.*, 2000, vol. 329, nr. 5-6, pp. 399-404.

[56] QUALTIERI, A., MORELLO, G., SPINICELLI, P., TODARO, M. T., STOMEO, T., MARTIRADONNA, L., DE GIORGI, M., QUÉLIN, X., BUIL, S., BRAMATI, A., HERMIER, J. P., CINGOLANI, R., DE VITTORIO, M.. Nonclassical emission from single colloidal nanocrystals in a microcavity: a route towards room temperature single photon sources. In: *New J. Phys.*, 2009, vol. 11, pp. 033025/1-9.

[57] GOLDSTEIN, L., GLAS, F., MARZIN, J. Y., CHARASSE, M. N., LE ROUX, G.. Growth by molecular beam epitaxy and characterization of InAs/GaAs strained-layer superlattices. In: *Appl. Phys. Lett.*, 1985, vol. 47, pp. 1099-1101.

[58] BARNES, W. L., BJÖRK, G., GERARD, J. M., JONSSON, P., WASEY, J. A. E., WORTHING, P. T., ZWILLER, V.. Solid-state single photon sources: light collection strategies. In: *Eur. Phys. J. D*, 2002, vol. 18, pp. 197-210.

[59] MOREAU, E., ROBERT, I., GERARD, J. M., ABRAM, I., MANIN, L., THIERRY-MIEG, V.. Single-mode solid-state single photon source based on isolated quantum dots in pillar microcavities. In: *Appl. Phys. Lett.*, 2001, vol. 79, pp. 2865-2867.

[60] CHANG, W.-H., CHEN, W.-Y., CHANG, H.-S., HSIEH, T.-P., CHYI, J.-I., HSU, T.-M.. Efficient Single-Photon Sources Based on Low-Density Quantum Dots in Photonic-Crystal Nanocavities. In: *Phys. Rev. Lett.*, 2006, vol. 96, pp. 117401/1-4.

[61] ENGLUND, D., FARAON, A., FUSHMAN, I., STOLTZ, N., PETROFF, P., VUCKOVIC, J.. Controlling cavity reflectivity with a single quantum dot. In: *Nature*, 2007, vol. 450, pp. 857–861.

[62] FARAON, A., ENGLUND, D., BULLA, D., LUTHER-DAVIES, B., EGGLETON, B. J., STOLTZ, N., PETROFF, P., VUCKOVIC, J.. Local tuning of photonic crystal cavities using chalcogenide glasses. In: *Appl. Phys. Lett.*, 2008, vol. 92, pp. 043123/1-3.

[63] MOSOR, S., HENDRICKSON, J., RICHARDS, B. C., SWEET, J., KHITROVA, G., GIBBS, H. M., YOSHIE, T., SCHERER, A., SHCHEKIN, O. B., DEPPE, D. G.. Scanning a photonic crystal slab nanocavity by condensation of xenon. In: *Appl. Phys. Lett.*, 2005, vol. 87, pp. 141105/1-3.

[64] HAFT, D., SCHULHAUSER, C., GOVOROV, A. O., WARBURTON, R. J., KARRAI, K., GARCIA, J. M.. SCHOENFELD, W., PETROFF, P. M., Magneto-optical properties of ring-shaped self-assembled InGaAs quantum dots. In: *Physica E*, 2002, vol. 13, pp. 165-169.

[65] HÖGELE, A., SEIDL, S., KRONER, M., KARRAI, K., WARBURTON, R. J., GERARDOT, B. D., PETROFF, P. M.. Voltage-Controlled Optics of a Quantum Dot. In: *Phys. Rev. Lett.*, 2004, vol. 93, pp. 217401/1-4.

[66] VAMIVAKAS, A. N., ZHAO, Y., LU, C.-Y., ATATÜRE, M.. Spin-resolved quantum-dot resonance fluorescence. In: *Nat. Phys.*, 2009, vol. 5, pp. 198-202.

[67] ATES, S., ULRICH, S. M., REITZENSTEIN, S., LÖFFLER, A., FORCHEL, A., MICHLER, P.. Post-Selected Indistinguishable Photons from the Resonance Fluorescence of a Single Quantum Dot in a Microcavity. In: *Phys. Rev. Lett.*, 2009, vol. 103, pp. 167402/1-4.

[68] FARAON, A., FUSHMAN, I., ENGLUND, D., STOLTZ, N., PETROFF, P., VUCKOVIC, J.. Coherent generation of non-classical light on a chip via photon-induced tunnelling and blockade. In: *Nat. Phys.*, 2008, vol. 4, pp. 859–863.

[69] FATTAL, D., DIAMANTI, E., INOUE, K., YAMAMOTO, Y.. Quantum Teleportation with a Quantum Dot Single Photon Source. In: *Phys. Rev. Lett.*, 2004, vol. 92, pp. 037904/1-4.

[70] JAYAKUMAR, H., PREDOJEVIC, A., KAUTEN, T., HUBER, T., SOLOMON, G. S., WEIHS, G.. Time-bin entangled photons from a quantum dot. In: *Nat. Commun.*, 2014, vol. 5, pp. 4251/1-5.

[71] REITHMAIER, G., LICHTMANNECKER, S., REICHERT, T., HASCH, P., MÜLLER, K., BICHLER, M., GROSS, R., FINLEY, J. J.. On-chip time resolved detection of quantum dot emission using integrated superconducting single photon detectors. In: *Sci. Rep.*, 2013, vol. 3, pp. 1901/1-6.

[72] INTALLURA, P. M., WARD, M. B., KARIMOV, O. Z., YUAN, Z. L., SEE, P., SHIELDS, A. J., ATKINSON, P., RITCHIE, D. A.. Quantum key distribution using a triggered quantum dot source emitting near 1.3 μm. In: *Appl. Phys. Lett.*, 2007, vol. 91, pp. 161103/1-3.

[73] POOLEY, M. A., ELLIS, D. J. P., PATEL, R. B., BENNETT, A. J., CHAN, K. H. A., FARRER, I., RITCHIE, D. A., SHIELDS, A. J.. Controlled-NOT gate operating with single photons. In: *Appl. Phys. Lett.*, 2012, vol. 100, pp. 211103/1-4.

[74] AGARWAL, G. S.. *Quantum Statistical Theories of Spontaneous Emission and their Relation to other Approaches*. Berlin: Springer, 1974. 135 p.

[75] FICEK, Z., SWAIN, S.. *Quantum Interference and Coherence: Theory and Experiments*. New York: Springer-Verlag, 2005. 420 p.

[76] KIFFNER, M., MACOVEI, M., EVERS, J., KEITEL, C. H.. Vacuum-Induced Processes in Multilevel Atoms. In: *Prog. Optics*, 2010, vol. 55, pp. 85-197.

[77] ZHU, S.-Y., SCULLY, M. O.. Spectral Line Elimination and Spontaneous Emission Cancellation via Quantum Interference. In: *Phys. Rev. Lett.*, 1996, vol. 76, nr. 3, pp. 388-391.

[78] MARTINEZ, M. A. G., HERCZFELD, P. R., SAMUELS, C., NARDUCCI, L. M., KEITEL, C. H.. Quantum interference effects in spontaneous atomic emission: Dependence of the resonance fluorescence spectrum on the phase of the driving field. In: *Phys. Rev. A*, 1997, vol. 55, nr. 6, pp. 4483-4491.

[79] PASPALAKIS, E., KNIGHT, P. L.. Phase Control of Spontaneous Emission. In: *Phys. Rev. Lett.*, 1998, vol. 81, nr. 2, pp. 293-296.

[80] KEITEL, C. H.. Narrowing Spontaneous Emission without Intensity Reduction. In: *Phys. Rev. Lett.*, 1999, vol. 83, nr. 7, pp. 1307-1310.

[81] POSTAVARU, O., HARMAN, Z., KEITEL, C. H., High-Precision Metrology of Highly Charged Ions via Relativistic Resonance Fluorescence. In: *Phys. Rev. Lett.*, 2011, vol. 106, nr. 3, pp. 033001/1-4.

[82] HEEG, K. P., WILLE, H.-C., SCHLAGE, K., GURYEVA, T., SCHUMACHER, D., USCHMANN, I., SCHULZE, K. S., MARX, B., KÄMPFER, T., PAULUS, G. G., RÖHLSBERGER, R., EVERS, J.. Vacuum-Assisted Generation and Control of Atomic Coherences at X-Ray Energies. In: *Phys. Rev. Lett.*, 2013, vol. 111, pp. 073601/1-5.

[83] GARRAWAY, B. M., KNIGHT, P. L.. Cavity modified quantum beats. In: *Phys. Rev. A*, 1996, vol. 54, nr. 4, pp. 3592-3602.

[84] PATNAIK, A., AGARWAL, G. S.. Cavity-induced coherence effects in spontaneous emissions from preselection of polarization. In: *Phys. Rev. A*, 1999, vol. 59, nr. 4, pp. 3015-3020.

[85] DAS, S., PÁLFFY, A., KEITEL, C. H.. Quantum interference effects in an ensemble of ^{229}Th nuclei interacting with coherent light. In: *Phys. Rev. C*, 2013, vol. 88, nr. 2, pp. 024601/1-14.

[86] GERARDOT, B. D., BRUNNER, D., DALGARNO, P. A., KARRAI, K., BADOLATO, A., PETROFF, P. M., WARBURTON, R. J.. Dressed excitonic states and quantum interference in a three-level quantum dot ladder system. In: *New J. Phys.*, 2009, vol. 11, pp. 013028/1-11.

[87] CIORNEA, V., MACOVEI, M. A.. Cavity-output-field control via interference effects. In: *Phys. Rev. A*, 2014, vol. 90, nr. 4, 043837/1-4.

[88] DAS, S., AGARWAL, G. S.. Protecting bipartite entanglement by quantum interferences. In: *Phys. Rev. A*, 2010, vol. 81, nr. 5, pp. 052341/1-6.

[89] TANG, Z.-H., LI, G.-X., FICEK, Z.. Entanglement created by spontaneously generated coherence. In: *Phys. Rev. A*, 2010, vol. 82, pp. 063837/1-11.

[90] HARRIS, S. E.. Electromagnetically Induced Transparency. In: *Phys. Today*, 1997, vol. 50, nr. 7, pp. 36-42.

[91] MACOVEI, M., EVERS, J., KEITEL, C. H.. Phase control of collective quantum dynamics. In: *Phys. Rev. Lett.*, 2003, vol. 91, nr. 23, pp. 233601/1-4.

[92] MACOVEI, M. A.. Enhancing superfluorescence via decay interference, In: *J. Phys. B: At. Mol. Opt. Phys.*, 2007, vol. 40, nr. 2, pp. 387-392.

[93] PASPALAKIS, E., KNIGHT, P. L.. Phase control of spontaneous emission. In: *Phys. Rev. Lett.*, 1988, vol. 81, nr. 2, pp. 293-296.

[94] MACOVEI, M., KEITEL, C. H.. Super-bunched photons via a strongly pumped near-equispaced multiparticle system. In: *Phys. Rev. B*, 2007, vol. 75, nr. 24, pp. 245325/1-7.

[95] XIE, X.-T., MACOVEI, M., KIFFNER, M., KEITEL, C. H.. Probing quantum superposition states with few-cycle laser pulses. In: *J. Opt. Soc. Am. B*, 2009, vol. 26, nr. 10, pp. 1912-1917.

[96] SADEGHI, S. M., LEFFLER, S. R., MEYER, J.. Quantum interferences and gain processes in optically-driven n-doped quantum wells with X configurations. In: *Opt. Commun.*, 1998, vol. 151, pp. 173-186.

[97] ROSENCHER, E., BOIS, Ph.. Model system for optical nonlinearities: Asymmetric quantum wells. In: *Phys. Rev. B*, 1991, vol. 44, nr. 20, pp. 11315-11327.

[98] FROGLEY, M. D., DYNES, J. F., BECK, M., FAIST, J., PHILLIPS, C. C.. Gain without inversion in semiconductor nanostructures. In: *Nat. Mater.*, 2006, vol. 5, nr. 3, pp. 175-178.

[99] PHILLIPS, M., WANG, H.. Spin coherence and electromagnetically induced transparency via exciton correlations. In: *Phys. Rev. Lett.*, 2002, vol. 89, nr. 18, pp. 186401/1-4.

[100] DYNES, J. F., FROGLEY, M. D., BECK, M., FAIST, J., PHILLIPS, C. C.. ac Stark splitting and quantum interference with intersubband transitions in quantum wells. In: *Phys. Rev. Lett.*, 2005, vol. 94, nr. 15, pp. 157403/1-4.

[101] SERAPIGLIA, G. B., PASPALAKIS, E., SIRTORI, C., VODOPYANOV, K. L., PHILLIPS, C. C.. Laser-induced quantum coherence in semiconductor quantum well. In: *Phys. Rev. Lett.*, 2000, vol. 84, nr. 5, pp. 1019-1022.

[102] CEBAN, V., MACOVEI, M. A.. Cavity quantum interferences with three-level atoms. In: *J. Opt. Soc. Am. B*, 2016, vol. 33, pp. 942-946.

[103] CEBAN, V.. Phase-dependent quantum interferences with three-level artificial atoms. In: *Rom. J. Phys.*, 2017, vol. 62, pp. 207/1-8.

[104] NICHOLS, E. F., HULL, G. F.. A Preliminary Communication on the Pressure of Heat and Light Radiation. In: *Phys. Rev.*, 1901, vol. 13, pp. 307-320.

[105] ABBOTT, B. et al.. Observation of a kilogram-scale oscillator near its quantum ground state. In: *New J. Phys.*, 2009, vol. 11, pp. 073032/1-13.

[106] KLECKNER, D., BOUWMEESTER, D.. Sub-kelvin optical cooling of a micromechanical resonator. In: *Nature*, 2006, vol. 444, pp. 75–78.

[107] COLE, G. D., WILSON-RAE, I., WERBACH, K., VANNER, M. R., ASPELMEYER, M.. Phonon-tunnelling dissipation in mechanical resonators. In: *Nature Comm.*, 2011, vol. 2, pp. 231/1-8.

[108] KLECKNER, D., PEPPER, B., JEFFREY, E., SONIN, P., THON, S. M., BOUWMEESTER, D.. Optomechanical trampoline resonators. In: *Opt. Express*, 2011, vol. 19, pp. 19708/1-9.

[109] FAVERO, I., STAPFNER, S., HUNGER, D., PAULITSCHKE, P., REICHEL, J., LORENZ, H., WEIG, E. M., KARRAI, K.. Fluctuating nanomechanical system in a high finesse optical microcavity. In: *Opt. Express*, 2009, vol. 17, pp. 12813-12820.

[110] STAPFNER, S., OST, L., HUNGER, D., REICHEL, J., FAVERO, I., WEIG, E. M.. Cavity-enhanced optical detection of carbon nanotube Brownian motion. In: *Appl. Phys. Lett.*, 2013, vol. 102, pp. 151910/1-5.

[111] VERBRIDGE, S. S., PARPIA, J. M., REICHENBACH, R. B., BELLAN, L. M., CRAIGHEAD, H. G.. High quality factor resonance at room temperature with nanostrings under high tensile stress. In: *J. Appl. Phys.*, 2006, vol. 99, pp. 124304/1-8.

[112] WANG, X., ZHU, D., YANG, X., YUAN, L., LI, H., WANG, J., CHEN, M., DENG, G., LIANG, W., LI, Q., FAN, S., GUO, G., JIANG, K.. Stressed carbon nanotube devices for high tunability, high quality factor, single mode GHz resonators. In: *Nano Research*, 2018, vol. 11, pp. 5812–5822.

[113] JAYICH, A. M., SANKEY, J. C., BORKJE, K., LEE, D., YANG, C., UNDERWOOD, M., CHILDRESS, L., PETRENKO, A., GIRVIN, S. M., HARRIS, J. G. E.. Cryogenic optomechanics with a Si3N4 membrane and classical laser noise. In: *New J. Phys.*, 2012, vol. 14, pp. 115018/1-17.

[114] FLOWERS-JACOBS, N. E., HOCH, S. W., SANKEY, J. C., KASHKANOVA, A., JAYICH, A. M., DEUTSCH, C., REICHEL, J., HARRIS, J. G. E.. Fiber-cavity-based optomechanical device. In: *Appl. Phys. Lett.*, 2012, vol. 101, pp. 221109/1-4.

[115] CHAN, J., SAFAVI-NAEINI, A. H., HILL, J. T., MEENEHAN, S., PAINTER, O.. Optimized optomechanical crystal cavity with acoustic radiation shield. In: *Appl. Phys. Lett.*, 2012, vol. 101, pp. 081115/1-4.

[116] VERHAGEN, E., DELEGLISE, S., WEIS, S., SCHLIESSER, A., KIPPENBERG, T. J.. Quantum-coherent coupling of a mechanical oscillator to an optical cavity mode. In: *Nature*, vol. 482, pp. 63–67.

[117] NGUYEN, D. T., BAKER, C., HEASE, W., SEJIL, S., SENELLART, P., LEMAITRE, A., DUCCI, S., LEO, G., FAVERO, I.. Ultrahigh Q-frequency product for optomechanical disk resonators with a mechanical shield. In: *Appl. Phys. Lett.*, 2013, vol. 103, pp. 241112/1-5.

[118] MA, R., SCHLIESSER, A., DEL'HAYE, P., DABIRIAN, A., ANETSBERGER, G., KIPPENBERG, T. J.. Radiation-pressure-driven vibrational modes in ultrahigh-Q silica microspheres. In: *Opt. Lett.*, 2007, vol. 32, pp. 2200-2202.

[119] FAVERO, I., MARQUARDT, F.. Focus on optomechanics. In: *New J. Phys.*, 2014, vol. 16, pp. 085006/1-8.

[120] POOT, M., VAN DER ZANT, H. S. J.. Mechanical systems in the quantum regime. In: *Phys. Rep.*, 2012, vol. 511, pp. 273-335.

[121] ARMOUR, A. D., BLENCOWE, M. P., SCHWAB, K. C.. Entanglement and Decoherence of a Micromechanical Resonator via Coupling to a Cooper-Pair Box. In: *Phys. Rev. Lett.*, 2009, vol. 88, pp. 148301/1-4.

[122] XUE, F., WANG, Y. D., SUN, C. P., OKAMOTO, H., YAMAGUCHI, H., SEMBA, K.. Controllable coupling between flux qubit and nanomechanical resonator by magnetic field. In: *New. J. Phys.*, 2007, vol. 9, pp. 35–35

[123] RABL, P., CAPPELLARO, P., DUTT, M. V. G., JIANG, L., MAZE, J. R., LUKIN, M. D.. Strong magnetic coupling between an electronic spin qubit and a mechanical resonator. In: *Phys. Rev. B*, 2009, vol. 79, pp. 041302/1-4.

[124] WILSON-RAE, I., ZOLLER, P., IMAMOGLU, A.. Laser Cooling of a Nanomechanical Resonator Mode to its Quantum Ground State. In: *Phys. Rev. Lett.*, 2004, vol. 92, pp. 075507/1-4.

[125] YEO, I., DE ASSIS, P.-L., GLOPPE, A., DUPONT-FERRIER, E., VERLOT, P., MALIK, N. S., DUPUY, E., CLAUDON, J., GERARD, J. M., AUFFEVES, A., NOGUES, G., SEIDELIN, S., POIZAT, J-PH., ARCIZET, O., RICHARD, M.. Strain-mediated coupling in a quantum dot–mechanical oscillator hybrid system. In: *Nat. Nanotech.*, 213, vol. 9, pp. 106–110.

[126] WEI, Y.-J., HE, Y., HE, Y.-M., LU, C.-Y., PAN, J.-W., SCHNEIDER, C., KAMP, M., HÖFLING, S., MCCUTCHEON, D. P. S., NAZIR, A.. Temperature-Dependent Mollow Triplet Spectra from a Single Quantum Dot: Rabi Frequency Renormalization and Sideband Linewidth Insensitivity. In: *Phys. Rev. Lett.*, 2014, vol. 113, pp. 097401/1-5.

[127] DIEDRICH, F., BERQUIST, J. C., ITANO, W. M., WINELAND, D. J.. Laser Cooling to the Zero-Point Energy of Motion. In: *Phys. Rev. Lett.*, 1989, vol. 62, nr. 4, pp. 403–406.

[128] MONROE, C., MEEKHOF, D. M., KING, B. E., JEFFERTS, S. R., ITANO, W. M., WINELAND, D. J., GOULD, P.. Resolved-Sideband Raman Cooling of a Bound Atom to the 3D Zero-Point Energy. In: *Phys. Rev. Lett.*, 1995, vol. 75, nr. 22, pp. 4011–4014.

[129] HAMANN, S. E., HAYCOCK, D. L., KLOSE, G., PAX, P. H., DEUTSCH, I. H., JESSEN, P. S.. Resolved-Sideband Raman Cooling to the Ground State of an Optical Lattice. In: *Phys. Rev. Lett.*, 1998, vol. 80, nr. 19, pp. 4149-4152.

[130] MORIGI, G., ESCHNER, J., KEITEL, C. H.. Ground State Laser Cooling Using Electromagnetically Induced Transparency. In: *Phys. Rev. Lett.*, 2000, vol. 85, nr. 21, pp. 4458–4461.

[131] EVERS, J., KEITEL, C. H.. Double-EIT ground-state laser cooling without blue-sideband heating. In: *Europhys. Lett.*, 2004, vol. 68, nr. 3, pp. 370-376.

[132] MACOVEI, M. A., XIE, X.-T.. Two-photon cooling of a nonlinear quantum oscillator. In: *Opt. Commun.*, vol. 282, pp. 3930-3933.

[133] CERBU, M., MACOVEI, M. A., LI G.-X.. Cooling a two-level emitter in photonic-crystal environments. In: *Phys. Rev. A*, vol. 89, pp. 013837/1-5.

[134] GU, W.-J., LI, G.-X.. Quantum interference effects on ground-state optomechanical cooling. In: *Phys. Rev. A*, 2013, vol. 87, nr. 2, 025804/1-5.

[135] MACOVEI, M. A.. Cooling a quantum circuit via coupling to a multiqubit system. In: *Phys. Rev. A*, 2010, vol. 81, nr. 4, pp. 043411/1-5.

[136] ROCHELEAU, T., NDUKUM, T., MACKLIN, C., HERTZBERG, J. B., CLERK, A. A., SCHWAB, K. C.. Preparation and detection of a mechanical resonator near the ground state of motion. In: *Nature (London)*, 2010, vol. 463, nr. 7277, pp. 72-75.

[137] CEBAN, V., MACOVEI, M. A.. Enhanced cooling for stronger qubit-phonon couplings. In: *Rom. Rep. Phys.*, 2018, vol. 70, pp. 407/1-8.

[138] KÜTT, W., ALBRECHT, W., KURZ, H.. Generation of Coherent Phonons in Condensed Media. In: *IEEE J. Quantum Electron.*, 1992, vol. 28, nr. 10, pp. 2434-2444.

[139] BARTELS, A., DEKORSY, TH., KURZ, H.. Coherent Zone-Folded Longitudinal Acoustic Phonons in Semiconductor Superlattices: Excitation and Detection. In: *Phys. Rev. Lett.*, 1999, vol. 82, nr. 5, pp. 1044-1047.

[140] EZZAHRI, Y., GRAUBY, S., RAMPNOUX, J. M., MICHEL, H., PERNOT, G., CLAEYS, W., DILHAIRE, S., ROSSIGNOL, C., ZENG, G., SHAKOURI, A.. Coherent phonons in Si/SiGe superlattices. In: *Phys. Rev. B*, 2007, vol. 75, nr. 19, pp. 195309/1-11.

[141] JING, H., ÖZDEMIR S. K, XIN-YOU LÜ, ZHANG J., YANG L., NORI F.. PT -Symmetric Phonon Laser. In: *Phys. Rev. Lett.*, 2014, vol. 113, nr. 5, pp. 053604/1-5.

[142] WANG, H., WANG, Z., ZHANG, J., ÖZDEMIR, Ş. K., YANG, L., LIU, Y.. Phonon amplification in two coupled cavities containing one mechanical resonator. In: *Phys. Rev. A*, 2014, vol. 90, pp. 053814/1-14.

[143] WU, H., HEINRICH, G., MARQUARDT, F.. The effect of Landau–Zener dynamics on phonon lasing. In: *New J. Phys.*, 2013, vol. 15, nr. 12, pp. 123022/1-11.

[144] BHATTACHERJEE, A. B., BRANDES, T.. Phonon Laser Effect and Dicke-Hepp-Lieb Superradiant Phase Transition in Magnetic Cantilever Coupled to a Bose Einstein Condensate. In: *Can. J. Phys.*, 2013, vol. 91, pp. 639-644.

[145] FIGUEIREDO ROQUE, T., VIDIELLA-BARRANCO, A.. Dissipation-driven squeezed and sub-Poissonian mechanical states in quadratic optomechanical systems. In: *arXiv:1406.1987 [quant-ph]*, 2014, pp. 1-10.

[146] KRONWALD, A., MARQUARDT, F., CLERK, A. A.. Arbitrarily large steady-state bosonic squeezing via dissipation. In: *Phys. Rev. A*, 2013, vol. 88, nr. 6, pp. 063833/1-10.

[147] POSHAKINSKIY, A. V., PODDUBNY, A. N.. Time-dependent photon correlations for incoherently pumped quantum dot strongly coupled to the cavity mode. In: *J. Exp. Theor. Phys.*, 2014, vol. 145, nr. 2, pp. 237-249.

[148] CHUU, C.-S., SCHRECK, F., MEYRATH, T. P., HANSSEN, J. L., PRICE, G. N., RAIZEN, M. G.. Direct Observation of Sub-Poissonian Number Statistics in a Degenerate Bose Gas. In: *Phys. Rev. Lett.*, 2005, vol. 95, pp. 260403/1-4.

[149] JACQMIN, Th., ARMIJO, J., BERRADA, T., KHERUNTSYAN, K. V., BOUCHOULE, I.. Sub-Poissonian Fluctuations in a 1D Bose Gas: From the Quantum Quasicondensate to the Strongly Interacting Regime. In: *Phys. Rev. Lett.*, 2011, vol. 106, 230405/1-4.

[150] MERLO, M., HAUPT, F., CAVALIERE, F., SASSETTI, M.. Sub-Poissonian phononic population in a nanoelectromechanical system. In: *New J. Phys.*, 2008, vol. 10, nr. 2, pp. 023008/1-12.

[151] CEBAN, V., MACOVEI, M. A.. Sub-Poissonian phonon statistics in an acoustical resonator coupled to a pumped two-level emitter. In: *J. Exp. Theor. Phys.*, 2015, vol. 121, pp. 793–798.

[152] GRANGIER, P., ASPECT, A., VIGUE, J.. Quantum Interference Effect for Two Atoms Radiating a Single Photon. In: *Phys. Rev. Lett.*, 1985, vol. 54, pp. 418-421.

[153] EICHMANN, U., BERGQUIST, J. C., BOLLINGER, J. J., GILLIGAN, J. M., ITANO, W. M., WINELAND, D. J., RAIZEN, M. G.. Young's interference experiment with light scattered from two atoms. In: *Phys. Rev. Lett.*, 1993, vol. 70, pp. 2359-2362.

[154] NEUZNER, A., KÖRBER, M., MORIN, O., RITTER, S., REMPE, G.. Interference and dynamics of light from a distance-controlled atom pair in an optical cavity. In: *Nat. Photon.*, 2016, vol. 10, pp. 303-306.

[155] RAIMOND, J. M., BRUNE, M., HAROCHE, S.. Manipulating quantum entanglement with atoms and photons in a cavity. In: *Rev. Mod. Phys.*, 2001, vol. 73, pp. 565–582.

[156] TANAS, R., FICEK, Z.. Stationary two-atom entanglement induced by nonclassical two-photon correlations. In: *J. Opt. B : Quantum Semiclass. Opt.*, 2004, vol. 6, pp. S610–S617.

[157] URBAN, E., JOHNSON, T. A., HENAGE, T., ISENHOWER, L., YAVUZ, D. D., WALKER, T. G., SAFFMAN, M.. Observation of Rydberg blockade between two atoms. In: *Nat. Phys.*, 2009, vol. 5, pp. 110–114.

[158] GAËTAN, A., MIROSHNYCHENKO, Y., WILK, T., CHOTIA, A., VITEAU, M., COMPARAT, D., PILLET, P., BROWAEYS, A., GRANGIER, P.. Observation of collective excitation of two individual atoms in the Rydberg blockade regime. In: *Nat. Phys.*, 2009, vol. 5, pp. 115–118.

[159] EVERS, J., KIFFNER, M., MACOVEI, M., KEITEL, C. H.. Geometry-dependent dynamics of two Λ-type atoms via vacuum-induced coherences. In: *Phys. Rev. A*, 2006, vol. 73, pp. 023804/1-7.

[160] PENG, J., LI, G.-X.. Effects of the dipole-dipole interaction on dynamic properties and atomic coherent trapping of a two-atom system. In: *Phys. Rev. A*, 1993, vol. 47, pp. 4212–4218.

[161] DICKE, R. H.. Coherence in spontaneous radiation processes. In: *Phys. Rev.*, 1954, vol. 93, pp. 99-110.

[162] DEVOE, R. G., BREWER, R. G.. Observation of Superradiant and Subradiant Spontaneous Emission of Two Trapped Ions. In: *Phys. Rev. Lett.*, 1996, vol. 76, pp. 2049–2052.

[163] MACOVEI, M., KEITEL, C. H.. Laser Control of Collective Spontaneous Emission. In: *Phys. Rev. Lett.*, 2003, vol. 91, pp. 123601/1-4.

[164] SCULLY, M. O., FRY, E. S., OOI, C. H. R., WÓDKIEWICZ, K.. Directed Spontaneous Emission from an Extended Ensemble of N Atoms: Timing Is Everything. In: *Phys. Rev. Lett.*, 2006, vol. 96, pp. 010501/1-4.

[165] SKRIBANOWITZ, N., HERMAN, I. P., MACGILLIVRAY, J. C., FELD, M. S.. Observation of Dicke Superradiance in Optically Pumped HF Gas. In: *Phys. Rev. Lett.*, 1973. vol. 30, pp. 309–312.

[166] GROSS, M., HAROCHE, S.. Superradiance: an essay on the theory of collective spontaneous emission. In: *Phys. Rep.*, 1982, vol. 93, pp. 301-396.

[167] KEITEL, C. H., SCULLY, M. O., Süssmann G.. Triggered superradiance. In: *Phys. Rev. A*, 1992, vol. 45, pp. 3242-3249.

[168] ANDREEV, A. V., EMEL'YANOV, V. I., IL'INSKII, Yu. A.. *Cooperative Effects in Optics. Superfluorescence and Phase Transitions.* London: IOP Publishing, 1993. 470 p.

[169] SCULLY, M. O., SVIDZINSKY, A. A.. The Super of Superradiance. In: *Science*, 2009, vol. 325, pp. 1510-1511.

[170] CONG, K., ZHANG, Q., WANG, Y., NOE, G. T., BELYANIN, A., KONO, J.. Dicke superradiance in solids. In: *J. Opt. Soc. Am. B*, 2016, vol. 33, pp. C80-C101.

[171] DE BOER, S., WIERSMA, D. A.. Dephasing-induced damping of superradiant emission in J-aggregates. In: *Chem. Phys. Lett.*, 1990, vol. 165, pp. 45-53.

[172] FROLOV, S. V., GELLERMANN, W., OZAKI, M., YOSHINO, K., VARDENY, Z. V.. Cooperative Emission in π-Conjugated Polymer Thin Films. In: *Phys. Rev. Lett.*, 1997, vol. 78, pp. 729–732.

[173] BAUMANN, K., GUERLIN, C., BRENNECKE, F., ESSLINGER, T.. Dicke quantum phase transition with a superfluid gas in an optical cavity. In: *Nature (London)*, 2010, vol. 464, pp. 1301–1306.

[174] CHUDNOVSKY, E. M., GARANIN, D. A.. Phonon Superradiance and Phonon Laser Effect in Nanomagnets. In: *Phys. Rev. Lett.*, 2004, vol. 93, nr. 25, pp. 257205/1-4.

[175] CEBAN, V., LONGO, P., MACOVEI, M. A.. Fast phonon dynamics of a nanomechanical oscillator due to cooperative effects. In: *Phys. Rev. A*, 2017, vol. 95, 023806/1-5.

[176] BRANDES, T., KRAMER, B.. Spontaneous Emission of Phonons by Coupled Quantum Dots. In: *Phys. Rev. Lett.*, 1999, vol. 83, nr. 15, pp. 3021-3024.

[177] TIGHINEANU, P., DAVEAU, R. S., LEHMANN, T. B., BEERE, H. E., RITCHIE, D. A., LODAHL, P., STOBBE, S.. Single-Photon Superradiance from a Quantum Dot. In: *Phys. Rev. Lett.*, 2016, vol. 116, pp. 163604/1-6.

[178] LONGO, P., KEITEL, C. H., EVERS, J.. Tailoring superradiance to design artificial quantum systems. In: *Sci. Rep.*, 2016, vol. 6, pp. 23628/1-6.

[179] SCULLY, M., ZUBAIRY, M.. *Quantum optics*. Cambridge: Cambridge University Press, 1997. 624 p.

[180] GERRY, CH. C., KNIGHT, P. L.. *Introductory Quantum Optics*. Cambridge: Cambridge University Press, 2004. 332p.

[181] CASIMIR, H.. On the attraction between two perfectly conducting plates. In: *Proc. Kon. Ned. Akad. Wetensch.*, 1948, vol. B51, pp. 793-795.

[182] SOYKAL, Ö. O., RUSKOV, R., TAHAN, Ch.. Sound-Based Analogue of Cavity Quantum Electrodynamics in Silicon. In: *Phys. Rev. Lett.*, 2011, vol. 107, pp. 235502/1-5.

[183] EKINCI, K. L., ROUKES, M. L.. Nanoelectromechanical systems. In: *Rev. Sci. Instrum.*, 2005, vol. 76, pp. 061101/1-12.

[184] NAZIR, A., MCCUTCHEON, D. P. S.. Modelling exciton–phonon interactions in optically driven quantum dots. In: *J. Phys.: Condens. Matter*, 2016, vol. 28, pp. 103002/1-26.

[185] WEISSKOPF, V., WIGNER, E.. Calculation of the natural line width on the basis of Dirac's theory of light. In: *Z. Phys.*, 1930 , vol. 63, pp. 54–73.

[186] KIRA, M., KOCH, S. W.. *Semiconductor Quantum Optics*. Cambridge: Cambridge University Press, 2012. 658 p.

[187] PURI, R. R.. *Mathematical Methods of Quantum Optics.* Berlin Heidelberg: Springer-Verlag, 2001. 289 p.

[188] JAMES, D. F. V.. Quantum Computation with Hot and Cold Ions: An Assessment of Proposed Schemes, In: *Fortschr. Phys.*, 2000, vol. 48, pp. 823-837.

[189] TAN, R., LI, G.-X., FICEK, Z.. Squeezed single-atom laser in a photonic crystal. In: *Phys. Rev. A*, 2008, vol. 78, nr. 2, pp. 023833/1-11.

[190] MACOVEI, M., EVERS, J., LI, G.-X., KEITEL, C. H.. Strong-Field Spatial Interference in a Tailored Electromagnetic Bath. In: *Phys. Rev. Lett.*, 2007, vol. 98, nr. 4, pp. 043602/1-4.

[191] QUANG, T., KNIGHT, P. L., BUZEK, V.. Quantum collapses and revivals in an optical cavity. In: *Phys. Rev. A*, 1991, vol. 44, pp. 6092-6096.

[192] JHA, P. K., SVIDZINSKY, A. A., SCULLY, M. O.. Coherence enhanced transient lasing in XUV regime. In: *Laser Phys. Lett.*, 2012, vol. 9, nr. 5, pp. 368-376.

[193] BOGOLUBOV, N. N. JR., QUANG, T., SHUMOVSKY, A. S.. Double optical resonance in a system of atoms. In: *Phys. Lett. A*, 1985, vol. 112, nr. 6-7, pp. 323-326.

[194] CEBAN, V.; MACOVEI, M.A.. Quantum Interferences with Equidistant Three-Level Quantum Wells. In: *IFMBE Proceedings. V. 77. Springer, Cham, 2019. 4th International Conference on Nanotechnologies and Biomedical Engineering. ICNBME 2019.* September 18-21, 2019, Chisinau, Moldova, pp. 155—159.

[195] IONICIOIU, R.. Quantum information and quantum technologies. In: *Rom. Rep. Phys.*, 2015, vol. 67, nr. 4, pp. 1300-1318.

[196] LI, J.-J., ZHU, K.-D.. All-optical mass sensing with coupled mechanical resonator systems. In: *Phys. Rep.*, 2013, vol. 525, nr. 3, pp. 223-254.

[197] BRAGINSKY, V. B., MANUKIN, A. B.. *Measurement of Weak Forces in Physics Experiments.* Chicago: University of Chicago Press, 1977. 153 p.

[198] JÄGER, S. B., COOPER, J., HOLLAND, M. J., MORIGI, G.. Dynamical Phase Transitions to Optomechanical Superradiance. In: *Phys. Rev. Lett.*, 2019, vol. 123, pp. 053601/1-6.

[199] JIANG, Y.-J., LÜ, H., JING, H.. Superradiance-Driven Phonon Laser. In: *Chin. Phys. Lett.*, 2018, vol. 35, pp. 044205/1-4.

[200] MONTENEGRO, V., COTO, R., EREMEEV, V., ORSZAG, M.. Ground-state cooling of a nanomechanical oscillator with N spins. In: *Phys. Rev. A*, 2018, vol. 98, pp. 053837/1-12.

Responsibility Declaration

I, hereby, confirm that the scientific results presented in the thesis refer to my investigations. I understand, that in the contrary case I have to face the consequences.

Victor Ceban

10 July, 2020

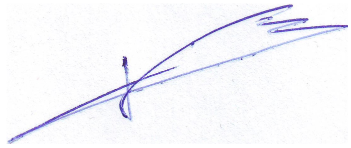

CURRICULUM VITAE: Victor CEBAN

Current position: scientific researcher
Professional Address: off. 221, Laboratory of Quantum Photonics,
Institute of Applied Physics,
5, Academiei str., Chisinau, Moldova.

Date of birth: 4 July 1987
Nationality: Moldavian, Romanian
Phone Number: +373 (0) 69656219
E-mail: victor.ceban@phys.asm.md
Web page: www.phys.asm.md/en/personalpages/vceban

Employment history:

Scientific researcher at the Institute of Applied Physics (in present - since 2014)

Studies:

Ph.D. student at Institute of Applied Physics, Moldova **(2015-2019)**
Thesis "Quantum behaviors of optical and optomechanical systems possessing articial atoms"
Master degree at University Paris-Sud XI, France **(2013)**
Statistical and Numerical Modeling of Complex Systems
Licence degree at University of Bordeaux I, France **(2009)**
First degree in Physics
Lyceum „Gheorghe Asachi", Moldova **(2006)**
Sciences Francophone Baccalaureate.

Internships:

Max-Planck Institute für Kernphysik (MPIK), Heidelberg, Germany **(2015)**
Theory Division, "Correlated and X-ray Quantum Dynamics" group, duration: 3 months
Laboratory „ Aimé Cotton " (LAC), Orsay, France **(2013)**
Study of the dynamics of an molecular ultracold gas in a magnetical trap, duration 4 months
Laboratory of Applied Optics (LOA), ENSTA, Palaiseau, France **(2011)**
Study of the stretcher-compressor system for X-ray lasers, duration: 4 months
Laboratory of Physics of Gases and Plasma (LPGP), Orsay, France **(2010)**
Study of the slowing of fast ions in hot and dense plasma, duration: 3 months
Center for Intense Lasers and Applications (CELIA), Bordeaux, France **(2009)**
Study of the state of the surface of an optical fiber, duration 3 months

Participation to scientific projects:

Bilateral Moldo-German Project 13.820.05.07/GF (2013-2015)
National Institutional Project 15.817.02.09F (2015-2019)
National Institutional Project 20.80009.5007.07 (2020-2023)

Publications:

International journals:

- **V. Ceban**, M.A. Macovei, *"Enhanced cooling for stronger qubit-phonon couplings"*, Rom. Rep. Phys. **70**, 407 (2018)
- **V. Ceban,** *"Phase-dependent quantum interferences with three-level artificial atoms"*, Rom. J. Phys. **62**, 207 (2017)
- **V. Ceban,** P. Longo, M.A. Macovei, *"Fast phonon dynamics of a nanomechanical oscillator due to cooperative effects",* Phys. Rev. A **95**, 023806 (2017)
- **V. Ceban**, M.A. Macovei, *"Cavity quantum interferences with three-level atoms"*, J. Opt. Soc. Am. B **33**, 942 (2016).
- **V. Ceban,** M.A. Macovei, *"Phonon statistics in an acoustical resonator coupled to a pumped two-level emitter"*, J. Exp. Theor. Phys. **121**, 793 (2015).
- C. Deutsch, N.A. Tahir, M. Barriga-Carrasco, **V. Ceban,** P. Fromy, D. Gilles, D. Leger, G. Maynard, B. Tashev, L. Volpe, *"Multiple scattering in electron fluid and energy loss in multi-ionic targets"*, Nucl. Instrum. Methods Phys. Res A **733**, 39 (2014).

National Journals and Conference Proceedings:

- **V. Ceban,** M. A. Macovei *"Quantum Interferences with Equidistant Three-Level Quantum Wells"* In: 4th International Conference on Nanotechnologies and Biomedical Engineering 2019. IFMBE Proceedings 77, 155-159 (2020). Springer, Cham.
- **V. Ceban,** M. Macovei "*The quantum dynamics of a nanomechanical resonator coupled to two quantum dots"* In: Proceedings of the 9th International Conference of "Microelectronics and Computer Science" pp. 37-40, October 19-21, 2017, Chisinau, Moldova.
- **V. Ceban,** M.A. Macovei, *"Quantum dynamics of acoustical phonon statistics"*, Fizică și Tehnică **2**, 18-22 (2015).
- S. Carlig, **V. Ceban,** M.A. Macovei, *"Optomechanical systems – A bridge between nano- and macro- worlds"*, Akademos **4**, 21-27 (2015).

Conferences:

Talks:

- **V. Ceban**, M.A. Macovei, "Quantum interferences with equidistant three level quantum wells", ICNBME (2019).
- **V. Ceban**, M.A. Macovei, "Single-phonon quantum dynamics with nonlinear mechanical resonators", MSCMP (2018).
- **V. Ceban**, "Collective effects in phonon generation with artificial atoms", Perspectivele și Problemele Integrării în Spațiul European al Cercetării și Educației (2017).
- **V. Ceban**, M.A. Macovei, "The quantum dynamics of a nanomechanical resonator coupled to two quantum dots", ICMCS (2017).
- **V. Ceban**, "Quantum behaviors in optomechanical systems possessing artificial atoms", Humboldt Kolleg (2017).
- **V. Ceban**, "Quantum cooling beyond the secular approximation", Perspectivele și Problemele Integrării în Spațiul European al Cercetării și Educației (2016).
- **V. Ceban**, "Cavity quantum dynamics with three level atoms", MSCMP (2016).

- **V. Ceban**, “Quantum interferences in cavity-atom systems”, Tendințe Contemporane ale Dezvoltării Științei (2016).
- **V. Ceban**, M.A. Macovei, “Quantum dynamics of acoustical phonon statistics”, Light and Photonics (2015).

Posters and other:

- Poster: **V. Ceban**, „Phonon statistics in an acoustical cavity”, Tendințe Contemporane ale Dezvoltării Științei (2015).
- Poster: **V. Ceban,** M.A. Macovei, „Quantum dynamics of phonon lasing”, MSCMP (2014).
- Materials Editor and Secretary of the LIGHTtalk: Power of photonics (Moldova), Workshop „Light in Life” (2016).

Scholarships:

Scholarship of the World Federation of Scientists. Duration: 1 year (2017).
Scholarship of the Government of Moldova “V. Belousov”. Duration: 1 year (2016).
Max-Planck Society stipend for Ph.D. students. Duration: 3 months (2015).

Other information:

Scientific interests: quantum optics, quantum optomechanics, laser physics.
Programming languages: C, R, Wolfram Mathematica, Maple.
Languages: Romanian (native), French (DALF B2), English (TOEIC score: 835), Russian.